EXPERIMENTAL INVESTIGATION OF THE OPTICAL MEASUREMENT METHOD FOR DETECTING DUST AND GAS FLAMES IN A FLAME ACCELERATION TUBE

Development of Experimental Apparatus

Ivar Børtnes Kalvatn

A thesis submitted in partial fulfilment of the
requirements for the degree of *Master of Science* in
the subject of Physics; Process Safety Technology

Department of Physics and Technology
University of Bergen
Bergen, Norway
June 2009

Table of Contents

APPENDICES:

Abstract

This thesis describes an experimental investigation of flame propagation in a 3.6-meter Flame Acceleration Tube (FAT) by the use of optical probes for flame detection and dust concentration measurements. The experiments in the FAT took place in the workshop of GexCon AS at Fantoft, Bergen. Fellow Master Student Gisle A. Enstad, who took part in the shared experiments, describes the impedance flame detection method in his thesis.

Flame detection and dust concentration probes were made. Preliminary tests were performed at the University of Bergen in the 20-litre explosion vessel of the USBM type. The final design of the probes implements both the optical and impedance based measurement method. In the preliminary phase of this work, the FAT was equipped with instrumentation cables and power supplies for measurement probes and electrically operated valves. A complete logging system with cables, a logging card from National Instruments and software for running the experiments was also set up as a part of this project.

Closed vessel experiments were performed with both maize starch and propane/air mixtures in the FAT. As the FAT was fitted with six circular windows at one side, the experiments could be recorder with a high-speed camera. A general trend in the results from the experiments was that the optical method detected the flame earlier than the impedance method. Video observations tended to measure the flame arrival time earlier than the optical method on gas and later on dust, while the impedance method were later than the other two. A thermocouple was also used as a reference to the other methods and it showed good correlation with the optical/impedance probe, as it measured the flame arrival time between the times measured by the two other principles.

Acknowledgements

I am profoundly grateful for the help provided by my supervisors, Trygve Skjold and Bjørn J. Arntzen, throughout this project. A special thank goes to Kåre Slettebakken, Leif Egil Sandnes and Roald Langøen at the Mechanical workshop at the University who made a lot of the equipment used in the project, including the measurement probes. Werner Olsen, chief engineer at the Section for Microelectronics at the UiB, have provided help with the design of almost every electrical circuit in this project, including arc generators, amplifiers and signal generators. Professor Rolf K. Eckhoff has been very helpful with both his insight in explosion phenomena, and for funding parts of this project. The staff at the workshop at GexCon AS has been very helpful and lent equipment to this project. A great deal of thanks goes to Justin J.Meager who has been proofreading parts of this thesis in his spare time. And last but not the least, many thanks goes to fellow master student Gisle A.Enstad for the excellent cooperation during this project.

1 Introduction

Apart from chapter 1.1.4 this chapter is similar to chapter 1 in Enstad (2009).

1.1 Motivation

The dust explosion phenomenon can be explained by an example from the daily life (Eckhoff, 2003). When lighting a bonfire, it is normal to whittle parts of the wood into smaller parts to make it easier to ignite. The subdivision also increases the combustion rate due to the increased specific surface area between the wood (fuel) and air (oxidizer). By dividing the wood into increasingly smaller parts, one eventually obtains dust particles with characteristic size typically below 100 μm. If a cloud, or mechanical suspension, of such wood dust is ignited, a flame can propagate rapidly through the cloud, creating a dust explosion.

Many materials can generate explosible dust clouds, including coal, sawdust, grain, flour, maize starch, sugar, plastics, aluminium, and titanium. Explosible dust clouds are more likely to occur inside process equipment, rather than outside. They can arise from activities such as pneumatic transport, milling, spray drying, etc., and can involve equipment such as bucket elevators, silos, grinding mills, and filters. Hence, dust explosions represent a hazard in a variety of industries.

1.1.1 Accidental dust explosions

Throughout the years, many people have lost their lives and/or been injured in accidental dust explosions. Material damages from dust explosions also result in considerable economic loss. Recent statistics from the U.S. Chemical Safety and Hazard Investigation Board (CSB, 2006) show that the dust explosion hazard is still a major problem in the powder handling industry Figure 1-1 suggest that the problem has worsened in the recent years, but this trend may be influenced by lack of reporting of minor incidents in the early years.

The following examples from Eckhoff (2003) and CSB (2006) illustrates that dust explosions can occur in many different types of industries:

- Wheat grain dust explosion in silo, Stavanger port silo, 1970
- Dust explosion in a silicon powder grinding plant at Bremanger, Norway 1972, five workers killed
- Fish meal factory, Norway 1975, one person killed
- Atomized aluminium powder production plant at Anglesey, UK 1983
- Methane/coal dust explosion in a coal storage silo at a cement works in San Bernardino County, California 1984
- Smoldering gas explosion in a silo plant in Stavanger, November 1985
- Polyethylene dust explosion, Kinston, North Carolina 2003, six workers killed
- Resin dust explosion, Corbin, Kentucky 2003, seven workers killed
- Sugar dust explosion at Imperial Sugar, Savannah, Georgia, February 7, 2008, 14 deaths and 38 injuries

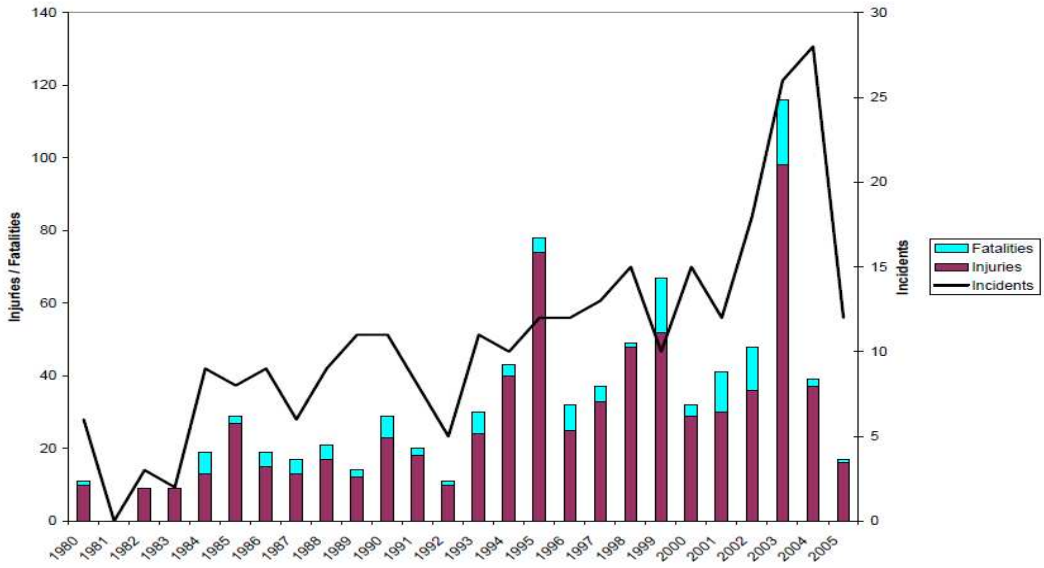

Figure 1-1 Dust incidents, injuries, and fatalities in the US from 1980 to 2005 (CSB, 2006)

1.1.2 Prevention and mitigation

The risk associated with an activity is determined by the probability and the consequence of events that inflict various types of loss: fatalities, injuries, material damage, downtime, loss of reputation, etc. There are two main categories of measures to reduce the risk posed by dust explosions (Eckhoff, 2003): prevention and mitigation. Prevention reduces the probability, and mitigation reduces the consequence. Table 1-1 provides an overview of the means for preventing and mitigating dust explosions in the process industries.

Table 1-1 Overview of means for preventing and mitigating dust explosions in the process industries (Eckhoff, 2003)

<table>
<tr><th colspan="2">Prevention</th><th rowspan="2">Mitigation</th></tr>
<tr><th>Preventing explosive dust clouds</th><th>Preventing ignition sources</th></tr>
<tr><td rowspan="2">Inerting by N_2, CO_2 and rare gases</td><td rowspan="2">Smouldering combustion in dust, dust flames</td><td>Reduce explosible cloud size</td></tr>
<tr><td>Partial inerting</td></tr>
<tr><td>Intrinsic inerting</td><td>Other types of open flames (e.g. hot work)</td><td>Isolation (sectioning)</td></tr>
<tr><td>Inerting by adding inert dust</td><td>Hot surfaces</td><td>Venting</td></tr>
<tr><td>Dust concentration outside explosible range</td><td>Electric spark and arcs, electrostatic discharges</td><td>Pressure resistant construction</td></tr>
<tr><td rowspan="2"></td><td rowspan="2">Heat from mechanical impact (metal sparks and hot spots)</td><td>Automatic suppression</td></tr>
<tr><td>Good housekeeping (dust removal/cleaning)</td></tr>
</table>

Preventive measures may in some situations be sufficient to reduce the dust explosions risk to acceptable levels. However, it is often necessary to apply mitigating measures, either passive, such as explosion venting or pressure resistant constructions, or active, such as automatic suppression and isolation systems. Sensors that detect the explosion in its incipient stages, either from the increase in pressure or the flame itself, trigger active mitigation systems. Reliable and robust methods for flame detection are therefore important to realise fast and effective suppression and isolation systems.

1.1.3 Flame detection – an overview

A flame can be detected by instruments that measures properties of the flame directly, or through phenomena that could result from flame propagation (e.g. increased pressure or smoke). Flame detection by measuring IR and/or UV radiation is the most used principle in instruments that are commercial available today, but other principles is also in use. Ray (1978) provides a useful review of the physical techniques that can be used to detect and give warning of fire. Figure 1-2 shows some of the different instruments available today.

Figur 1-2 Instruments for detecting flames or flame related properties: 1) combined IR and UV flame detector from Net-Safety Monitoring Inc., 2) IR smoke detector from Det-Tronics, 3) piezoelectric pressure sensor from Kistler, 4) and thermocouples from Jackson Oven Supply.

Flame detection is important both for industry and in research. In industry, it can be used to monitor combustion processes, or for activating suppression and isolation systems. In the context of research, quantitative information about flame propagation and flame-related properties is needed to investigate and understand combustion phenomena (e.g. through the validation of numerical models). Thus, the purpose of flame detectors differs in the two cases.

It is very important that instruments designed for industrial applications are reliable and can run for a long time with minimum maintenance. Instruments intended for dust explosion protection will usually operate under relatively harsh conditions inside process equipment such as bucket elevators, mills, filters, etc. Most flame sensors will never be activated by an explosion, but should a flame occur, the sensor should detect the flame fast enough for the active mitigation system to isolate or extinguish the flame.

Robustness and lifetime is usually less important in research, but it is desiarable that the sensor provides additional information about the flame, such as temperature and flame thickness. The flame sensor will not run for long periods, but rather in short intervals during the experiments, and some maintenance between tests can usually be afforded.

The following principles for flame detection/measurements have been identified in the context of active mitigating systems:

- pressure measurements in partially or fully closed systems (*e.g.* pressure transducers)
- measuring flame temperature (*e.g.* thermocouples and photosensors)

- measuring the dielectricity and/or resistivity in the flame (*e.g.* ionization gauges and impedance probes)
- measuring the speed of sound (e.g. acoustic transducers and receivers)

In the context of dust explosion research it is of interest to combine two or more of these principles to get additional information about the flame propagation, and to compare the results from the different principles. The use of pressure transducers and thermocouples are quite common in dust explosion experiments. Different versions of optical probes, usually photodiodes, are used to some extent. However the remaining principles are rarely used, and a combination of different principles within the same probe is even rarer.

1.1.4 The optical measurement principle applied to dust explosions

Optical measurements are applied in dust explosion research for monitoring dust concentrations, for detecting flames, and for measuring flame temperatures. The principle used for measuring dust concentrations is based on attenuation of light. As monochromatic radiation propagates through the atmosphere, its radiance is attenuated exponentially according to the law of Beer-Lambert-Bouguer (Levi, 1980). The attenuation is a combined effect of absorption and scattering, where the absorbed radiation is transformed into heat, and the scattered radiation is redistributed angularly. If one assumes that the attenuation is proportional to the concentration of the absorbing and scattering particles (Beer's law), one can estimate the concentration of a dust cloud by measuring the attenuation of light that passes through the cloud. This can be done by the use of a light emitting diode (LED) that emits light at a certain range of wavelengths, and register the light that reaches a photodiode (PD). This way, the measured signal at the PD will depend on the radiation from the LED, and the attenuation of the radiation as it travels from the LED to the PD.

1.2 Present Work

1.2.1 Experimental approach

The present work involves an experimental study of flame detection by various means in the 3.6-meter flame acceleration tube (FAT) illustrated in Figure 1-3. The experiments involve constant volume explosions with either propane-air mixtures or clouds of maize starch in air. In the basic experimental setup, an ignition source initiates the combustion process in one end of the tube, thermocouples measure flame propagation along the length of the tube, and piezoelectric pressure transducers measure pressure development inside the tube. The experimental approach is similar to that of Pu *et al.* (1988), but with a somewhat larger apparatus, and with an up to date data acquisition systems.

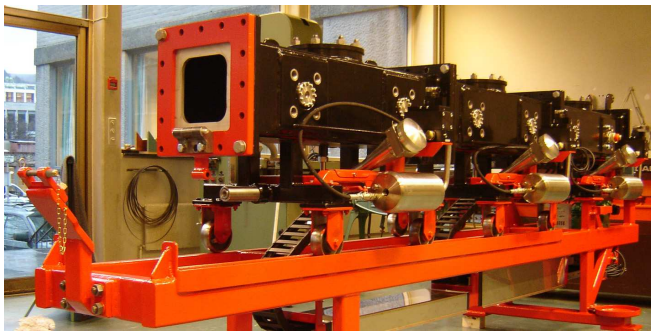

Figure1-3 The 3.6 meter flame acceleration tube used in the experiment; the internal cross-section of the tube is 0.27m × 0.27 m.

The experiments were performed in co-operation with fellow master student Gisle A. Enstad and PhD student Trygve Skjold. This thesis focuses on the optical flame detection/measurement principle, whereas Enstad describes the impedance principle. Instrumentation and small-scale laboratory work took place at the Dust Explosion Laboratory at the Department of Physics and Technology, University of Bergen. Prototyping of the flame sensors were done in a 20-litre explosion vessel of the USBM type (Skjold, 2003). Prior to testing of the measurement systems, the FAT was equipped with power supplies for instrumentation and automation, as well as a dust dispersion system, a gas-filling system, and an ignition system.

1.2.2 Aim

The aim of the present work is to identify reliable and robust means of detecting turbulent flames in dust-air suspensions and gaseous mixtures. Such measurements are important both for practical applications (*e.g.* suppression and isolation systems), and for fundamental experimental and computational studies of turbulent flame propagation (*e.g.* the determination of burning velocity and flame thickness of the turbulent flame brush). This thesis will focus on the optical flame detection/measurement principle, and in particular on the development of a probe that fits both industrial and research related demands.

2 Basic Concepts and Previous Work

Apart from chapter 2.2.2 this chapter is similar to chapter 2 in Enstad (2009).

2.1 Concepts and Definitions

2.1.1 Turbulence

Turbulence is a property of the flow, not the fluid. In the present context, turbulence influences the dispersion process, the residence time of the dust cloud, ignitability, and not the least the burning velocity. Eckhoff(2003) describes turbulence in the context of a dust cloud as "*a state of rapid internal, more or less random movement of small elements of the dust cloud relative to each other in three dimensions*". One may distinguish between two sources of turbulence in the case of a dust explosion. First, the initial turbulence is the turbulence which is at place where the dust cloud is formed, typically within process equipment. Second, the turbulence generated ahead of the flame front by expansion-induced turbulence, is depending on the flow and geometry of the system.

In the case of dust dispersion, turbulence is the most important property of the flow. In fact, turbulence is needed for the dust to be dispersed at all. A common way to disperse dust in experiments is to use pressurised air and disperse the dust through some kind of a nozzle or perforated tube/pipe, thus generating turbulence.

Turbulence determines the residence time of the dust cloud. The more turbulence, the longer it will take before the dust in the dust cloud settles out. Therefore, a simple way to study the influence of turbulence on the explosibilty of a dust cloud is to vary the delay between dispersion and ignition. The longer delay, the lower is the level of turbulence.

The ignitability of a dust cloud is highly influenced by the turbulence, because the turbulence cools the ignition zone by convective heat transfer. Hence, the ignition energy required to ignite a dust cloud increases with increasing level of turbulence. The ignition source itself creates turbulence and affect the combustion process. A chemical igniter, for instance, will create more turbulence than an electric spark.

In a burning dust cloud, turbulence will promote mixing of hot burned/burning dust with the unburned cloud. Hence, the flame front is not a well-defined planar surface, but rather a mixture of burned, burning, and unburned parts. As a result, the burning velocity of a turbulent dust cloud is much larger than that of a laminar dust cloud. In experiments, expansion-induced turbulence that affects the flame speed can be generated by inserting objects in the explosion vessel, thus changing the geometry, and the flame speed can be measured for different levels of turbulence (Pu *et. al*., 1988).

2.1.2 Combustion

Combustion involves exothermic chemical reactions between a fuel (usually a hydrocarbon) and an oxidant (usually air). In the context of chemical explosions, combustion is not always straightforward to define precisely because of various borderline cases, which complicate a precise definition. According to Arrhenius, the reaction rate will never equal zero, thus there will always be some rate of combustion whenever a fuel is mixed with an oxidiser. The question is then how to define combustion in a useful way. In this thesis, combustion is

defined as the rapid oxidation of a fuel, accompanied by heat release, light emission and ion generation in the reaction zone. This definition fits the different measurement methods, light emission and heat release suits optical and thermocouples while ion generation fits the impedance method.

2.1.3 Flames

A flame can be defined as the zone where the combustion processes takes place. Thus, combustion characteristics, such as heat release, ion density in the form of free radicals and emission of light, will define the flame.

Exothermic combustion often results in emission of visible light, although this is not always the case. For instance, hydrogen flames are not readily visible. Several processes are taking place in a flame, such as heat release, heat transport and mass transport. Decomposition of the reacting molecules at high temperatures produces free radicals, such as OH and CH among others. It is possible to measure these radicals, as they alter the physical behaviour of the medium. For example, both the electrical conductivity and the dielectric constant in a flame are different from the unreacted mixture. These effects are utilised for making flame sensors.

Radiation from a flame is due to heat production and emission of light. The light is a result of both black body radiation and spectral band emission, which gives the flame a specific colour. Spectral band emission is used to identify different species of molecules within the flame with laser spectroscopy. Black body emission however, requires a surface to emit light. In dust explosions the dust particles provide the surface. Fuel-rich hydrocarbon flames form small particles of carbon or soot. These particles radiate bright light. In premixed flames close to stoichiometric concentrations, the combustion is more complete, resulting in less carbon particles, thus less red/yellow colour of the flame. Such flames often have a blue colour, associated with the spectrum band of CH and C_2.

Pyrolysis of organic dust particles releases gas from the surface. The gases mix with the oxidiser, by diffusion and turbulence, and burn. At moderate turbulence levels, the mixing of fuel and oxidiser is the slowest process, and defines how fast the dust cloud burns. If the turbulence level is high, the slowest process is the surface reaction. The surface reaction depends on the temperature and the specific surface area of the particles. For metal particles, melting and evaporation replace pyrolysis.

Table 2-1 summarises the main categories of flames according to initial conditions and mode of fluid motion. In explosions, the fuel and oxidizer is always premixed. However, expansion-induced turbulence can determine the mixing state of fuel/oxidizer. In coalmine explosions for instance, a methane/air-explosion can whirl up layers of coal dust, which again is ignited by the primary explosion.

Table 2-1 Different types of flames

Fuel/Oxidizer mixing	Fluid Motion	Examples
Premixed	Turbulent	Gasoline engines
	laminar	Bunsen burner
Nonpremixed	Turbulent	Torch
	Laminar	Candle

In some cases the dispersion is due to dust falling through air, thus turbulence is not needed. The turbulence level of the flame is one of the key parameters to predict the violence of an explosion. Turbulence can in extreme cases lead to detonation, making the explosion much more devastating. This mechanism is almost as important as the reactivity of the fuel, making it a crucial point in venting area dimensioning.

Figure 2-1 illustrates the Borghi diagram for turbulent combustion (Borghi, 1984). This diagram shows the relation between turbulence parameters and the reaction rate of the mixture. If the turbulent velocity fluctuations are smaller than the laminar flame speed ($v` < S_L$), the flame will be wrinkled or laminar, depending on the length scale of the turbulence (the x-axis of the diagram). Length scale is associated with the size of the turbulent eddies. At the smallest length scale, Kolmogorov length scale l_K, the time for ½ revolutions equals the diffusion time across the diameter. The geometrical dimensions of the system define the largest length scale, the integral length scale l_0.

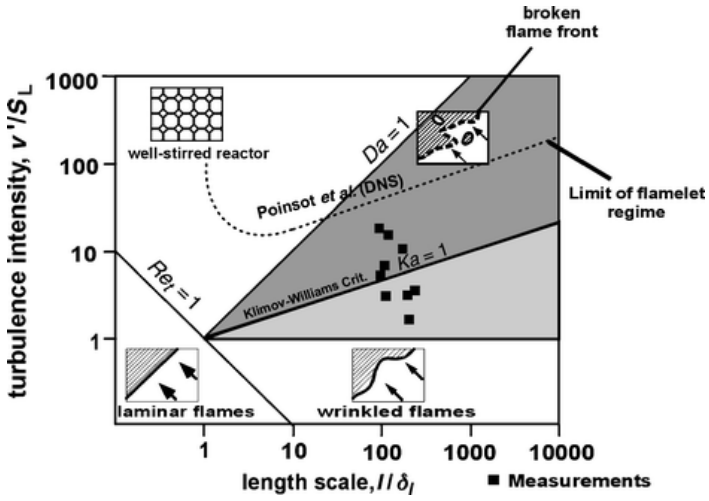

Figure 2-1 Borghi diagram. (from Borghi 1984)

If the flame thickness is smaller than the Kolmogorov length scale the flame is characterised as a laminar premixed flame, embedded in turbulence. This occurs under the line where *Ka = 1*, where the Karlovitz number *Ka* is given by (2.1).

$$Ka = \frac{\tau_L}{\tau_K} \qquad \textbf{(2.1)}$$

Where τ_L is the time scale of the laminar flame, $\tau_L = \delta_L / S_L$, and τ_K the Kolmogorov time scale, $\tau_K = (\nu/e)^{0.5}$. δ_L is the laminar flame thickness, S_L is the laminar burning velocity, ν is the kinematic viscosity and e is the dissipation rate. The Damkölher number *Da* relates the for chemical time scale to the turbulent time (2.2). If the fluid motion is faster than the reaction (Da > 1) it results in well stirred reaction. The flame can be very thick under these circumstances. If the number is smaller than 1 the flame will be torn apart, resulting in a large area of reaction. The Damköhler number is given by:

$$Da = \frac{l_0 \cdot S_L}{v` \cdot \delta_L} \qquad \textbf{(2.2)}$$

Where l_0 is the integral length scale, δ_l the laminar flame thickness, S_l the laminar burning velocity and v' the turbulent velocity fluctuation.

2.1.4 Explosions

The word 'explosion' is often used for rapid release of energy, resulting in the propagation a pressure wave through the surrounding medium. Explosions can have devastating consequences, and great efforts are made to both prevent them from happen and mitigate the consequences. In the present context, an explosion is defined as rapid combustion resulting in pressure build-up. Five fundamental criteria must be satisfied for a chemical explosion to occur:

I) Fuel – a flammable material

II) Oxidizer – usually oxygen from air

III) Explosible mixture of fuel and oxidiser

IV) Confinement – some degree of confinement is usually required for pressure build-up to occur.

V) Ignition source – electrical sparks are besides chemical igniters usually applied for experimental work. The ignition source can influence the progress of the explosion.

2.1.5 Some differences between gas and dust

Explosive gas mixtures and dust clouds exhibit similar ignition and combustion properties Eckhoff (2005):

- reasonably well-defined flammability and explosibility limits
- laminar burning velocities and quenching distances
- strong influence of turbulence on the burning velocity
- detonation made of flame propagation
- adiabatic constant-volume explosion pressure of similar magnitudes
- reasonably well-defined minimum ignition energies
- minimum ignition temperatures for given experimental conditions

However, there is a vast difference in the way explosive clouds/mixtures arise and behaves. Whereas explosible gas mixtures are most likely to arise from a leak, explosible dust clouds often exist within various types of process equipment such as filters and bucket elevators under normal operating conditions Furthermore, dust layers accumulated outside process equipment can generate secondary dust clouds and secondary dust explosions. Finally, a cloud of dust particles suspended in air will settle after a while, unlike a gas mixture.

Another important difference is that dust is flammable both as a dust cloud, with concentrations between the lower and upper flammability limits, and as a settled layer of dust. In combustible gas however, flame propagation is only possible with gas concentrations within the lower and upper flammability limits. It is therefore important to remove dust between tests when dealing with experiments. If not, dust from previous tests will take part in the combustion. This makes testing with dust time-consuming compared to testing with gas because of the time needed for cleaning.

2.2 Previous Work

2.2.1 Flame propagation in dust explosions

Limited attention has thus far been given to the investigation of the effect of obstacles on flame propagation in dust clouds. This is nevertheless a relevant topic for both explosion safety and the modelling of dust flames, since turbulence induced by the air/dust mixture passing such obstacles will result in flame acceleration.

The first large-scale experiments to investigate flame propagation in large length to diameter galleries were the ones described by Hall (1890). Similar work has been done later in response to the many disastrous explosions in coalmines. Many of these experiments were performed in large scale, with tubes 100 – 250 m long, and turbulence induced by wall friction. The flame velocities measured in these experiments vary from 50 to 800 m/s. Detonation can also be achieved, if the tube is long enough or the wall roughness increased.

Bartknecht (1971) investigated flame propagation in tubes with one end open. He used an external dispersion system, which generated a dust cloud along the whole tube length. This was achieved by injecting dust from externally pressurised reservoirs. By using this technique, he was able to avoid the use of a primary explosion to initiate the dust explosion. This resulted in well-defined conditions for the experiment, and more reproducible results. However, one may discuss whether these conditions are comparable to the ones in more realistic situations. Bartknecht also conducted experiments by placing the dust as a layer inside the tube, and let the air velocity in front of the explosion generate the dust cloud. The deflagration was initiated with a turbulent methane/air explosion at the closed end of the tube. This resulted in lower flame speeds and maximum pressures, and shows the importance of performing experiments as close to the realistic condition as possible. His work showed a close agreement between the K_{St} value and violence of the explosion in the tubes. The K_{St} values were measured in a 1 m^3 closed explosion vessel. The 1 m^3 vessel used by Bartknecht was the prototype of the International Standards Organization method to determine K_{St} values (ISO, 1985).

A lot of work has been done in explosion vessels without expansion-induced turbulence during combustion. By varying the delay between dispersion and spark ignition, and vary the strength of the dispersion, one can correlate the measured rate of pressure rise (dP/dt) and turbulence. Kauffman *et. al.* (1984) investigated the effect of turbulence on dust explosions in a 0.95 m^3 vessel. It was assumed isotropic turbulence, and a hot wire anemometer measured the level of turbulence in the absence of dust. The presence of dust complicates the turbulence measurements, but Kauffman et al. was unable to account for this. Tezok et al. (1985) extended the work of Kauffman et al. His results corresponded with what Kauffman found. Tezok also used an optical probe for measuring the flame thickness, which was found to be in the range of 0.15 to 0.7 m.

Pu et al. (1988) investigated the influence of obstacles on a propagating dust flame. Pu used two tubes, one 0.91 and one 1.86 m long. Both tubes were equipped with rings to induce turbulence. The small tube was equipped with two high-quality schlieren glasses for visualizing the process. The dispersion system consisted of a dust feeder on the top of the vertical tube. The dust fell down, forming an explosible dust cloud. Pictures from the schlieren system were used for analysing the flame. In the larger tube it was used one piezoelectric transducer, for pressure measurement, and eight ionization probes, to investigate the flame velocity. The dust was dispersed through two dispersion pipes located at one of the tube walls. Experiments were performed for both methane-air mixtures and clouds of maize starch in air. It was found that flame propagation in lean methane-air mixtures had similarities

with flame propagation in the dust clouds. This result may suggest that there are similar processes in the gaseous phase, which is not further discussed in her article.

Klein (2005a, 2005b) experimented with dust explosions in a closed vessel system at TNO. The apparatus consisted of two 1 m^3 vessels connected with pipes of various lengths, with or without obstacles and a 90° bend. The dust was ignited in one of the 1 m^3 vessels. It was also conducted tests with different types of dusts, such as coal, silicon and potato starch, and with various configurations of ignition position and venting. The introduction of either obstacles or a 90° bend in the connecting pipe resulted in enhanced pressure piling for all the dusts, because of delayed jet ignition in the secondary vessel.

Holbrow (2004, 2005a, 2005b) performed tests on a larger system, consisting of two cylindrically vented vessels (20 m^3 and 2 m^3) connected by a pipe with a sharp bend of 90°. The pipe was of diameter 0.5 or 0.25 m. The dust was dispersed from four 2.3 l pressurized reservoirs, one at the 2 m^3 vessel, and three at the 20 m^3 vessel. The ignition source was located in the larger vessel and consisted of electric fuse heads and 25 g of black powder (50 kJ). Six pressure transducers located in both vessels and pipe, and 8 thermocouples located in the centreline of the pipe measured the flame speed, as it propagated through the system. Holbrow found that the explosion more readily transmitted through the larger pipe (0.50 m) than the smaller one (0.25 m). The experiment produced results of poor repeatability. One of 25 tests produced significantly high pressure in the smaller secondary vessel (3 bar).

2.2.2 Previous work on the optical measurement principle

Many researchers have explored the optical measurements principle in order to measure flame arrival and concentrations in dust clouds. Some examples of such work are presented here.

Conti *et. al*. (1982) made an optical probe for monitoring dust explosions, based on the principle of light attenuation. An optical filter prevents the photodiode from reaching saturation when the flame passes by. This makes it possible to extend the measurements into the combustion zone. The probe was also fitted with air flushing of the windows in front of the diodes, to prevent dust from settling on the windows and disturb the measurements. Figure 2-2 shows the design of the probe.

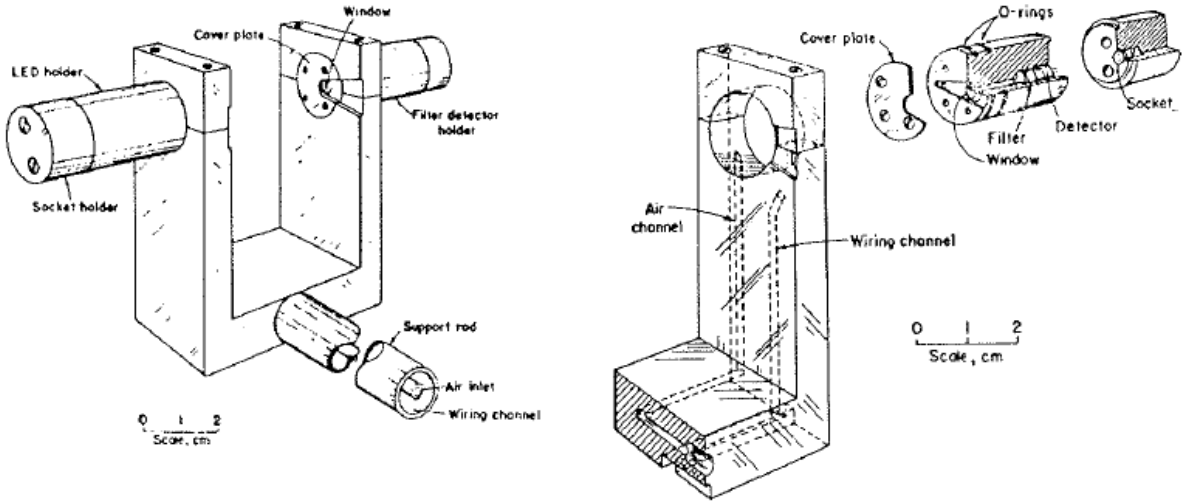

Figure 2-2 The optical probe described by Conti *et. al.* (1982)

Eckhoff *et. al.* (1985) performed vented maize starch explosions in a 236 m^3 silo. They used up to six optical probes for measuring the dust concentration in the silo and the flame arrival

times. The probes were somewhat simplified compared to the design of Conti *et. al.* (1982), yet they were able to successfully measure the dust concentration throughout the silo. However, even though the probes were thermally insulated by asbestos that in turn was covered by aluminium foil, many of the probes broke down due to the harsh environment in this large experimental setup. This underlined the need for a plug-in system where one can change damaged components within the probe.

Li *et. al.* (1995) performed experiments in a horizontal pipe in order to study deflagration to detonation transition supported by dust layers. The tube was 70 m long and 0.3 m in diameter, with one end closed, and the other end open to the atmosphere. A layer of dust was placed throughout the tube and a hydrogen explosion was initiated in the closed. The effect of moisture content, dust layer geometry, and dust concentration was investigated. In order to get an impression of the dust concentration as the dust was lifted by the initial shock, it was attempted to use optical probes. However, the optical probes did not detect any change in dust concentration after passage of the initial shock, and it changed only after the passage of the flame front. The most probable reason for this is that the concentration probes was placed in the centreline of the tube, and that the flame passed the probe while the entrained dust was below the probes. This emphasises the need to consider the positioning of the probes in advance, and especially if it is of interest or possible to use several probes over a cross section in order to get an impression of the concentration distribution.

Chen & Fan (2005) studied flame propagation through an aluminium particle cloud. They carried out experiments in a horizontal tube with an inner diameter of 0.14 m and length 12 m, and did measurements with piezoelectric pressure transducers and photodiodes. Figure 2-3 shows measurements done by the photodiodes. In addition, they used a hot wire anemometer to measure the level of turbulence generated by the pneumatic dispersion system without dust, and found that the turbulence decayed exponentially. Due to the low residence time of the aluminium-air suspensions, they triggered each of the 20 dispersion systems alongside the tube in turn. This way they were able to keep the aluminium particles in suspension until the arrival of the flame front.

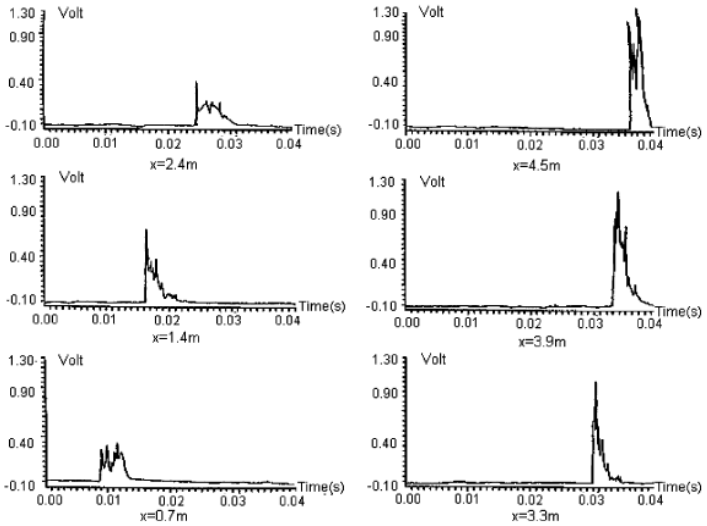

Figure 2-3 Typical signal of photodiode corresponding flame front in aluminium-air mixture, Chen & Fan (2005)

The principle of light extinction is also used to determine different particle characteristics. Cai *et. al.* (2005) performed in-line measurement of pneumatically conveyed particles by a light transmission fluctuation (LTF) method. They used a laser diode as the light source, and an optical fiber and a photodetector to measure the transmitted light. By measuring the fluctuation in the transmitted light, they were able to extract information about both the particle size and the particle concentration. The probes proved to be robust and reliable in operation. Their longest *in situ* test for pulverized coal monitoring went for over two years. They concluded that due to its low cost, good flexibility and high reliability, the LTF instrument was well suited for real-time, continous monitoring in hostile environments.

3 Experiments

This chapter describes the experimental equipment and experimental procedure. Apart from chapters 3.1.2 and 3.3.6 this chapter is similar to chapter 4 in Enstad (2009).

3.1 Preliminary Tests in the 20-litre Vessel at the UiB

The different measurement systems have been tested in the 20-litre USBM vessel at the Dust Explosion Laboratory, UiB (Skjold, 2003). Figure 3-1 shows a simplified schematic of the test facility, and Figure 3-2 shows a picture of the 20-litre vessel. A more detailed description of the test facility is given by Skjold(2003). The powder used in these tests is maize starch, usually at a nominal concentration of 500 g/m^3, which correspond to 10 g in the 20-litre vessel. The main purpose was to verify the functionality of the different measurement probes and the associated electronics.

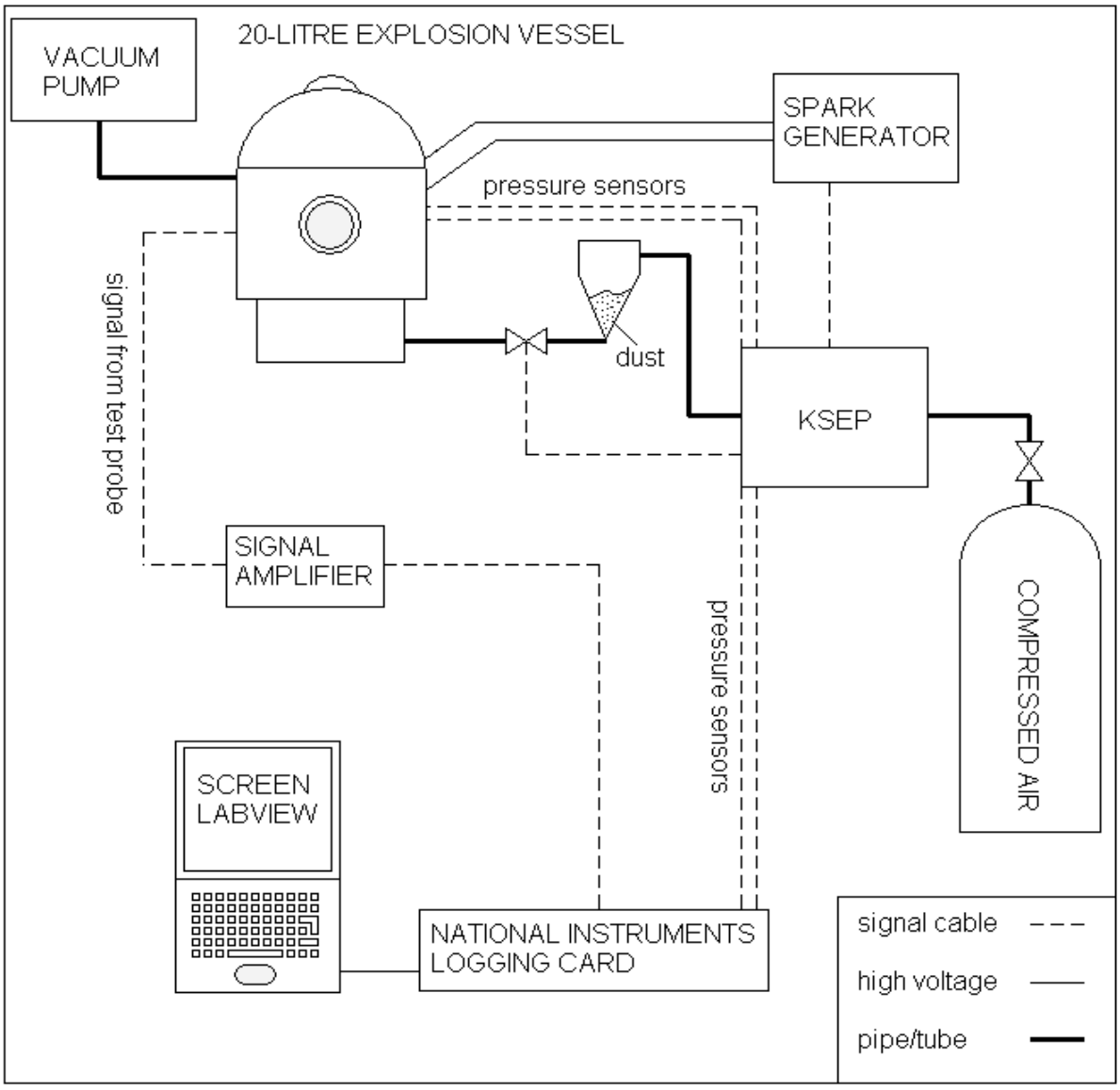

Figure 3-1 Simplified schematic for the 20-litre test facility at UiB

3.1.1 Experimental procedure

The spark gap is checked before the lid is closed. The vacuum pump lowers the pressure inside the vessel to 0.4 bar(a). A digital pressure indicator monitors the pressure inside the vessel. A desired amount of dust is then placed in the dust reservoir before a lid seals the reservoir. The reservoir is pressurised to 20 bar(g) with air from a 50 litre compressed air bottle. A digital pressure indicator monitors the pressure inside the reservoir. The spark generator is turned on and a flashing blue light indicates that the spark ignition is ready to be triggered. The Measurement and Control Unit, KSEP, runs the dust dispersion, triggering of the ignition source, and pressure measurements. A computer in the dust laboratory runs the KSEP software, that initiates and controls the sequence of events. The dust is dispersed through a dispersion nozzle and is ignited by an electrical arc discharge, or alternatively a chemical igniter. Two piezoelectric pressure sensors from Kistler measure the pressure development inside the vessel. Two separate charge amplifiers in the KSEP amplify the signal from the pressure sensors, and the resulting signals is registered by the logging card from National Instruments (NI USB-6259), transferred to a laptop, and processed by Labview. The signal from the test probe is processed in the same way i.e. with a signal amplifier, the NI-card, and a laptop. After the test, the spark generator is manually turned off and the remaining dust inside the vessel is removed with a brush and vacuum cleaner.

Figure 3-2 20-litre explosion vessel situated at the dust-explosion laboratory at the UiB. The two blue displays in the upper right corner are the digital pressure indicators for controlling the pressure in the vessel and dust reservoir pressure.

3.1.2 Optical probe for preliminary tests

The final probe design was too large to be tested in the 20-l vessel, and a smaller preliminary probe was made at the mechanical workshop at UiB. The design of the probe (Figure 3-3) used in the preliminary tests is similar to that of Conti *et.al.* (1982), but without flushing and optical filter. The principle of operation is described in chapter 3.3.6 and the electronics in Appendix A.6.2 and A.6.3. The probe has a path length of approximately 4 cm between the windows of the LED and PD, and the design of the power supply and signal amplification is similar to that of the final design. Since this was a simplified, preliminary probe that was not intended to last very long, the wires to and from the diodes was covered only by isolating tape. Thus after a few tests they would burn up and had to be changed. Since the diodes were glued to the diode holders, they could not be replaced in case they were damaged. By the use of setscrews, the diode holders were held in place so the holders as a whole could be replaced. Nevertheless, the diodes worked fine during the preliminary tests, and replacement of the diodes was not needed. Prior to experiments, the power supply to the LED was turned on, and it was confirmed that the PD registered the signal sent out by the LED. Since dust settled on the windows, due to the lack of a flushing system, the windows in front of the diodes were cleaned between each experiment. The wires connected to the diodes were checked after each test.

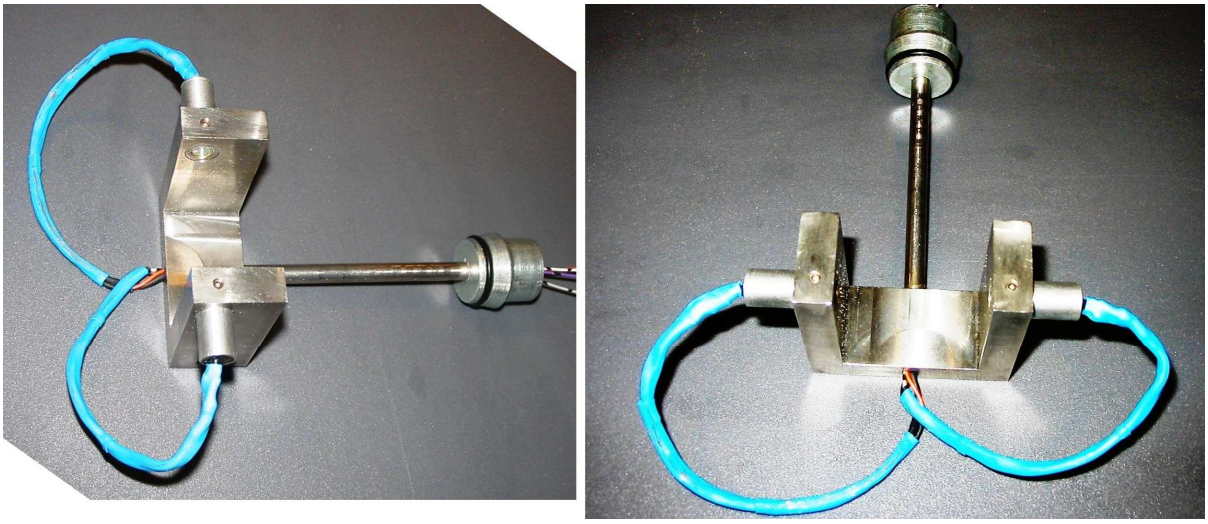

Figure 3-3 Preliminary optical probe

3.2 Preliminary Dispersion Experiments

The dispersion system is a crucial part of the experimental setup, and has been tested separately to document its ability to create well-dispersed dust clouds. The tests were performed in a section replica which was mounted with a plexiglas in front (Figure 3-4). A high speed camera was used to investigate the effectiveness of the nozzle to evenly distribute the dust and the shape of the dust cloud, with and without confinement. The time delay between the dispersion signal, to the first dust seen coming out of the nozzle gives a time delay of the pneumatic operated valve. The pressure in the reservoir is not recorded in this investigation. It was later recorded in FAT experiments, and it is of interest to compare the pressure-time curves with and without dust in the cyclone. Figure 3-4 shows the experimental setup and the view from the camera. For timing purposes, a LED-light was used (referred to as signal lamp on the schematics), indicating when the dispersion signal is sent. This signal is

sent from a NI-CAD card. To measure the pressure in the reservoir, before the test is performed, a manometer is used. The camera can record at a rate of 1200 fps, but this will compromise the quality of the frames. The rate used in this experiment is therefore 300 fps, giving it a time resolution of 0.0033 seconds per frame. Analysis of the videos is manually done, and is therefore subjective.

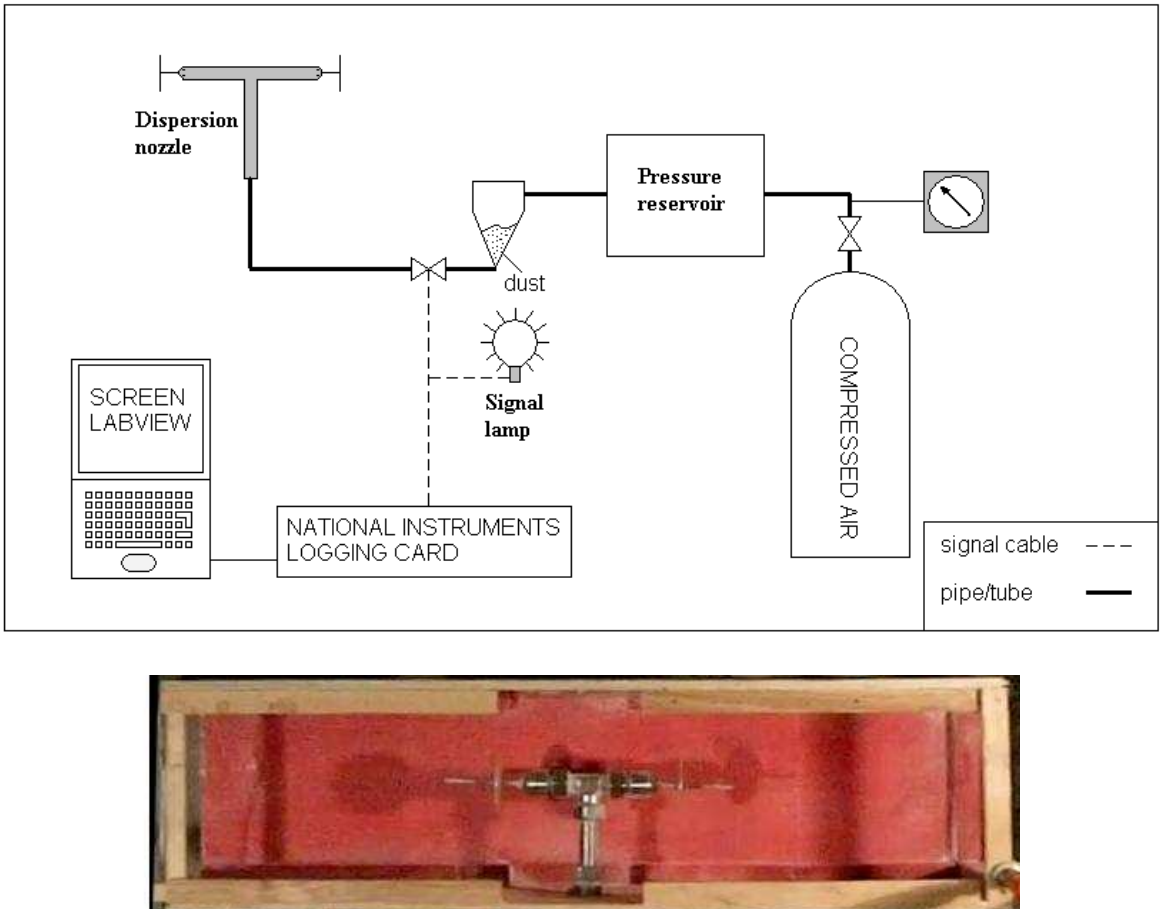

Figure 3-4 Upper: Schematics of the experimental setup Lower: the dispersion nozzle in the test rig

3.3 Experiments in the Flame Acceleration Tube (FAT)

The Experiments conducted with the complete FAT setup are closed vessel experiments. Both gas (propane) and dust (maize starch) are tested, and the results are compared. Experiments of gas mixtures were performed for 3% (often referred to as lean mixture), 4.5% (often referred to as stoichimetric mixture) and 6% (often referred to as rich mixture). The dust used in the experiments was maize starch, of nominal concentration 500 g/m^3 or 250 g/m^3. The concentration of different tests is given in appendix B.1.

3.3.1 The FAT

Figure 3-5 shows the FAT. The tube consists of three 1.2 m sections with internal cross section 0.27 x 0.27 m. one section is fixed and two of them are running on rails. This allows

easy access to the interior of the pipe, for cleaning and modifications. It is possible to place different types and numbers of obstructions inside the tube, to generate different levels of turbulence. One sidewall and the top of the tube are fitted with circular plexiglasses, in order to make the explosion visible from the outside. A high speed camera films the experiment.

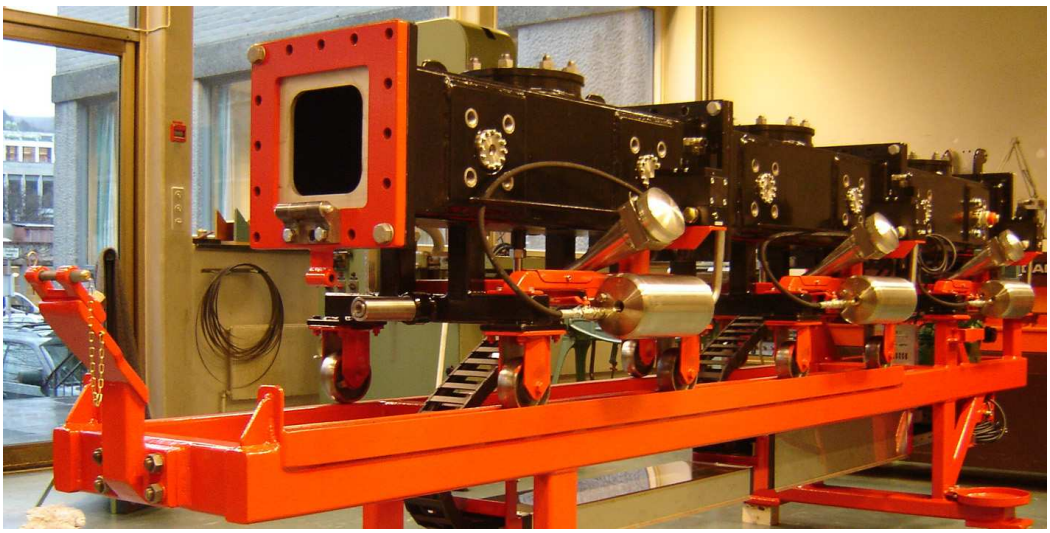

Figur 3-5 The Flame Acceleration Tube

3.3.2 Systems for dust dispersion and gas filling

When testing with gas a separate gas filling system is applied to the FAT. It consists of a flask with gas *e.g.* propane, six tube entries alongside the FAT with belonging valves, and valves to shut off gas from the flask and to bleed the tube system to get rid of air and gas in prior to filling. The vacuum pump evacuates down the pressure inside the vessel prior to gas filling. The concentration of gas is estimated based on pressure rise inside the FAT when filling gas. If a concentration of 4-volpercentage of gas in air is desired at atmospheric pressure, a pressure rise of 0.04 atm is needed. In order to optimize the concentration distribution in the FAT, the gas is in equal amounts let in at the six entries in turn. Pressurised air from the dust dispersion system mixes the gas prior to ignition. Figure 3-7 shows the system schematically.

If dust is to be tested, the dust is filled into the dust reservoirs (1A, 2A and 3A on schematics (Figure 3-7). The dust is dispersed by activating a pneumatic valve, actuated by the control system. This releases the pressurised air from the air reservoirs and disperses the dust. For more detailed information, see chapter 3.2. Note that the dispersion air is injected for both gas and dust experiments, in order to maintain the same initial conditions.

3.3.3 Control and data acquisition systems

A NI-CAD 6259 card, connected to a computer, performs both controlling and logging of the experiment. The card controls the timing of dispersion and ignition. This NI-CAD card is programmed by LabView software, which is documented in appendix A.7.2. The software enables the user to change all setup parameters, within the limitations of the card.

Control system

A tailor made power supply with opto-couplers and semiconductor relays was made to control the experiments. See switching circuits in Appendix A.5. A NI CAD (6259) sends signals to this power supply switching on and off the opto-couplers and semi conductor relays, controlling the valves and triggers the ignition. In order to be able to pre-program the output and maximize the accuracy of timing, the analogue output of the NI-CAD card is used. Digital

ports are used for: remote triggering of the experiment, to reset and activate the pressure measurement system and for turning on the LED indicator. A high speed camera records the explosion, and the LED indicates when the dispersion occurs.

A simple spark generator was built for igniting the gas explosion tests (Appendix A.2). The NI-CAD card is used to trigger the spark directly through an opto-coupler. However, reliable ignition of turbulent dust clouds requires a stronger ignition source, and for this purpose a 1 kJ chemical igniter was used. This chemical igniter need 24 volt to ignite. This is achived by one of the semiconductor-relay in the switching circuit, shown in Appendix A.

Sources of error, timing

The NI-CAD card is able to time trigging within 50 ns. Three separate semiconductor-relays operate the dispersion valves. The relays switch from off to on within 0.1 ms and use 0.75 ms from on to off. The valves use at most 20 ms to open, see section 4.2. Time delay for the spark-generator has not been measured, but the optocoupler trigging this system uses 5 us to switch on. The spark generator utilise a coil to generate high voltage. This coil will delay the spark, but it is probably negligible compared to the other sources of timing error. Time delay of activating the chemical igniters, was not determined.

Data acquisition system*

The experience from the work performed in this thesis shows that amplification of measured signal is important. One A/D converter reads all the channels. Switches inside the card choose which channel to read. If one channel is not satisfactory amplified, the signal from one channel would influence the signal read next. The reason may be stray capacitance, see documentation of the NI-CAD 6259, of 100 pF inside the NI-CAD card.

Sources of error, timing, A/D converters and measurements

The NI CAD card can record 1MS/s when multiple channels are in use, or 62.5 kS/s per channel. The resolution of the readings is 16 bits, which makes it possible to differentiate between 65536 levels. The maximum input voltage is +/- 10 V. The accuracy of the voltage reading in the NI-CAD card is relative to the maximum and minimum voltage set for the specific task, and varies from 0.019% (+/- 10 V) to 0.023% (+/- 2 V) (obtained from www.ni.com). Background noise and natural drifting of the electrical equipment represent additional source of error.

The light sensitivity of the high speed camera drops with increasing frame rates. This becomes a problem for lean gaseous flames, since less bright. At 600 fps the lean propane air flames were barely visible on the video. Richer mixtures give a flame easily seen, as the flame shines bright yellow. Since these results are manually processed, the results are subjective to some extend. Especially in cases of dust flames, because of illumination of the dust ahead of the flame. The frame rate also introduces inherent limits to the time resolution of the video measurements.

The pressure measurement consists of a pressure transducer and a charge amplifier. The amplifiers precision, according to documentation, is 1 % of charge amplified. This means that constant test conditions will give results varying with 1 %. The accuracy depends upon the setup of the amplifier, and the sensors. The sensors are also temperature dependent. To protect and insulate the sensors, red silicone covers the exposed end of the sensor. However some thermal drift is expected for prolonged measurements

3.3.4 Flame probes

In order to measure flame arrival times in the same position, probes with both capacitive plates and optical diodes has been designed. The probes are distributed through out the length of the pipe 0.6 m apart (Figure 3-6). The probes are designed to carry two optical pair of one sender and one receiver. In addition it is possible to fit in two acoustic sensor pairs. The probe is shown in Figure 3-6, and more comprehensive drawings are included in Appendix A.6.1.

Figure 3-6 Probe used in the FAT experiment.

Special probes with exposed junction thermocouples were designed to monitor flame arrival and to some extent flame temperature. The electronics, as well as a welding apparatus built for this application, are shown in Appendix A.3 and A.4. Thermocouples is a bit slower than the other measurements, since the temperature of the burning gas will have to heat the laminar boundary layer around the string, and the string it self. This physical restriction not only slow the response time regarding flame arrival, but also limits the information possible to retrieve from the combustion process.

3.3.5 Experimental procedures

Experimental procedure for the FAT – Gas

With reference to the schematic in Figure 3-7, the experimental procedure for the gas explosion tests in the FAT was as follows

1) start vacuum pump and open valves (16, 17 and 18) between the pump, FAT and pressure gauge P_1
2) evacuate the FAT to the desired pressure typically –0.33 bar(g) + desired partial pressure of gas monitored by the digital pressure indicator(P_1)
3) close valve 17 to pump and turn off vacuum pump
4) open valves 24, 25, 20 and 19 and fill pressurised air of 16 bar(g) from the flask into the reservoirs via the reservoir valves(11, 12 and 13) by the help of the digital pressure indicator(P2)
5) open valves 10, 9 and 1 to flush gas through the line to displace air in the system. Add 1/6 of total amount of gas, measured by partial pressure into the FAT via the valves 2, 3, 4, 5, 6 and 7. Use reduction valve (8) to control the flow accurately. The pressure inside the FAT should reach -0.33 bar(g)
6) close valve (8) to the fuel gas
7) adjust vacuum and reservoir pressure to -0.32 bar(g) and 16 bar(g), respectively, via valves (vacuum: 14 and 15, reservoirs: 21 and 22)
8) close needle valve (24) on flask of pressurised air and valve (20) between flask and FAT
9) check that the safety valve(16) is closed
10) activate the labview program and specify filename in labview
11) reset charge amplifiers for pressure measurements in reservoirs
12) close the reservoir valves (11, 12 and 13)
13) turn on the spark generator
14) secure the area
15) check that the test number is correct
16) turn on camera
17) push the trigger button
18) open exhaust valve
19) open FAT and connect ventilation system

Experimental procedure for the FAT - Dust

With reference to the schematic in Figure 3-7, the experimental procedure for the dust explosion tests in the FAT was as follows

1) open the door in the end of ignition and install a chemical igniter to the holder for spark gap / chemical igniter located inside tube at the point marked ignition
2) start vacuum pump and open valves (16, 17 and 18) between the pump, FAT and pressure gauge P_1
3) evacuate the FAT to the desired pressure typically –0.33 bar(g)
4) close valve 17 to pump and turn off vacuum pump
5) open valves 24, 25, 20 and 19 and fill pressurised air of 16 bar(g) from the flask into the reservoirs via the reservoir valves(11, 12 and 13) by the help of the digital pressure indicator(P_2)
6) fill desired amount of dust into dust reservoirs, 1A, 2A and 3A
7) adjust vacuum and reservoir pressure to -0.32 bar(g) and 16 bar(g), respectively, via valves (vacuum: 14 and 15, reservoirs: 21 and 22)
8) close needle valve (24) on flask of pressurised air and valve (20) between flask and FAT
9) check that the safety valve(16) is closed
10) activate the labview program and specify filename in labview
11) reset charge amplifiers for pressure measurements in reservoirs
12) close the reservoir valves (11, 12 and 13)
13) secure the area
14) check that the test number is correct
15) turn on camera
16) push the trigger button
17) open exhaust valve
18) open FAT and clean out remains from the experiment

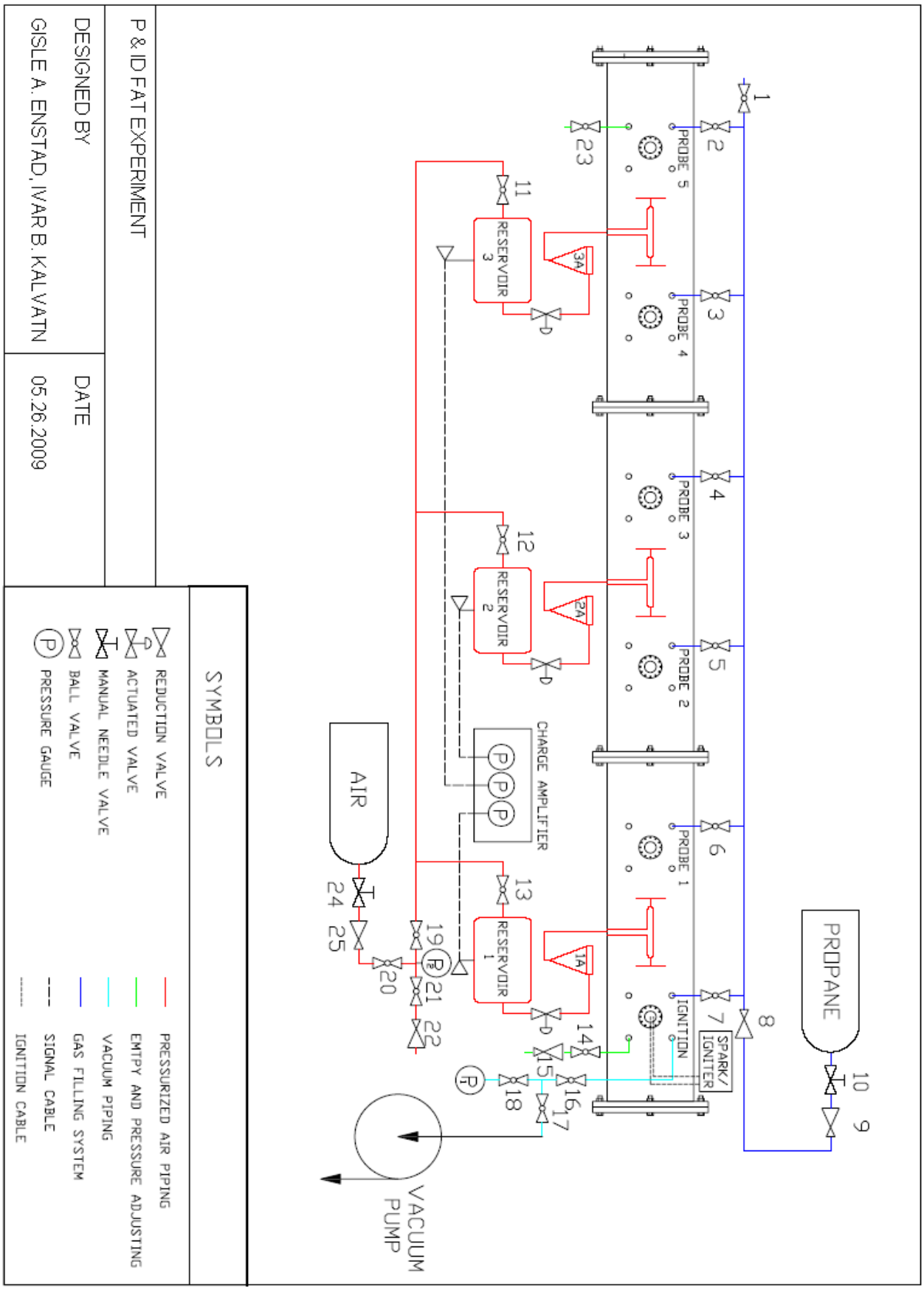

Figure 3-7 Schematics of experimental setup for the FAT

3.3.6 Optical probe

An optical probe is built into the flame probes described in 3.3.4. The probe uses a LED (IR2234 from Elfa) that emits radiation with a peak wavelength of 940 nm (infrared radiation) and a PD (OP 905 from Elfa) with a peak wavelength of 880 nm. An astable multivibrator powers the LED, and an electrical circuit with an operational amplifier processes the signal from the PD. Figure 3-8 shows a simplified schematic of the electronics for the optical probe. For more details, see Appendix A.6.2 and A.6.3.

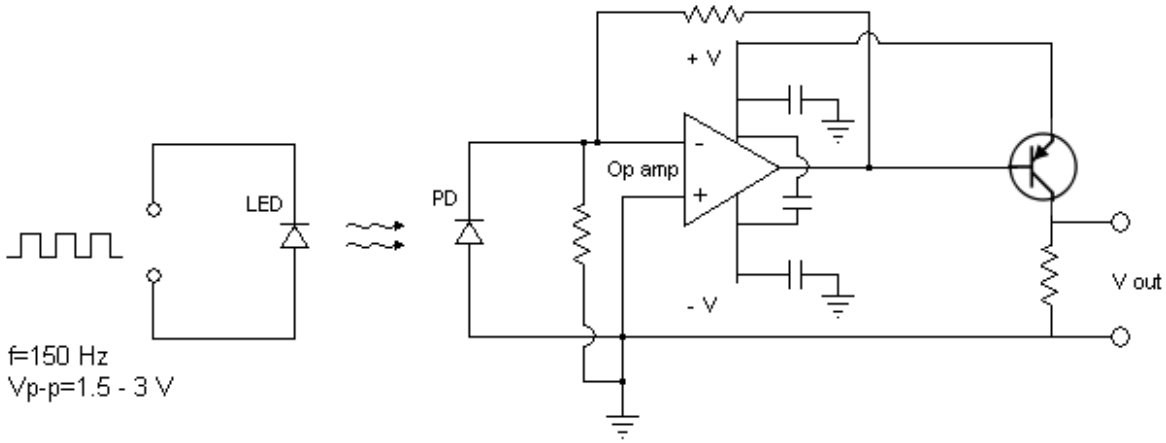

Figure 3-8 Simplified schematic of electrical circuit for the optical probe

The PD registers the square wave signal sent out by the LED, and when a dust cloud is present, the amplitude of the signal will decrease due to absorption and scattering. When the flame arrives, the PD will reach saturation, and thus detect the flame. The flame speed can then be estimated from the measured flame arrival times.

The infrared part of the spectrum is used to limit interference from visible light. Figure 3-9 shows the relative response vs. wavelength for the PD, the spectral distribution for the LED, and transmission vs. wavelength for the diode windows.

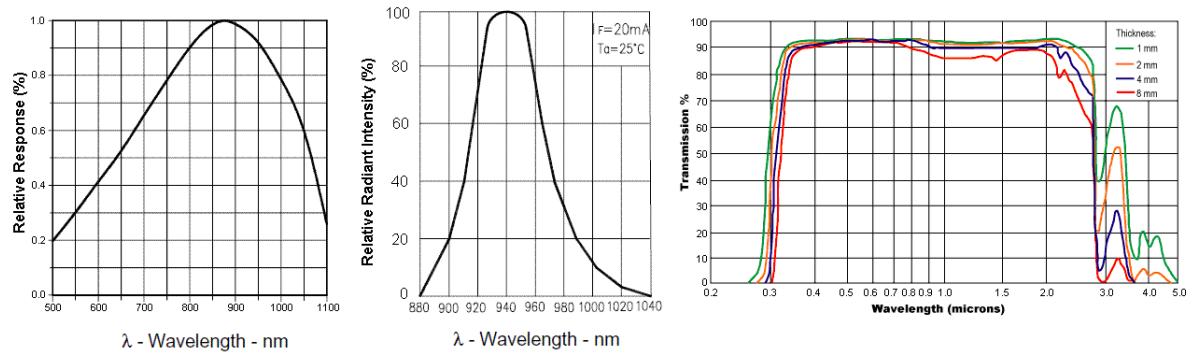

Figur 3-9 Relative response vs. wavelength for PD (left), spectral distribution for infrared diode (middle) and transmission vs. wavelength for diode windows (right).

As the figure shows, the PD will register a wide band of wavelengths, at least 500-1100 nm, while the band of wavelengths sent out by the LED is more narrow (900-1000 nm). The relative response of the PD at the peak wavelength of the LED is just above 90 %. At the peak wavelength, the PD will register radiation that corresponds to a temperature at about 3300 K, according to Wien's displacement law. Taking the energy distribution of a black body into account, as well as the relative response vs. wavelength curve, the PD will register a wide band of radiation. In other words, the PD will register radiation from the combustion because of the heat generated, thus reach saturation during the explosion because of the intensity of this radiation. Saturation of the PD during combustion can to some extent be avoided by applying an optical filter in front of the PD. However, no filter has been applied. Nevertheless, the windows in front of the diodes will offer some filtration. The window transmits radiation with wavelengths in the range 300 – 3000 nm (Figure 3-9).

In order to compare the different principles for flame detection it was decided to build a probe that would consist of the optical dust measurement, and the impedance measurement principle described in Enstad (2009). The design consists of a ring where the PD and LED are placed on opposite sides, pointing towards each other. In addition, acoustic transducers can be fitted to the probe in a similar manner. An advantage with the probe is that it allows one to replace damaged measure-heads, viewed in Figure 3-10, with new ones, without having to replace the whole probe. The LED and PDs within the measurement heads can easily be replaced as they are mounted directly into the measure heads. The probe is also fitted with an air flushing system, similar to that described by Eckhoff (1985), to keep the windows in front of the diodes clean. However, during initial testing with propane/air-mixtures it was found that the air-tubes to the measure-heads could not withstand the heat and pressure, and it was decided to disconnect the flushing system since it would not have worked without major rebuilding of the probe. More details on the flushing system and suggested improvements are found in Appendix A.6.4. Figure 3-10 shows the probe used for optical and impedance measurements. The motivation for the design is that the same ring will be used for measurements in a planned tube experiment. However, due to delivery problems, calibration in the glass tube has not been possible and this will be done in the future. Aluminium extension rings at both ends of the probe improves the aerodynamics of the probe, thus reduces the amount of expansion-induced turbulence caused by the probe. However, since this probe is highly intrusive when used in the FAT, it will contribute to a significant amount of expansion-induced turbulence. Therefore, the shape of the probe is not ideal for general use in the FAT, but in the glass tube it will fit perfectly.

Figure 3-10 Optical/impedance probe for monitoring gas and dust explosions(left) and measure-heads (right).

The inner diameter of the probe is 960 mm, and the distance from the outer surface of the diode windows to the diodes is 3 mm, which means that the pathway for the radiation from the LED to the PD is 966 mm. The signal generator for the LED and amplifier for the PD has been tuned to this distance based upon simple experiments at the dust explosion laboratory at UiB. Basically these tests involved sieving dust over the probe with different values of amplification and strength of the power fed into the LED. The tuning was therefore highly qualitative.

Potential error sources

In the context of flame detection, there are many uncertainties concerning the precision of the optical flame arrival measurements. First, the view angle of the PD is ±18° so the PD will detect the flame before it reaches the plane in the centre of the probe. However, when calculating flame speeds based on flame detection by the same type of probes, this effect will to some extent cancel out as long as all the PDs have the same view angle. Another effect that can disturb the measurements is reflected radiation within the FAT. Reflected radiation can reach the PD before the flame arrives, thus cause premature flame detection.

Since it is of interest to capture the flame with a high-speed video camera, the windows at the side of the FAT could not be covered. This means that light can reach the probes through the windows, thus disturb the measurements. To minimize these effects the PDs points away from the windows. It is furthermore important that the light conditions at the experiment site are the same for every experiment.

The response time of the PD is about 5 ns for both rise and fall times, defined from 10% to 90% of the total step height. The operational amplifier got a slew rate of 130 V/μs. This means that the amplifier requires approximately 40 ns for a voltage to change 5V. However, the interpretation of measurement data cannot be done to an accuracy better than about 1 ms, and this will therefore be the dimensioning limit for the accuracy of the flame detection measurements.

4 Results and Discussion

Chapter 4.2 is similar to chapter 5.2 in Enstad (2009).

4.1 Results from Preliminary Tests in the 20-litre Vessel at UiB

Only the results from measurements with the optical probe are presented here. Appendix B.2 presents the results from pressure sensors and thermocouples. The LED is powered by a square wave signal, as explained in Appendix A.6.2. Figure 4-1 shows the measurement results from a test in the 20-litre vessel with a simplified optical probe. As Figure 4-1 shows, the signal during dispersion is highly irregular with varying amplitude. This is probably due to the lack of a flushing system for cleaning the windows, and dust settling on the window. In addition, turbulence will affect the local dust concentration in the vessel. Compared to the FAT, the maximum level of turbulence in the 20-litre is higher, because of the smaller volume, and higher initial pressure difference between the dust reservoir and the vessel prior to dispersion. The ignition delay in the 20-litre is 60 ms, which is significantly shorter than in the FAT (700 ms) and this means that the dust cloud is given very little time to settle, thus the turbulence is relatively high at the time of ignition. This means that the dust concentration distribution will vary over time and will make the dust concentration measurements in the 20-litre more difficult.

Upon flame arrival, the PD will reach saturation due to the radiation from the flame and the lack of an optical filter to block this radiation. After saturation, the PD registers a square wave signal that slowly decreases. After a while, the amplitude of the signal from the photodiode stabilises on a level significantly lower than before combustion took place. This is because burnt dust settled on the windows in front of the diodes during the process, due to the absence of a flushing system, hence weakened the radiation registered by the PD.

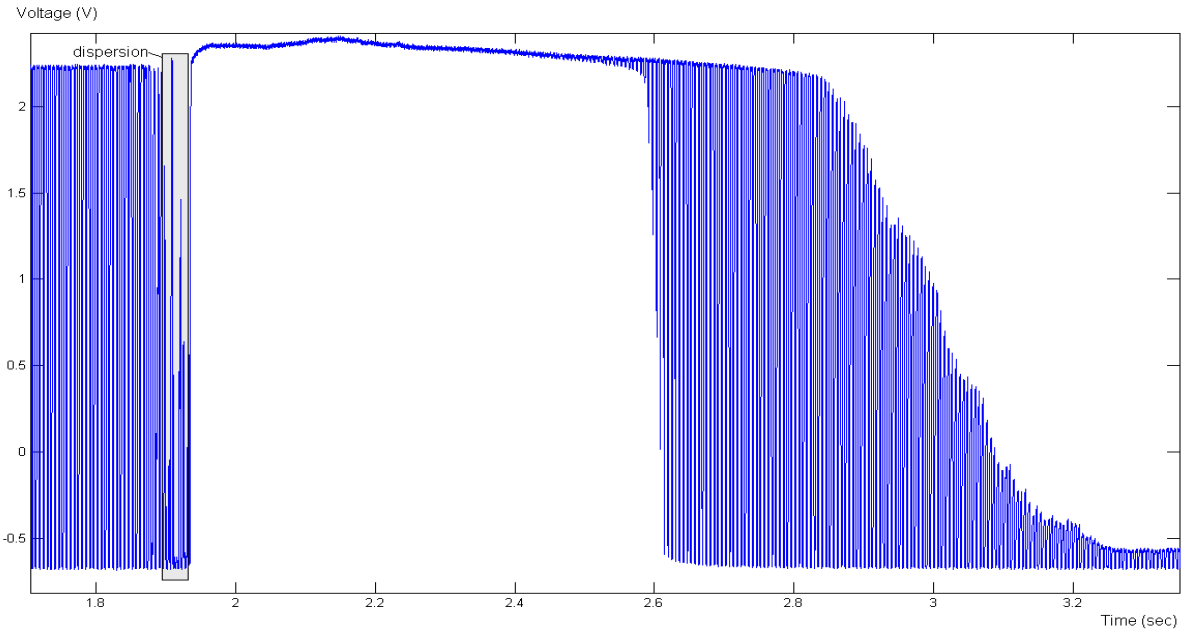

Figur 4-1 Result from test in the 20-litre vessel with the optical test probe

4.2 Results from Preliminary Dispersion Experiments in the FAT

This section presents the results from preliminary dispersion experiments in the FAT. Table 4-1 shows test configurations and test results and Figure 4-2 shows the pressure development in the reservoirs during dispersion. Figures 4-3 and 4-4 shows images from the dispersion tests and illustrates the strong effect of confinement.

Table 4-1 Test configuration and test results

Test number	**Configuration**	
1	Confined within box	
2	No confinment	
Time delay of dust		
Test Number	**Frames**	**Sec**
1	13	0,043
2	14	0,047
Time to fill box		
1	75	0,250

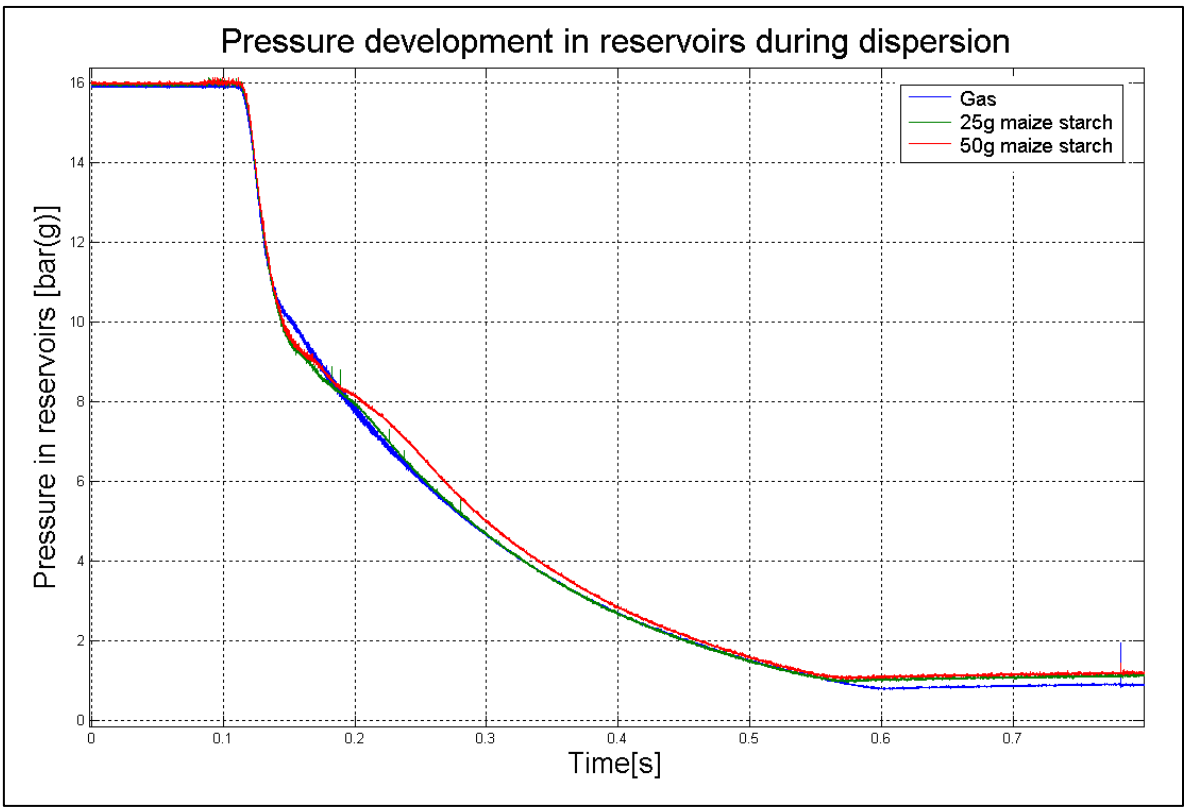

Figure 4-2 Pressure development in reservoirs during the dispersion process

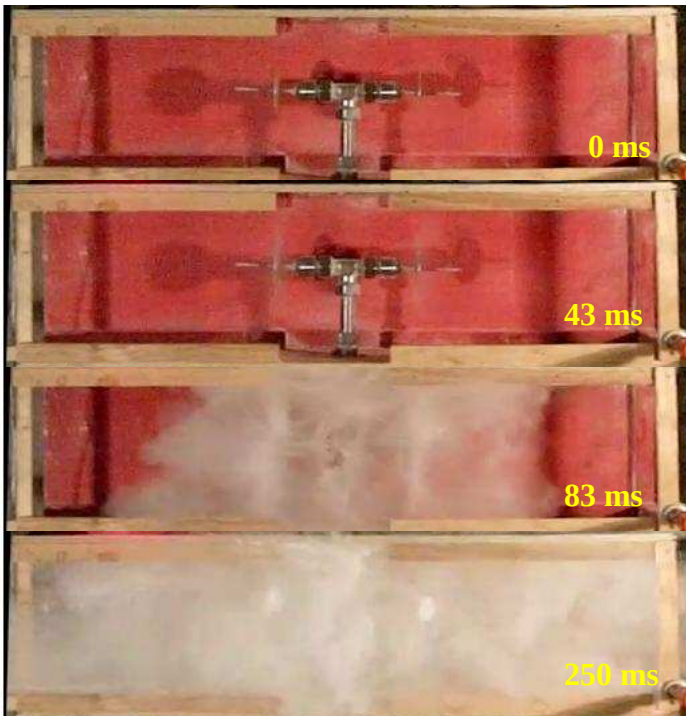

Figure 4-3 Images from dispersion confined within box.

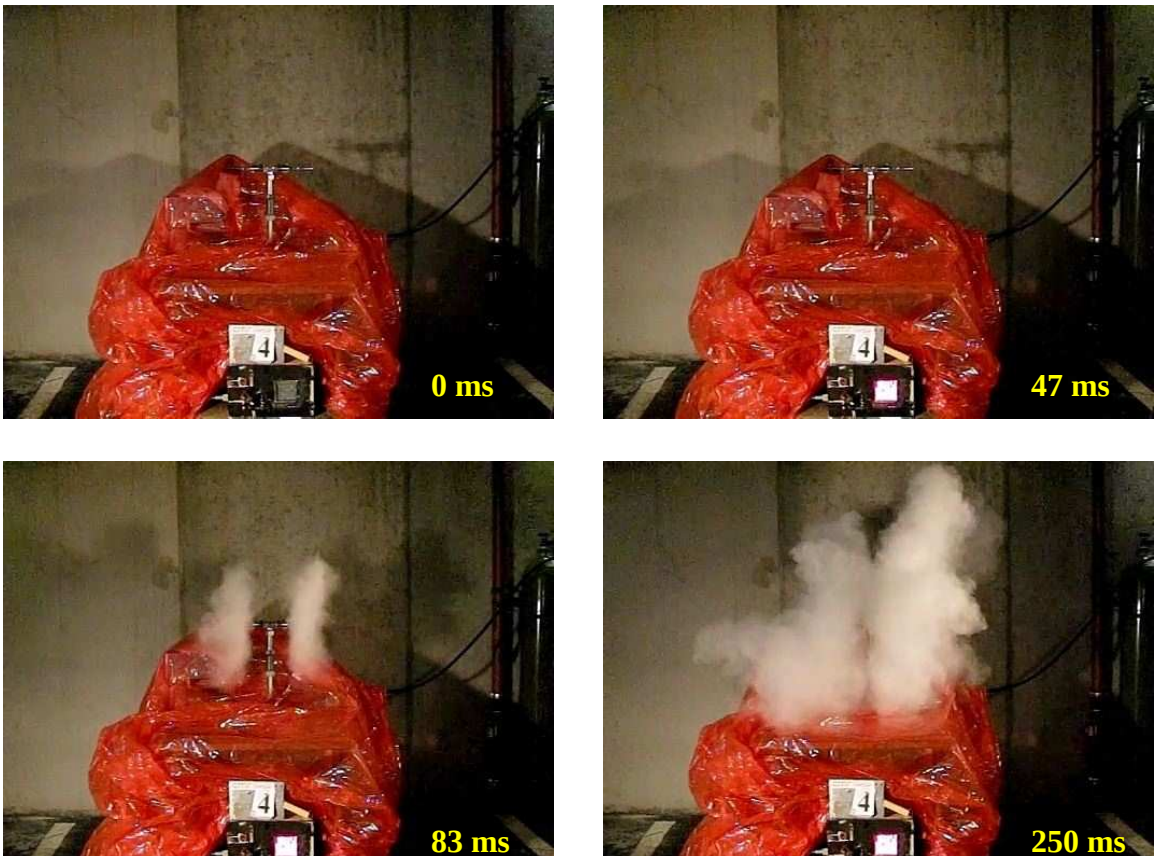

Figure 4-4 Images from dispersion test 2.

4.2.1 Analysis of pressure in reservoirs

Figure 4-2 shows the pressure time curves during dispersion tests. The introduction of dust in the dust reservoirs slows down the discharge rate, and hence pressure drop in the reservoir. It seems 25 and 50 gram of maize starch give approximately the same end pressure. The initial pressure drop that seems to be linear is probably sonic flow, and the reason for the linear pressure development is chocking. This sonic flow lasts a little longer in the experiments with dust.

The dispersion process is over after about 500 ms. The trigger signal is sent just before 0.1 s after the LabView program is activated, and the pressure drops up to 0.57 - 0.60 s. A shorter dispersion time would be advantageous. If the dispersion times were shorter, the dispersion could be differentiated in such a way that the last section of the FAT would disperse last. This would give more control with the mixture ratio in the pipe. To achieve this, the dispersion system would have to inflict less pressure drop, meaning that the number of bends and length of pipes must be reduced and the cross-section area of the connections increased. In some tests the valves did not close. The length of the signal sent was adjusted to 90 ms, since the valves seem to close after a certain time after the signal is stopped. Improvements to the system would be advantageous in order to get better control with the dispersion process.

4.3 Results from Flame Measurements in the FAT

Flame arrival measurements are presented and discussed for the optical measurement principle. The results are compared with the measurements done by the impedance/capacitive principle (Enstad, 2009), thermocouple and video observations. Table B-3 in Appendix B.1 shows a complete overview of the flame arrival measurements, as well as calculated flame speeds, for all tests. For an overview of the maximum pressure see Table B-2 in Appendix B.1. Video observations are done by the use of a high-speed camera with a time resolution of 600 frames per second. Appendix B.1 shows pictures from the videos recorded of test 7 and 16.

Flame Arrival

One of the major issues regarding flame detection with the optical probe is to define an unambiguous criterion for positive flame detection. Is it when the PD within the probe registers a specific change in radiation intensity, or when it reaches saturation? In this thesis, the first criterion has been used. One of the reasons for this is that in experiments with lean dust/air-mixtures, and propane/air-mixtures without initial turbulence, the PD did took quite some time to reach saturation. In addition, in the first experiments some of the channels on the NI-card were preset to an input range of ±5V, which meant that the measurements reached saturation at 5V. Figure 4-5 shows typical flame detection.

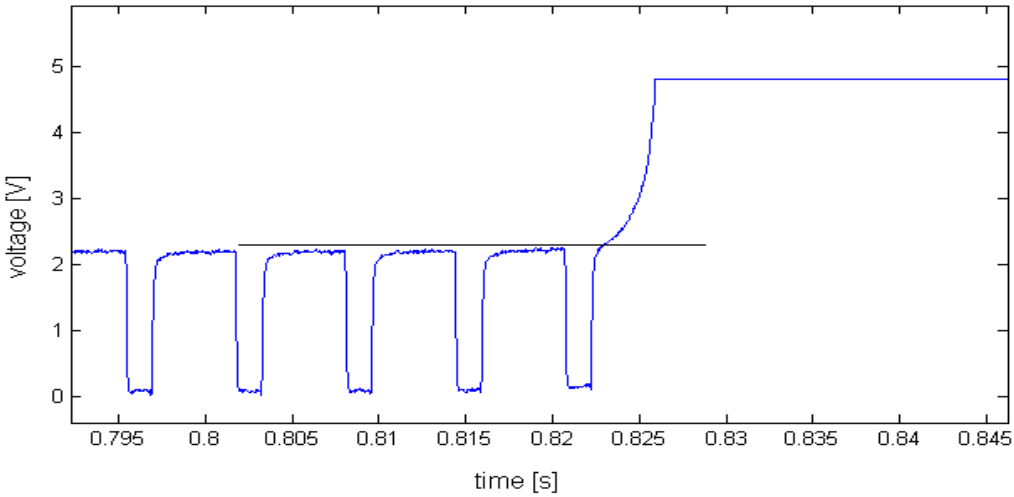

Figure 4-5 Flame detection with the optical probe**.**

If the only purpose with the optical probes were to measure flame arrival times, it would have been enough to use the PD, and not the LED. In that case, it would possibly have been easier to define the flame arrival times, due to the absence of the square wave signal. Hence, in an industrial situation were the main purpose is to detect a flame, only the PD would be used. However, the purposes of the optical probes used in this thesis have been to both measure flame arrival times and light attenuation.

As the measured signals from the PD showed a significant offset, probably because the op-amps were pushed to their limits in terms of amplification, the signals presented here are adjusted to zero volts. For the future, dual amplifiers are preferred to reduce the offset; however, the offset should not affect the flame detection. Times for flame arrival were measured with five probes along the FAT in most of the experiments. The exceptions are tests

19 and 20, where the first probe was disconnected in order to free logging channels for measurements in the air reservoirs.

4.3.1 Propane/air-mixtures

Tests with 3.0 vol%, 4.5 vol% and 6.0 vol% of propane in air were performed in the FAT. Flame arrival times, have been measured by the optical principle. Figures 4-7, 4-9, and 4-11 show results from flame speed measurements for some of the tests. *Speed 01* refers to estimated average flame speed based on time of ignition and measured flame arrival at probe 1, *speed 12* based upon flame detection at probes 1 and 2, etc. The dotted lines are fitted curves for each principle, and are mostly included for illustration. A curve that goes through all the points is preferred but for some measurements, the curves are fitted in a least square sense. This is because for these tests a curve that goes through the points will appear somewhat wrinkled. In order to be able to measure *speed 01*, the time of ignition has to be known. Since the trigger signal for ignition will affect the measured signal from the PD, and turn out as a spike on the measurements, the time of ignition relative to the measurements could be estimated. Figure 4-6 illustrates this spike for test 6.

Figures 4-8, 4-10, and 4-12 illustrate the deviation from the mean values of flame arrival and flame speeds, measured by the probes and video, for each principle. The deviation is defined as follows:

$$\sigma_i = \frac{t_{f,i} - \overline{t_f}}{\overline{t_f}} \qquad \textbf{(4.1)}$$

Where σ_i are a dimensionless measure for the deviation in observed flame arrival times obtained with measurement method i, $t_{f,i}$ flame arrival time determined with method i and $\overline{t_f}$ the average flame arrival time observed by all methods. Since the values used here for flame arrival is time relative to ignition, a relatively large deviation from the mean value of flame arrival for the first probe does not mean that the deviation in seconds is large than on the last probe.

Flame arrivals observed by the video are considerable earlier than for flame arrival measured by the probes. An explanation for this could be that reflection from the aluminium rings made it difficult to estimate flame arrival with the video, meaning it could lead to premature flame detection. It is generally not straightforward to observe ignition times from the video recordings. The optical principle seems to detect the flame early, compared to the impedance/capacitive method. The reason for this could be that the PD has a detection angle of ±18°, and hence may be within a range by reflection from the aluminium extension rings. For the future, it is therefore recommended for the aluminium rings to be painted/soothed in order to reduce reflection.

The maximum flame speed derived from the optical measurements is 200 m/s in, tests with 4.5 vol% propane in air. For the tests with 6.0 vol% of propane in air, the maximum flame speed was 100 m/s in test 12. In test 15, with 3.0 vol% propane in air without initial turbulence, a maximum flame speed of 14 m/s were measured between probe two and three. What is interesting is that *speed 34* measured by the optical probes are higher than for the other principles for most of the tests. This means that either probe three register the flame relatively late compared to the other principles, and/or probe four registers the flame early.

Figures 4-8, 4-10, and 4-12 suggest that probe four measures flame arrival earlier, compared to both the video and the impedance/capacitive measurements. However, in test 5, when flame propagation were only studied by the video, and test 6, when only the optical/impedance probe measured flame arrival time, the maximum flame speed were observed between probes three and four for all cases. It is also difficult to measure flame arrival with millisecond revolution due to the relatively gentle slope in the start of the flame detection signal. The accuracy of the flame speed is given by:

$$P = \frac{S_F \cdot dt}{L_t} \qquad \textbf{(4.2)}$$

Where P is the accuracy, S_F the measured flame speed and dt the time resolution. For fast flames, small variations in interpretation of the measurements would yield large variations in the estimated flame speeds. This is due to the short delay between the measured flame arrival times for the different probes. Therefore, the reading of the measured signals regarding flame detection is a major source of error. In addition, the number of tests are limited, and it is difficult to draw any final conclusions regarding the trends in the measured flame arrival times.

Due to the limited number of channels on the NI card, there were only two active thermocouples inside the FAT during most of the tests. However, the signal from one of the thermocouples was disturbed by other signals, and the results therefore only include data from one thermocouple. The thermocouple gives good correlation with both the optical and impedance probes and this supports the earlier observations suggesting that the video observations are inaccurate. The flame arrival time measured by the thermocouple tends to lie between the time measured by the optical and the impedance principles. However, since the thermocouple-wire used here are quite thick, *i.e.* 0.3 mm, it can be questioned if it reacts slow compared to a thinner type. Nevertheless, it serves as a reference for the other measurements/observations. Future studies should include measurements with a thinner thermocouple.

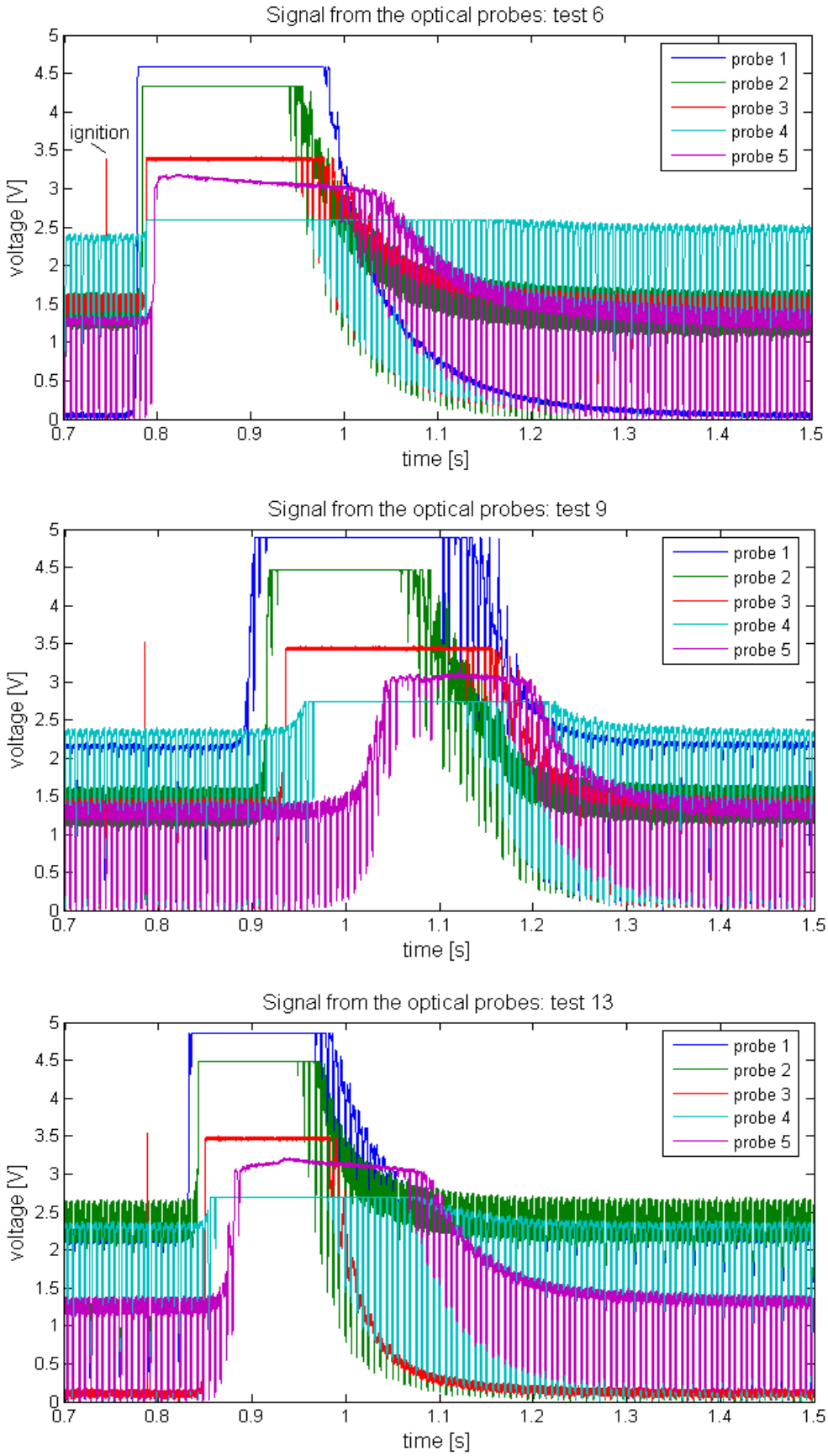

Figure 4-6 Signal from the optical probes. Test 6: 4.5 vol% propane in air. Test 9: 2.8 vol% propane in air without initial turbulence. Test 13: 6.0 vol% propane in air.

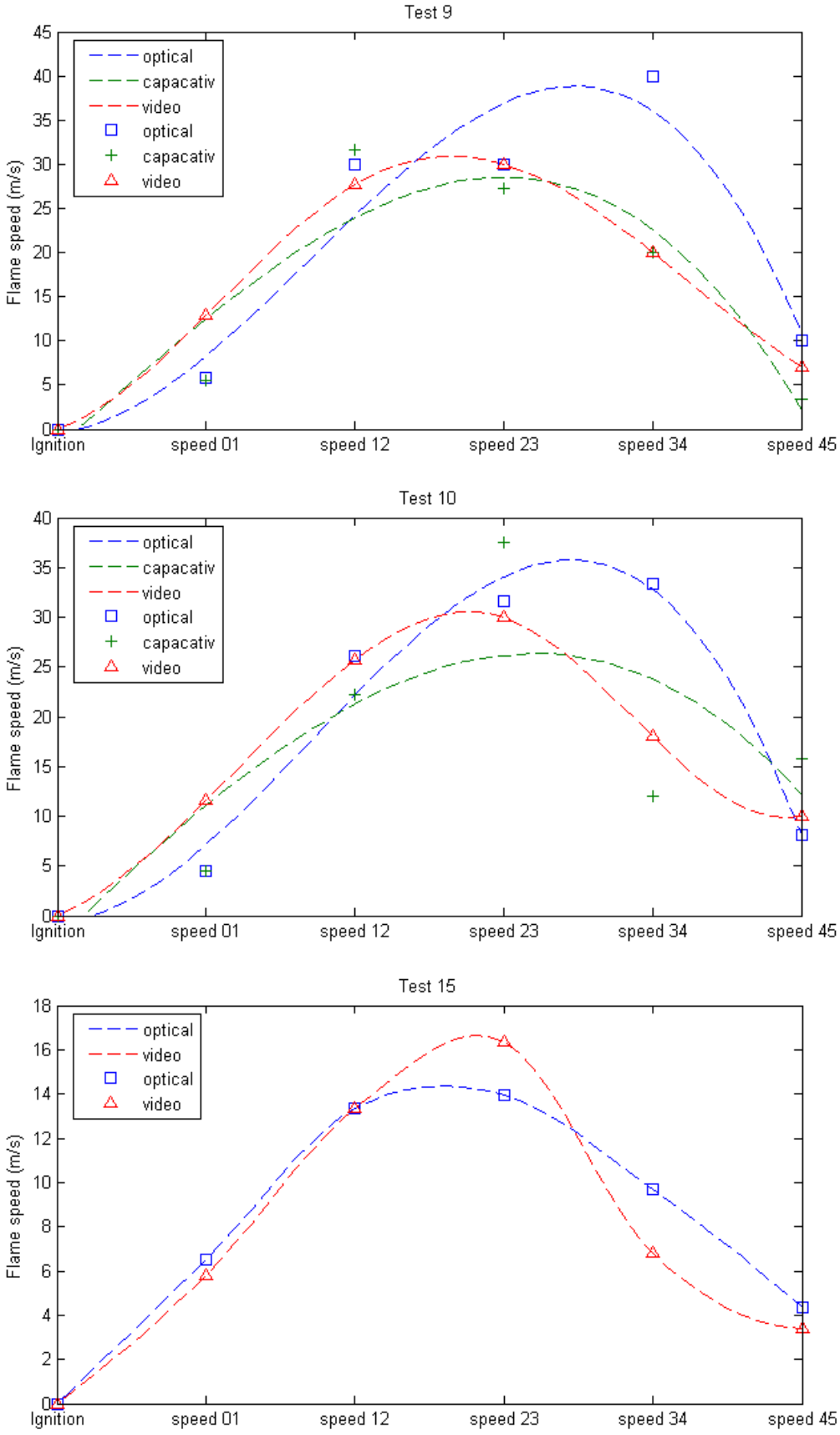

Figure 4-7 Flame speed measurements for tests with 3.0 vol% propane in air.

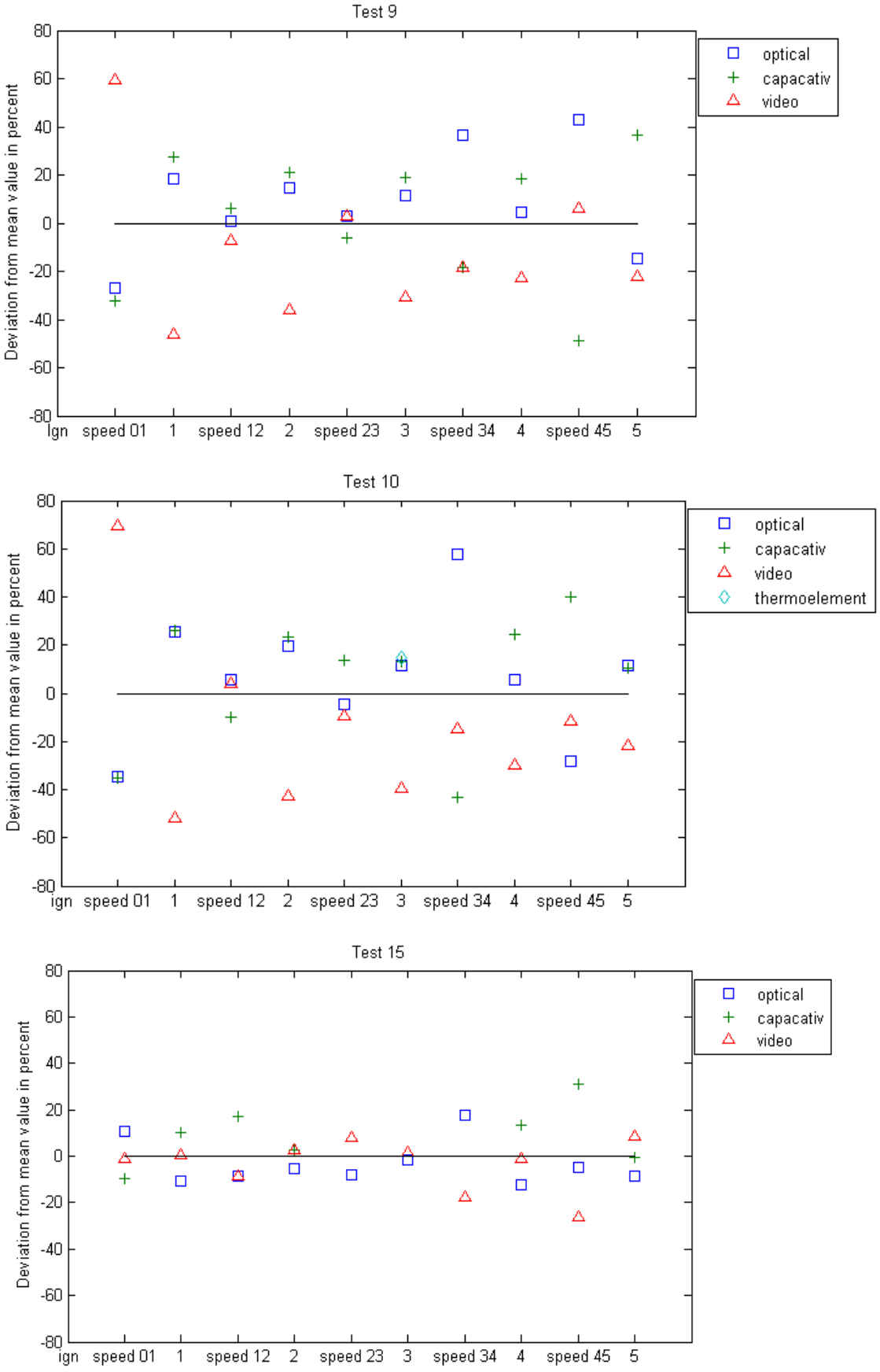

Figure 4-8 Deviation from mean values for flame arrival/speed measurements for the different measurement principles in tests with 3.0 vol% propane in air.

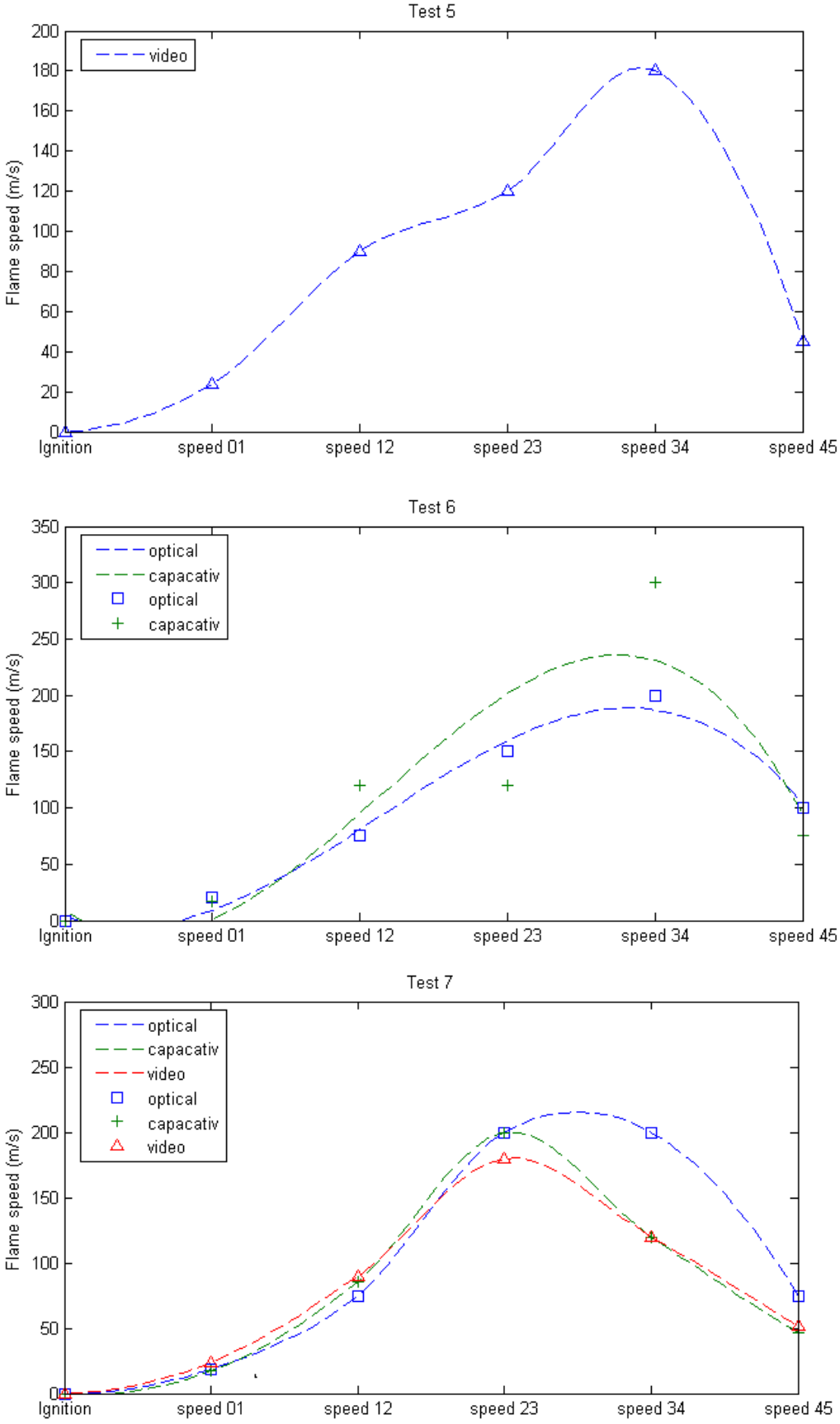

Figure 4-9 Flame speed measurements for tests with 4.5 vol% propane in air.

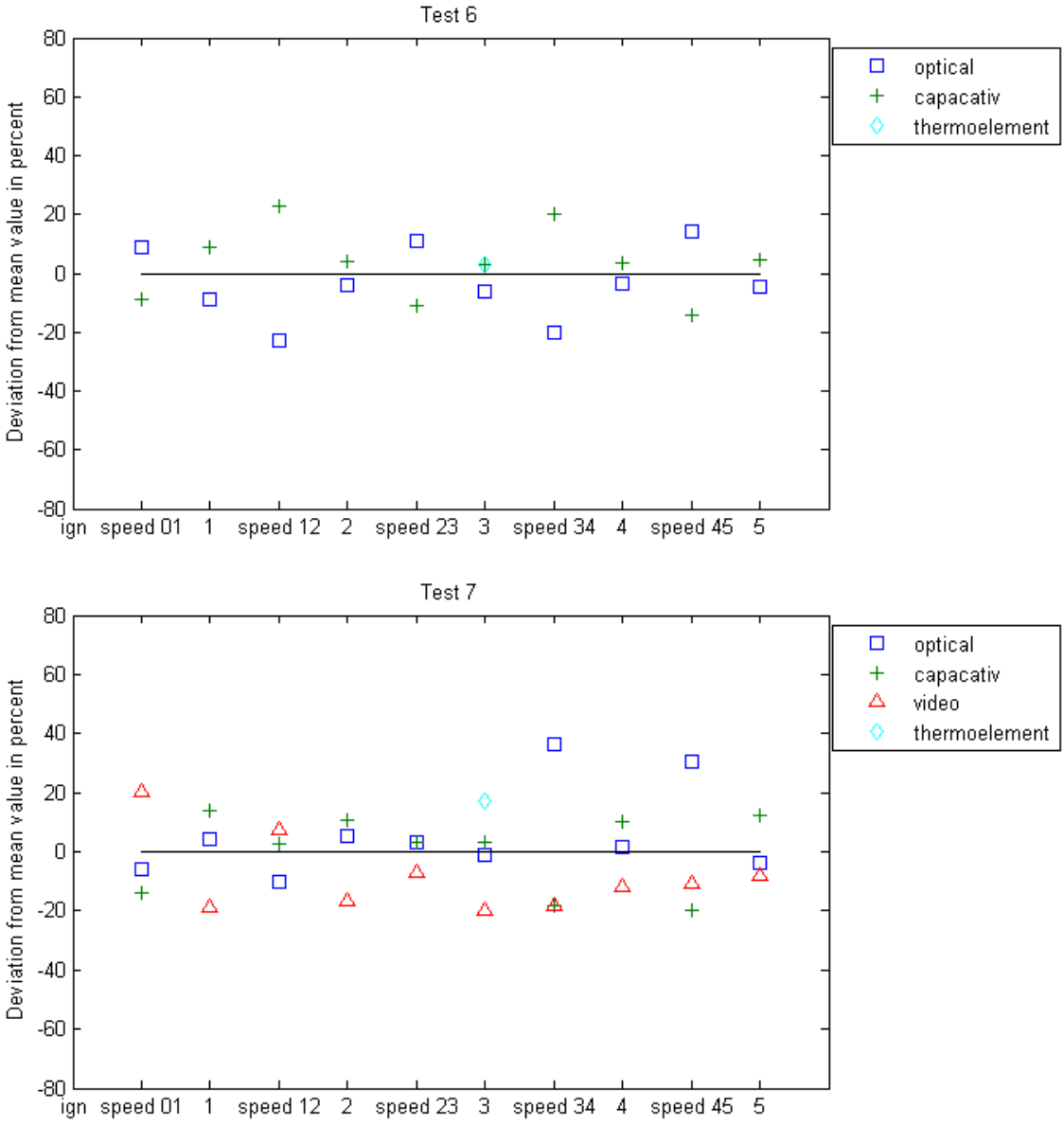

Figure 4-10 Deviation from mean values for flame arrival/speed measurements for the different measurement principles in tests with 4.5 vol% propane in air.

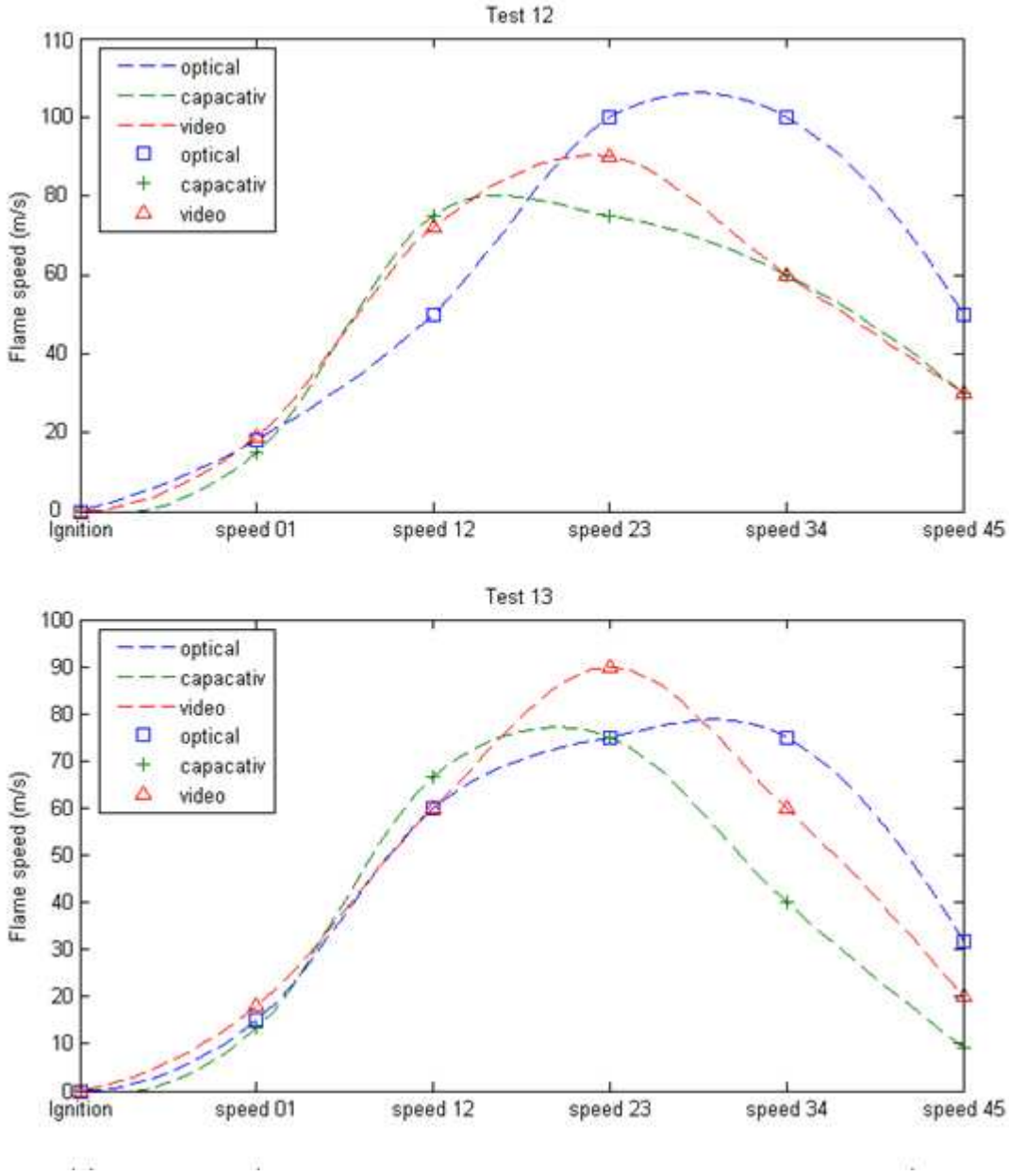

Figure 4-11 Flame speed measurements for tests with 6.0 vol% propane in air.

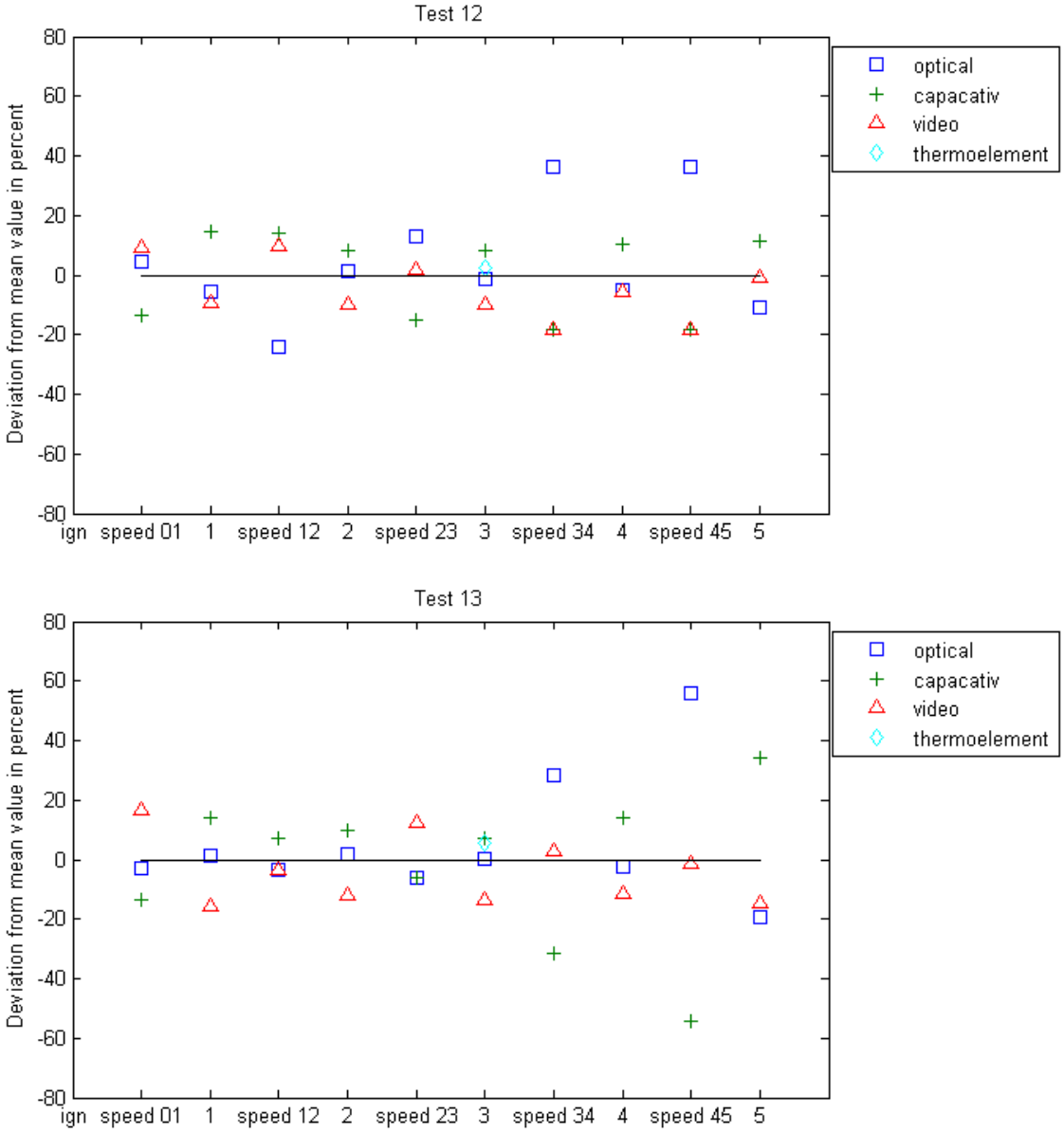

Figure 4-12 Deviation from mean values for flame arrival/speed measurements for the different measurement principles in tests with 6.0 vol% propane in air.

4.3.2 Experiments with maize-starch

Tests were performed with maize starch with nominal dust concentrations of 500 g/m^3 and 250 g/m^3. Figures 4-13 to 4-15 show results for flame speed/arrival measurements for these tests. For the two tests with a concentration of 250 g /m^3, the flame did not propagate throughout the tube. This is probably because the dust at the end of the tube had settled out before the flame arrived, and the induced turbulence was not enough to whirl up a sufficient amount of dust. This could have been solved by activating the three dispersion systems in sequence. However, this would require a redesign of the dispersion system, to get a smaller pressure drop through the system. This is because a smaller pressure drop would reduce the time needed for the dust to enter the FAT, thus give more room for adjusting dispersion timing before ignition.

The light emitted from the chemical igniter influences the first probe. The PD will first reach saturation because of the igniter, then the output voltage goes down before it reaches saturation again because of the flame arrival. The result from test 16 shown in Figure 4-16 shows this. Flame detection for the first probe is then defined as the lowest point between the two saturation points. When testing with maize starch, another phenomenon occurred on the measurements. As Figure 4-16 shows, a lot of noise were generated on the measurements during dispersion, which did not happen with gas, before it disappeared some 0.2 s before the time of ignition. This was also the case with the impedance measurements. One difference between dust and gas that perhaps could affect the measurements in such a way, is that dust will generate static electricity. One possibility is that the capacative plates is affected, and that the noise influences the optical measurements as the sensors lie close together inside the probe. Another possible explanation is that the grounding of the electronic circuits is not good enough. However, the noise has been filtered out when analysing the data and is therefore not present in the other figures. In an industrial situation, this noise must be removed, as the measurements should not generate noise in the presence of a highly turbulent dust cloud. The noise could trigger false alarms if it exceeds a certain trigger level for flame detection.

Flame Arrival and Flame Speed

The maximum flame speed measured by the optical probes in the experiments with maize starch was 46 m/s in test 16. As it turned out, maximum flame speeds were, for all principles except for the optical in test 16, measured between probe three and four for the three tests with 500 g/m^3 of maize starch. This is in contrast to the tests with propane where the impedance principle and the video observed maximum flame speeds between probes two and three, while the optical probes measured between probes three and four, which is the same as for dust. A possible explanation could be that the concentration is more ideal for flame propagation in that part of the tube, and/or that dust is relying more on expansion-induced turbulence than gas. However, a more probable explanation is that the pressure-rise developed slower because the burning rate for dust is lower than for gas. Thus, the maximum flame speed will appear later for dust than for gas, as there will be a lot of unburned dust behind the flame front, meaning that the pressure is lower. However, an analysis of the pressure development showed that the pressure developed quite similar for dust and gas (Figure 4-18).

Another difference between dust and gas in the measurements, is that flame arrival observed by the use of the video, compared to the optical/capacativ probe, is not as early for dust as for gas. The reason for this could be the reduced reflections from the aluminium rings in dust explosions, compared to gas, which means that it is easier to define flame arrival on the video.

The reason could also be that the flame front in dust clouds is diffuse, and that the flame arrival time observed on the video therefore occurs somewhat late. Another trend is that the PD measures flame arrival earlier than the video, and the impedance principle later, thus it indicates that the optical principle detects the flame too early, and the impedance to late. The deviation between the optical and impedance principle are similar for dust and gas flames, if one compares flames with approximately the same speed. However, the results for dust experiments shows less relative deviations on the charts, but this is mainly due to the video analysis agreeing more with the other measurements. Nevertheless, for the first probe the PD registers the flame earlier than the impedance principle, compared to the other probes. The reason for this could be the disturbance in the measurements from the chemical igniter.

Transmission, Flame Thickness and Flame Analysis

In the tests with a nominal maize starch concentration of 250 g/m^3, where the flame did not propagate all the way through the tube, the PD did not reach saturation for all of the probes that measured a flame. Figures 4-17 and 4-18 show results from these tests. The intensity of radiation measured by the PD fluctuates while the flame is present. This is especially clear for probe three in test 20, shown in Figure 4-17. These fluctuations indicate the irregularities and wrinkling of the flame. Based upon the time the PD measures an increased radiation relative to the LED radiation, and the measured flame speeds, a flame thickness in the area of 1.5-2 m could be indicated. This is about two to three times larger than the flame thickness measured by Tezok et. al. (1985), although his experiment did not imply obstacles to enhance turbulence. In general, to measure the flame thickness in such a geometry with a lot of obstructions, i.e. the probes and dispersion nozzles, have been difficult. For instance, in many of the tests the flame was visible along the whole length of the tube at the same time. However, it seems likely that more reliable flame thicknesses can be measured in the glass tube in the future, where the probe fits better, and the turbulence will be less intense.

Even though the flushing system for the optical probes did not work, transmission has been measured based upon the decrease in amplitude of the signal measured by the PD. The transmission is calculated based upon the amplitude during the process, and the start value of the amplitude:

$$T = \frac{A(t)}{A_{start}} \qquad \textbf{(4.3)}$$

Where A(t) is the amplitude of the signal during the measurements, and A_{start} is the start initial value of the amplitude. When a flame is present, the transmission will follow the flame signal in the plots because the amplitude is evaluated by calculating the mean value of the signal. Figures 4-16 to 4-18 show results from the tests with maize starch in the FAT. Due to the lack of a flushing system, the results are somewhat random. This is illustrated by the fact that there is little difference in the measured transmission in tests with maize starch of 250 and 500 g/m^3. The transmission during dispersion also seems constant, while one perhaps could expect that it decreased as dust settled down. In addition, after the explosion the transmission is considerably lower than before. This again indicates that dust has settled on the windows due to the lack of a flushing system. However, one interesting observation is that probe five seems to react later to the dispersion of dust than the other probes in all tests. A reason for this could be that probe five is the only probe that is directly exposed to only one dispersion nozzle,

while the other probes all have one dispersion nozzle at each side. This means that the build-up of the dust cloud seems to happen faster in the middle of the tube than at the ends. However, since probe three in test 19 also reacts late, the explanation could lie somewhere else. Another interesting observation is that the value of the start amplitude varies for each experiment, which could indicate inadequate cleaning of the diode windows between some of the experiments.

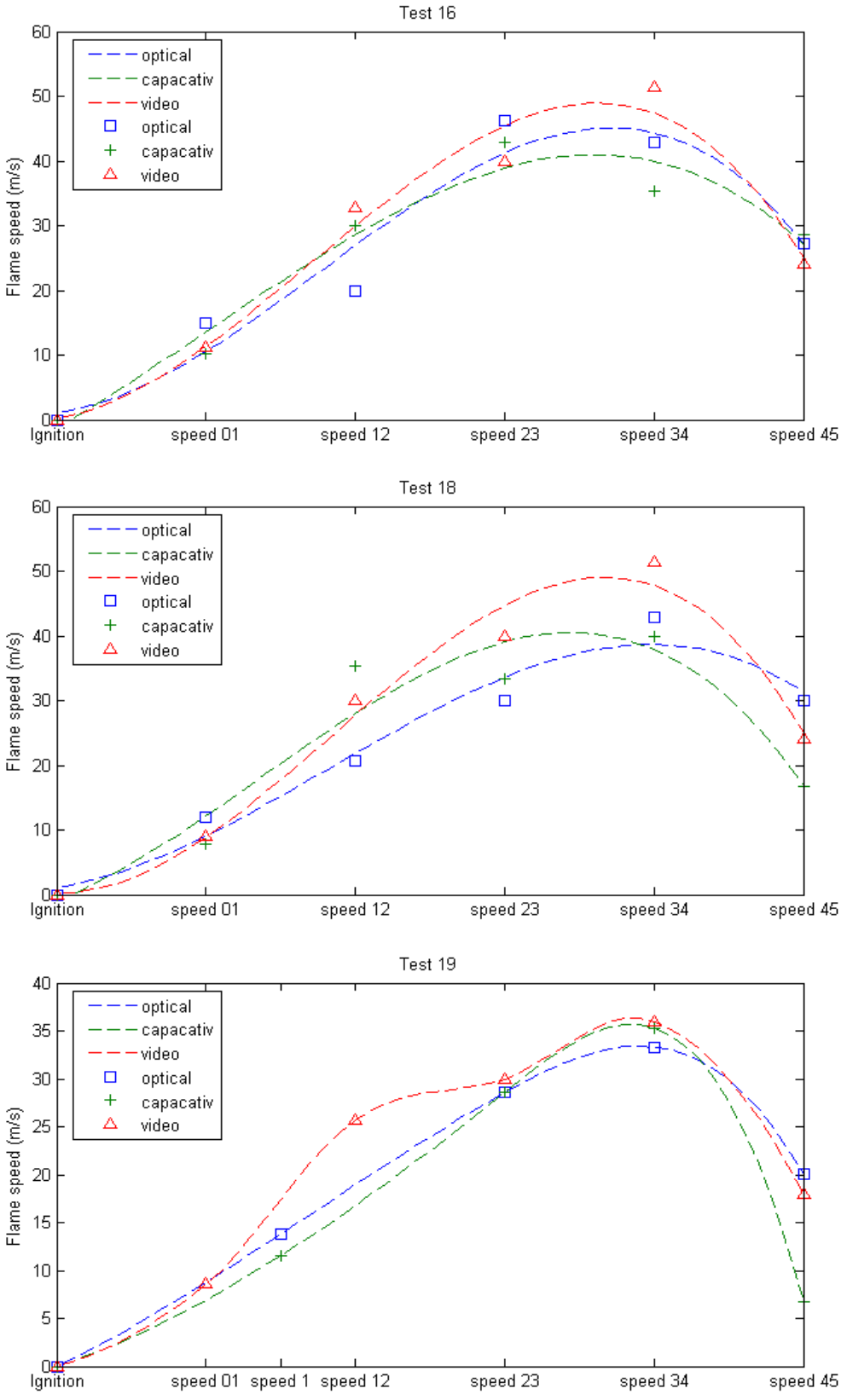

Figure 4-13 Flame speed measurements for tests with 500 g/m^3 of maize starch. Note that in test 19 the first probe was disconnected, thus *speed 1* refers to the flame speed derived from the time of ignition and measured flame arrival time at probe 2.

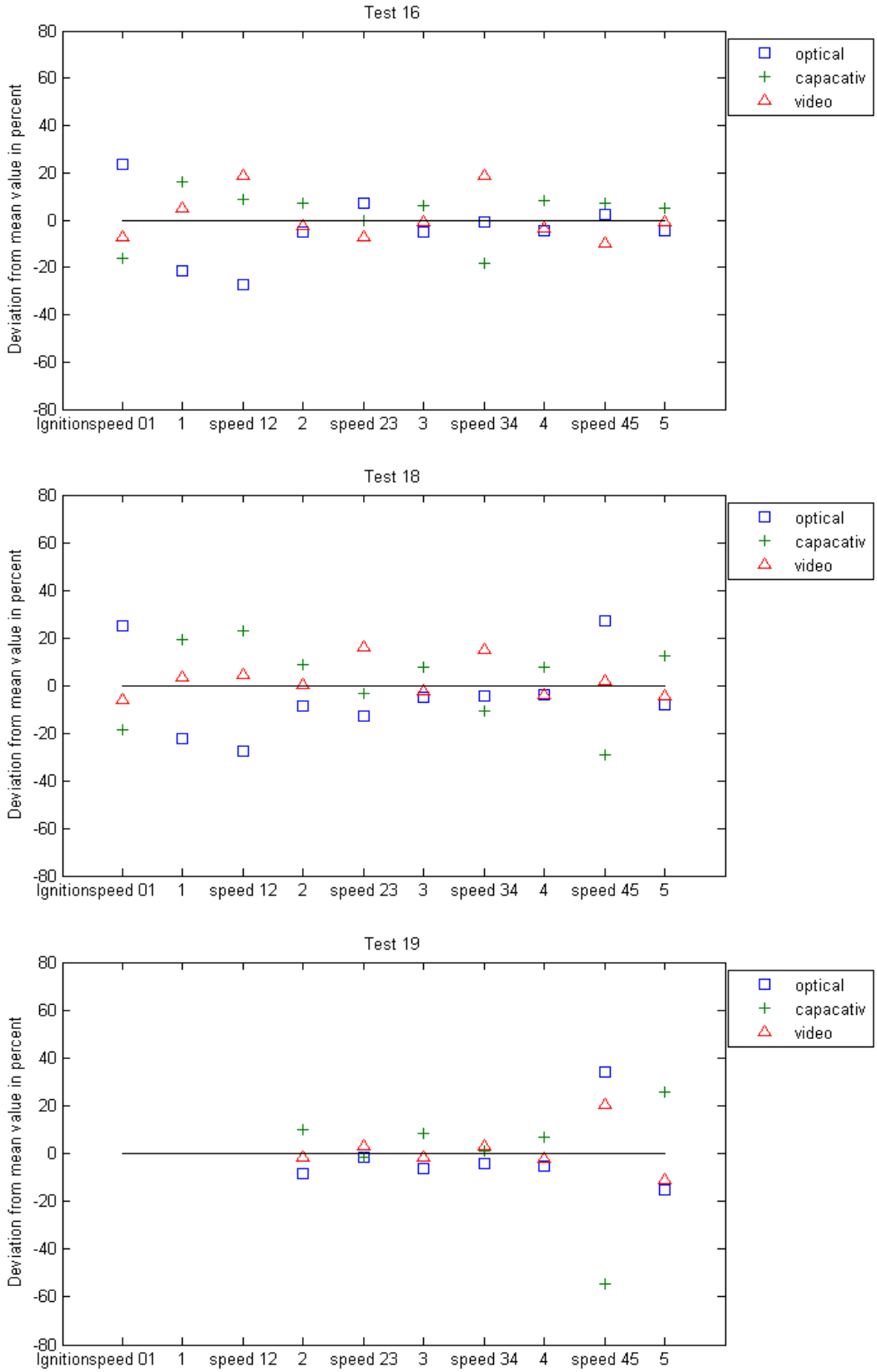

Figure 4-14 Deviation from mean values for flame arrival/speed measurements for the different measurement principles in tests with 500 g/m3 of maize starch.

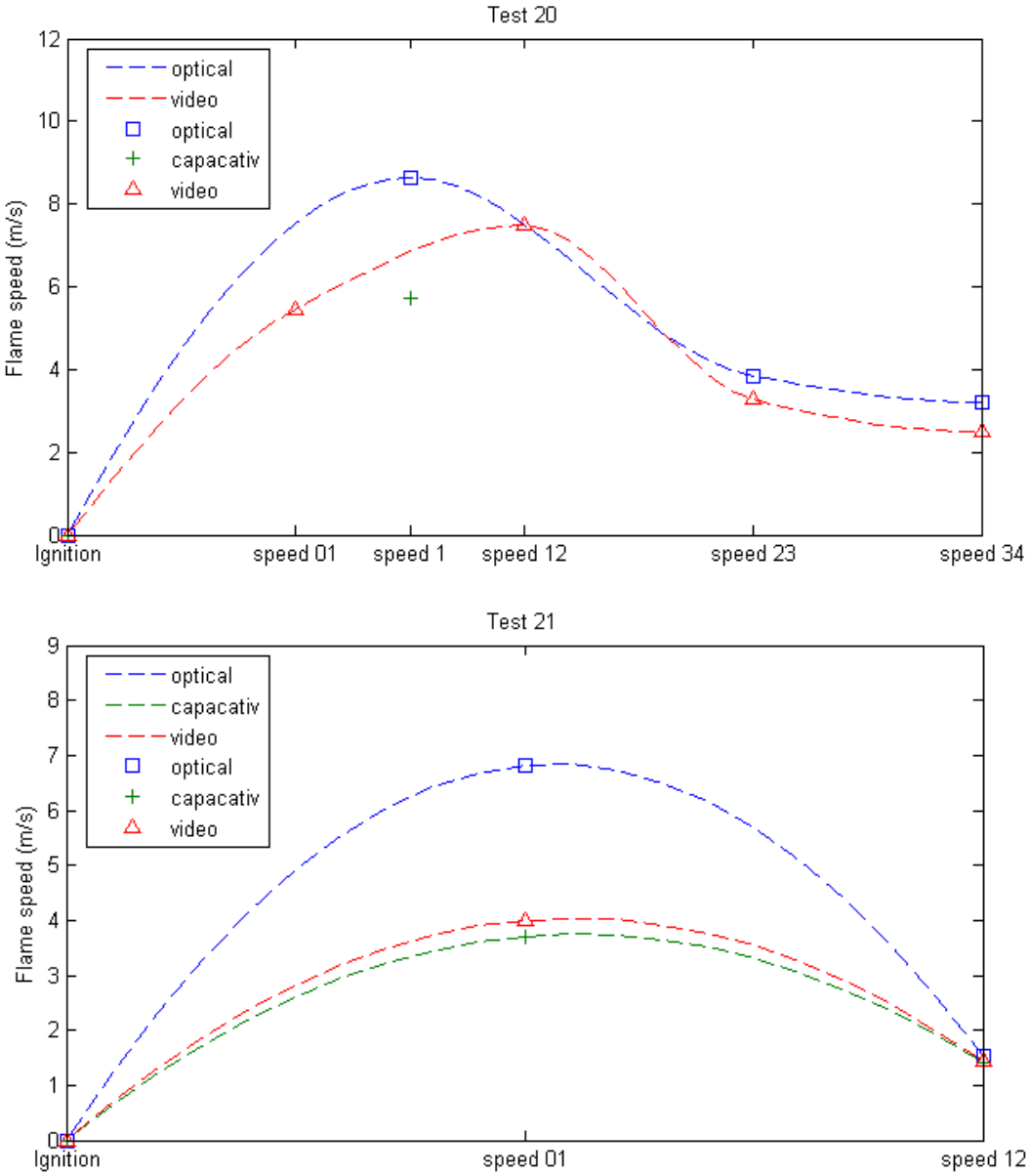

Figure 4-15 Flame speed measurements for tests with 250 g/m^3 of maize starch. Note that in test 20 the first probe was disconnected, thus *speed 1* refers to the flame speed derived from the time of ignition and measured flame arrival time at probe 2.

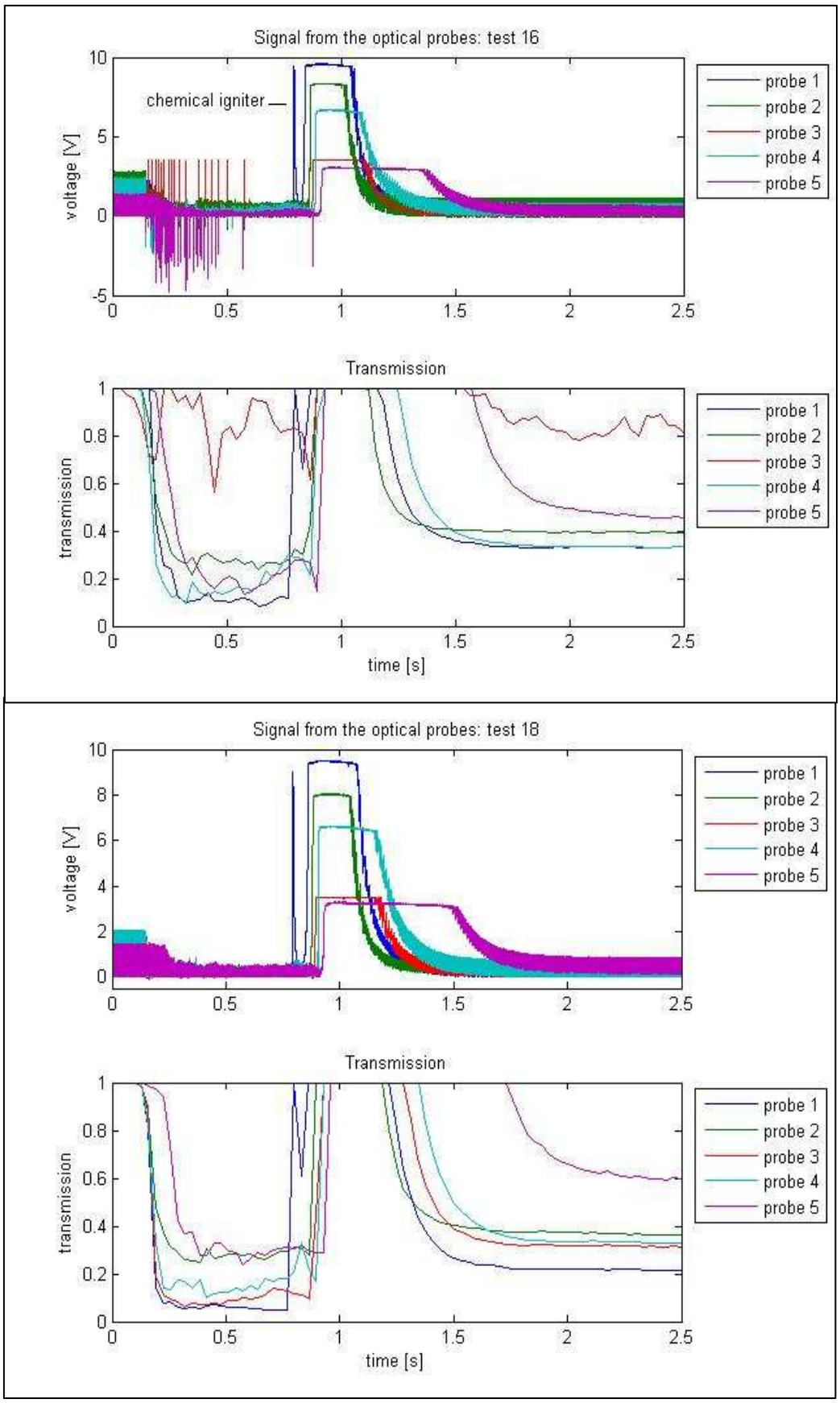

Figure 4-16 Signal from the optical probes and estimated transmission in tests with 500 g/m^3. Note that probe three in test 16 did not yield a sufficient amplitude to calculate transmission, due to problems with the LED. Nevertheless, it did do flame detection with the PD.

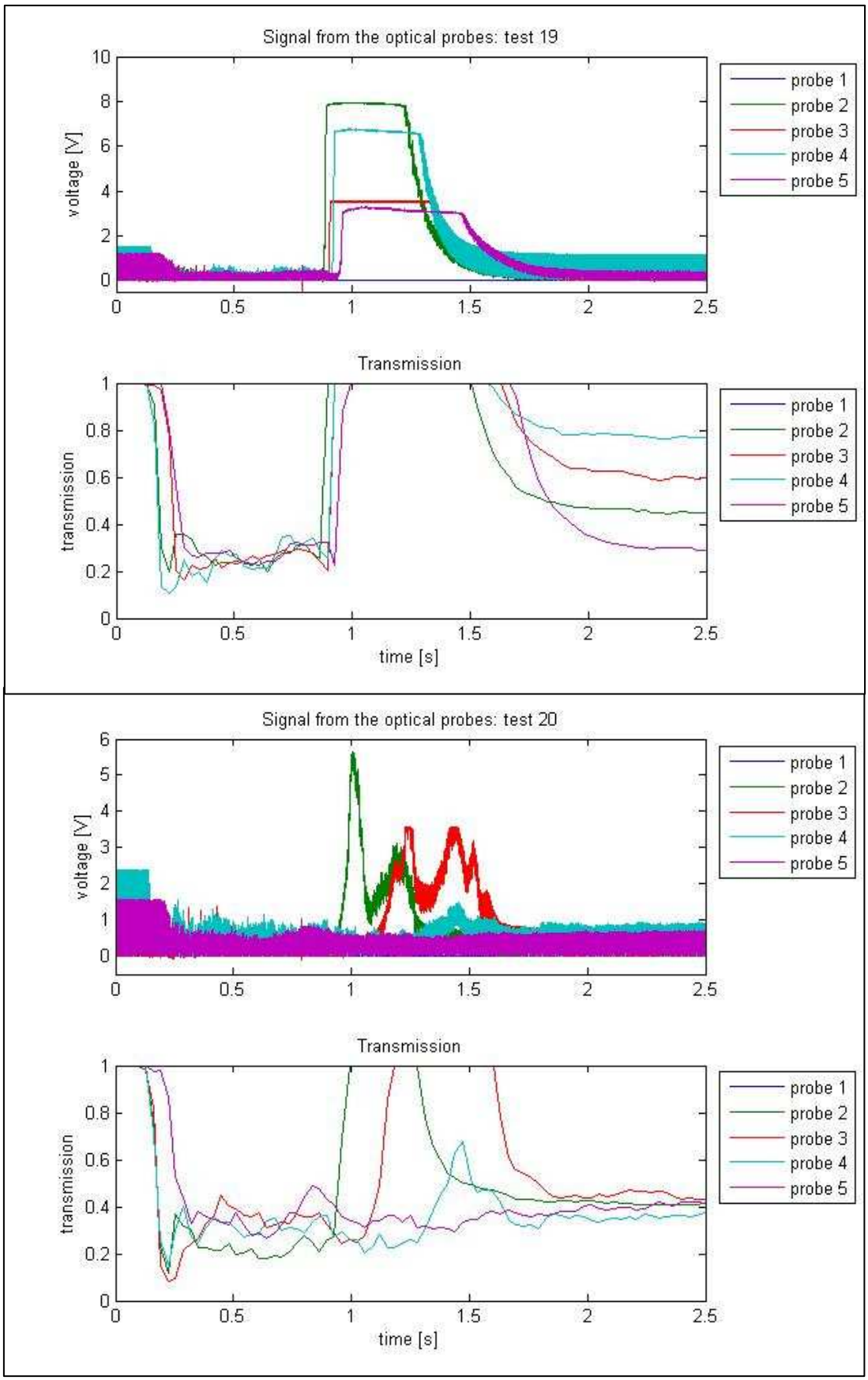

Figure 4-17 Signal from the optical probes and estimated transmission in tests with maize starch, where test 19 is with 500 g/m^3 and test 20 with 250 g/m^3. Note that in these tests the first optical/capacativ probe was not active due to the lack of logging channels because the reservoir pressures were measured.

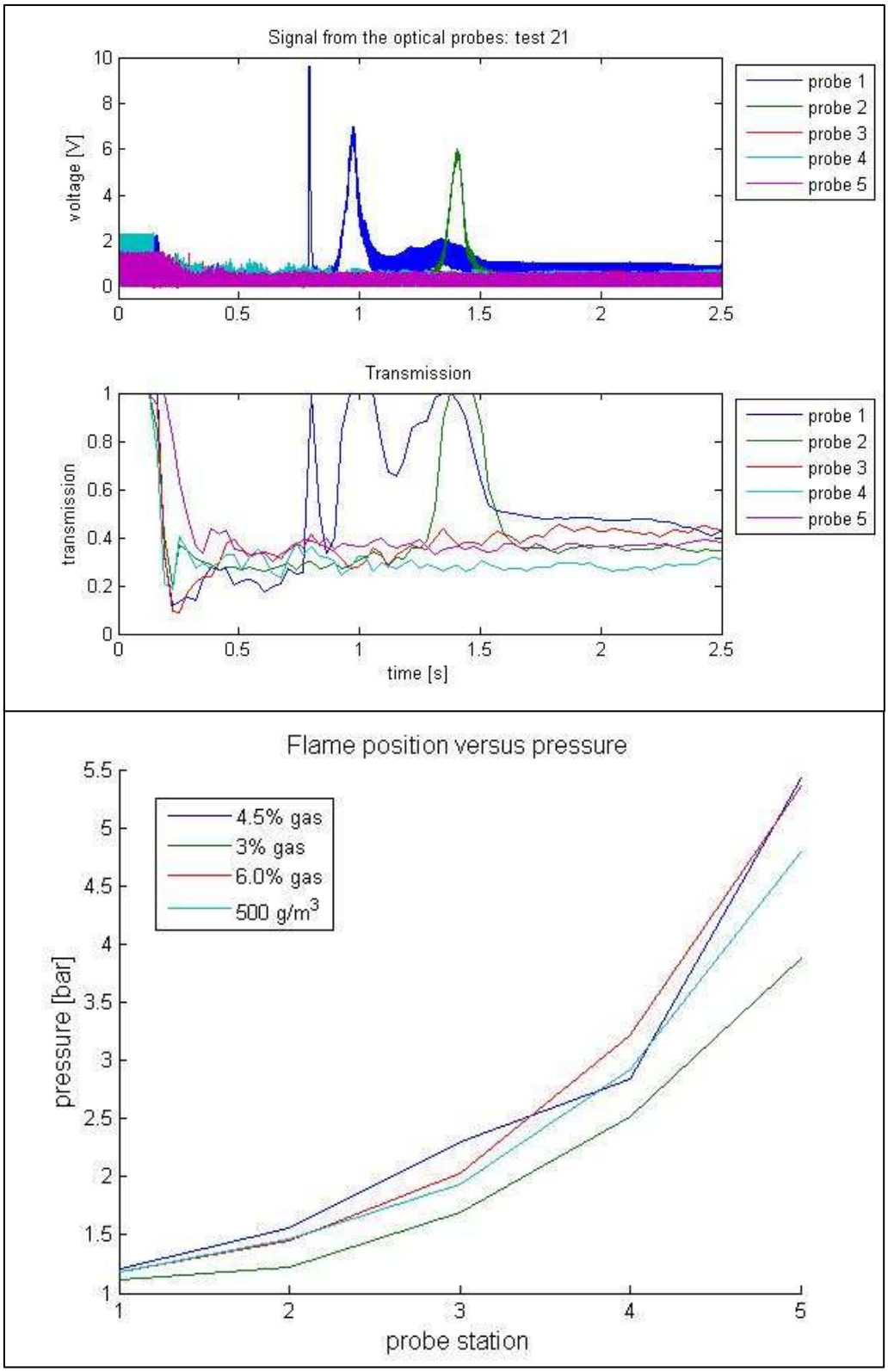

Figure 4-18 Upper: signal from the optical probes and estimated transmission in a test with maize starch in a concentration of 250 g/m^3. Lower: flame position vs. pressure for the different fuels and concentrations.

5 Conclusions

5.1 Apparatus

The 3.6 m Flame Acceleration Tube (FAT), situated in the laboratory workshop of GexCon AS, was equipped with a complete logging system, including cables, a logging card from National Instruments, a laptop, and a Labview program for running the experiment. The logging system worked adequately, although there were some problems with the logging card regarding disturbance between the analog input channels.

A simple arc generator was made for tests with gas/air-mixtures. Since it did not generate enough energy to work as a reliable ignition source for maize-starch/air-mixtures, chemical igniters were used for such tests.

Five measurement probes, including the optical and impedance sensors, were made at the workshop at the UiB. This work focused on the optical measurement method, whereas Enstad (2009) describes the impedance principle. The probe was designed as a ring, to fit a glass tube to be used in future experiments. In the FAT, the probe is highly intrusive and generates expansion-induced turbulence. The accompanying electronics for the optical probe includes signal generators for the LEDs, and amplifiers for the PDs.

5.2 Preliminary tests at the UiB

Before tests were performed in the FAT, preliminary tests were carried out in the 20-litre vessel at the dust-explosion laboratory at the UiB. Since the final probe design was too large to be tested in this vessel, a test probe was made. The main purpose of these tests were to optimise the measurement system i.e. signal generators, amplifiers, logging system etc. The results in these tests proved satisfactory.

5.3 Dispersion experiments

Prior to experiments in the FAT, the dispersion system were tested separately. The tests were performed in a replica of one section of the FAT with a glass-front, and monitored with a high-speed camera. The results showed that the dispersion of the dust were adequate, if not a bit slow. By reducing the pressure loss in the dispersion system, the dispersion process will be faster, hence give more room for individually triggering of each of the three dispersion systems.

5.4 Experiments with propane/air-mixtures in the FAT

Experiments with 3.0 vol%, 4.5 vol% and 6.0 vol% propane in air were performed in the FAT. Maximum flame speeds measured by the optical principle for these concentrations were 67 m/s, 200 m/s and 100 m/s respectively. The optical principle tended to measure the flame arrival time before the impedance method in the experiments, but after flame arrival time observed by the use of a high-speed camera. A possible reason for this could be reflections from the surroundings, leading to premature detection for the optical principle compared to the impedance principle, and even earlier detection on the video. In addition, a thermocouple was used and it gave good correlation with the optical and impedance principle, however it was not the fastest type of thermocouple.

5.5 Experiments with maize-starch in the FAT

Tests were performed with maize starch with nominal dust concentrations of 250 g/m^3 and 500 g/m^3 in the FAT. Maximum flame speeds measured by the optical principle for these concentrations were 9 m/s and 46 m/s respectively. As for gas, the optical principle detected the flame earlier than the impedance principle, while the flame arrival time observed by the use of the high-speed camera, tended to be between the two. In addition, the maximum flame speed appeared to occur closer to the end of the FAT for dust than for gas. The reason for this is probably that dust burn slower than gas, i.e. there was a lot of unburned dust behind the flame front, which means that pressure did not build up so fast.

5.6 Suggestions for further work

By improving the air flushing system it will be possible to keep the diode windows clean during tests. In addition, an optical filter can be applied in front of the photodiodes within the probe in order to be able to measure transmission during the presence of a flame. To be able to measure the concentration of dust in a dust cloud, the optical probes should be calibrated. For this to be done, a calibration apparatus must be made.

The acoustic measurement principle can be applied to the flame probes. It would also be advantageous to use thinner thermocouples that got a faster response time, as the ones used in this thesis are 0.3 mm thick. Further experiments can also be performed in the FAT. By applying rings inside the FAT to induce turbulence, the effect of obstacles on flame propagation can be studied. In addition, less intrusive probes should be designed for use in the FAT in order to minimize the effect from the measurement probes on flame propagation.

References

Bartknecht, W. (1971) “Brenngas-und staubexplosionen.” Forschungsbericht F45. Koblenz, Federal republic of Germany: Bundesinstitut für Arbeitsschuttz.

Borghi, R. In: Bruno C, Casci C (eds) (1984), *Recent Advances in Aerospace Science*, Pergamon, London

Cai, X., J.Li, X.Ouyang, Z.Zhao and M.Su. (2005) In-line measurement of pneumatically conveyed particles by a light transmission fluctuation method. *Flow Meas. and Instr*, 16, pp. 315-320

Chen, Z. & Fan, B. (2005), Flame propagation through aluminium particle cloud in a combustion tube. *Journal of Loss Prevention in the Process Industries* 18, pp. 13-19

Conti, R.S., K.L. Cashdollar and I. Liebman.(1982). Improved optical probe for monitoring dust explosions. *Rev. Sci. Instrum.*53 No. 3, pp. 311-313.

Dobashi, R. (2000). *Welding procedure of fine wire thermocouple.* Personal communication between R. Dobashi and R.K. Eckhoff, November 2000.

Eckhoff, R.K., K. Fuhre and G.H. Pedersen (1985), *Vented maize starch explosions in a 236 m^3 experimental silo.* Chr. Michelsen Institute, Bergen, Norway

Eckhoff, R.K. (2003), *Dust explosions in the Process industries*, third edition, Gulf Professional Publishing, Amsterdam

Eckhoff, R.K. (2005), *Explosion Hazards in the Process industries*, Gulf Professional Publishing, Houston, TX

Enstad, G.A. (2009), *Experimental Investigation of the Impedance Measurement Method for Detecting Dust and Gas Flames in a Flame Acceleration Tube*. Master Thesis, University of Bergen

Holbrow, P. (2004), DESC: *Interconnected vented explosion tests*. Report EC/04/30, HSL, Harpur Hill, Buxton, UK

Holbrow, P. (2005a), DESC: *Phase 2: Interconnected vented explosion tests*. Report EC/04/72, HSL, Harpur Hill, Buxton, UK

Holbrow, P. (2005b), Large scale explosions in vented coupled vessels. *International ESMG symposium*, Nürnberg, Germany, 11-13 October 2005 (7pp.).

ISO 6184-1 (1985). *Explosion Protection Systems – Part 1: Determination of Explosion Indices of Combustible Dusts in Air*. International Organization for Standardization.

Klein, A. J. J., van der Voort, M. M., van Zweden, A., & van Ierschot, P. G. A (2005a). Validating CFD-code 'DESC'; *Large scale dust explosions in linked enclosed vessels*, Report DV2 2005 CO24, TNO, Rijswiik, the Netherlands.

Klein, A. J. J., van der Voort, M. M., & Versloot, N. (2005b) *Large scale dust explosions in linked enclosed vessel*s. In: International ESMG symposium, Nürnberg, Germany, 11-13 October 2005, (9pp.).

Kauffman, C.W., S. R. Srinath, F. I. Tezok. (1984). Turbulent and accelerating dust Flames. *Proceedings of the 20th Symposium (International) on combustion/The Combustion Institute*

Levi, L. (1980), *Applied Optics*. Vol. 2, John Wiley & sons, New York, USA

Li, Y.C., W. Kauffman and M.Sichel (1995). An experimental study of deflagration to detonation transition supported by dust layers. *Combustion and Flame*, 100, pp. 505-515

Pu, K. Y., J. Mauzurkiewicz, J. Jarosinkski, C. W. Kauffman (1988). Comparative study of the influence of obstacles on the propagation of dust and gas flames. *Twenty-second symposium (International) on combustion/The Combustion Institute*

Rako, P. (2004). *Photodiode amplifiers changing light to electricity*. National Semiconductor Corporation, obtained from www.national.com

Ray, B. (1978). Detection of fires and explosions. *Phys. Technol*., Vol. 9

Siwek R. (1996). Determination of technical safety indices and factors influencing hazard evaluation of dusts. *Journal of Loss Prevention in the Process Industries* 9, pp.21-31.

Skjold, T. (2003). *Selected aspects of turbulence and combustion in 20-litre explosion vessels*. Cand. Scient. Thesis, University of Bergen

Skjold, T., R. K. Eckhoff, G. A. Enstad, I. B. Kalvatn, M. van Wingerden, K. van Wingerden (2008), A modified balloon experiment for dust explosions, *Thirty-second International Symposium on Combustion*, Work-in-Progress Poster Session, Montreal

Tezok, F., W. C. Kauffman, M. Sichel, J. A. Nicholls (1985). Turbulent burning velocity Measurments for dust/air mixtures in a constant volume spherical bomb. Paper presented at *10th International Colloquium on Dynamics of Explosions and Reactive systems*, Berkley, CA,

"The Temperature Handbook" (2004). Middlesex UK: Labfacility Ltd

U.S. Chemical Safety and Hazard Investigation Board, Investigation Report, *Combustible Dust Hazard Study*, 2006, Report No. 2006-H-1, obtained from www.csb.gov

Appendix A – Experimental Apparatus and Procedures

A.1 Dispersion System

The dispersion systems consist in essence of a pressurized reservoir, an outlet valve, a dust reservoir, and a dispersion nozzle. Figure A-1 shows the dispersion nozzles situated in the FAT. The desired amount of dust is placed inside the dust reservoir, while the pressure inside the pressurised reservoir is adjusted up to 16 bar(g). Before dispersion the pressure inside the FAT is pumped down to 0.65 bar(a) so that the pressure in the FAT after dispersion with pressurised air equals atmospheric pressure. The outlet valve between the pressurized reservoir and the dust reservoir is activated by a trigger signal from the computer and the dust is subsequently dispersed into the FAT via the dispersion nozzle. In order to be able to measure the pressure development during the dispersion process a piezoelectric pressure sensor can be fitted into the pressurised reservoir.

There are three of these dispersion systems in the FAT and each can be triggered in turn in order to optimize the dispersion relative to ignition. During testing with gas in the FAT instead of dust, the purpose of the dispersion system is to mix the gas with air. The gas is then filled into the FAT before dispersion via a separate gas filling system, and when the pressurised air flows out of the dispersion nozzles it creates turbulence and mixes the gas and air.

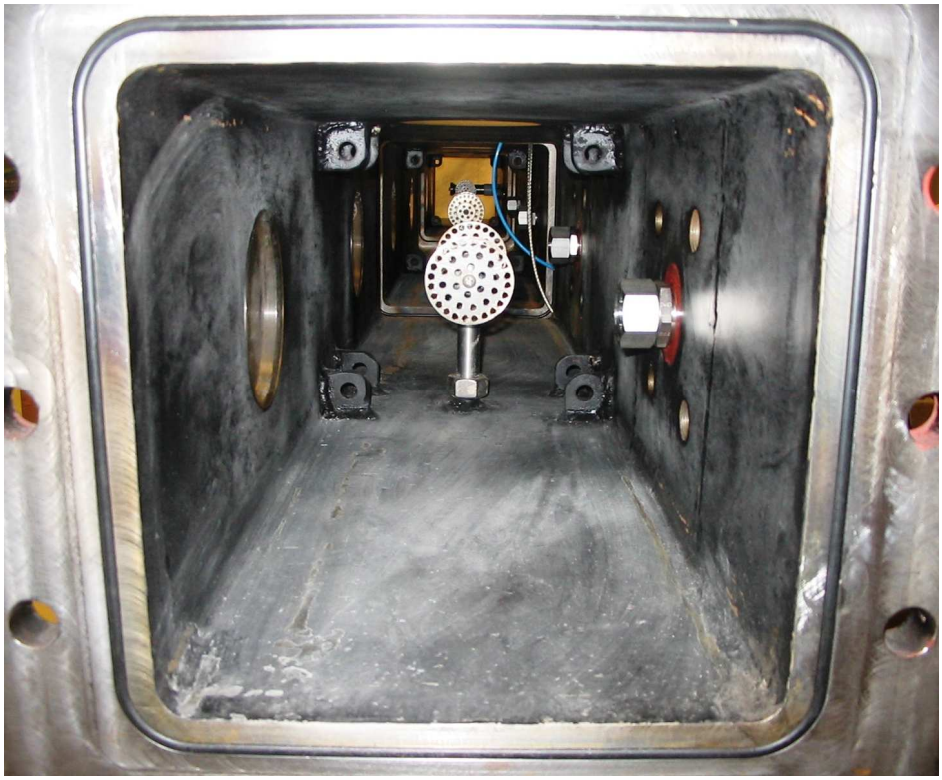

Figure A-1 Dispersion nozzles situated in the FAT

A.2 Electric Spark Generator

An electric spark generator has been made for preliminary experiments for both this project and others e.g. the modified balloon experiment. However, it did not generate enough energy to ignite pure dust clouds and was therefore only used for gas mixtures and hybrid mixtures with gas and dust. The energy generated has been estimated at around 50 mJ. Figure A-3 shows the schematic for the generator. The part list is shown in Table A-1 The electronics of the generator is built into a cabinet with the size of 25 x 20 x 11 cm (L x W x H) and a handle on the top. The electrical circuit board within the spark generator has been made at the UiB.

The basic principle of the generator is to discharge a capacitor that has been loaded by electricity from the regular power net. Either a negative or a positive flank of voltage can manually, or externally trigger the spark generator. The desired setting is chosen on the front panel of the spark generator. The possibility to externally trigger the spark discharge makes it easy to trigger the spark from a computer, thus it is implemented in the Labview program for running the FAT experiment. Figure A-2 below shows the inner parts of the generator.

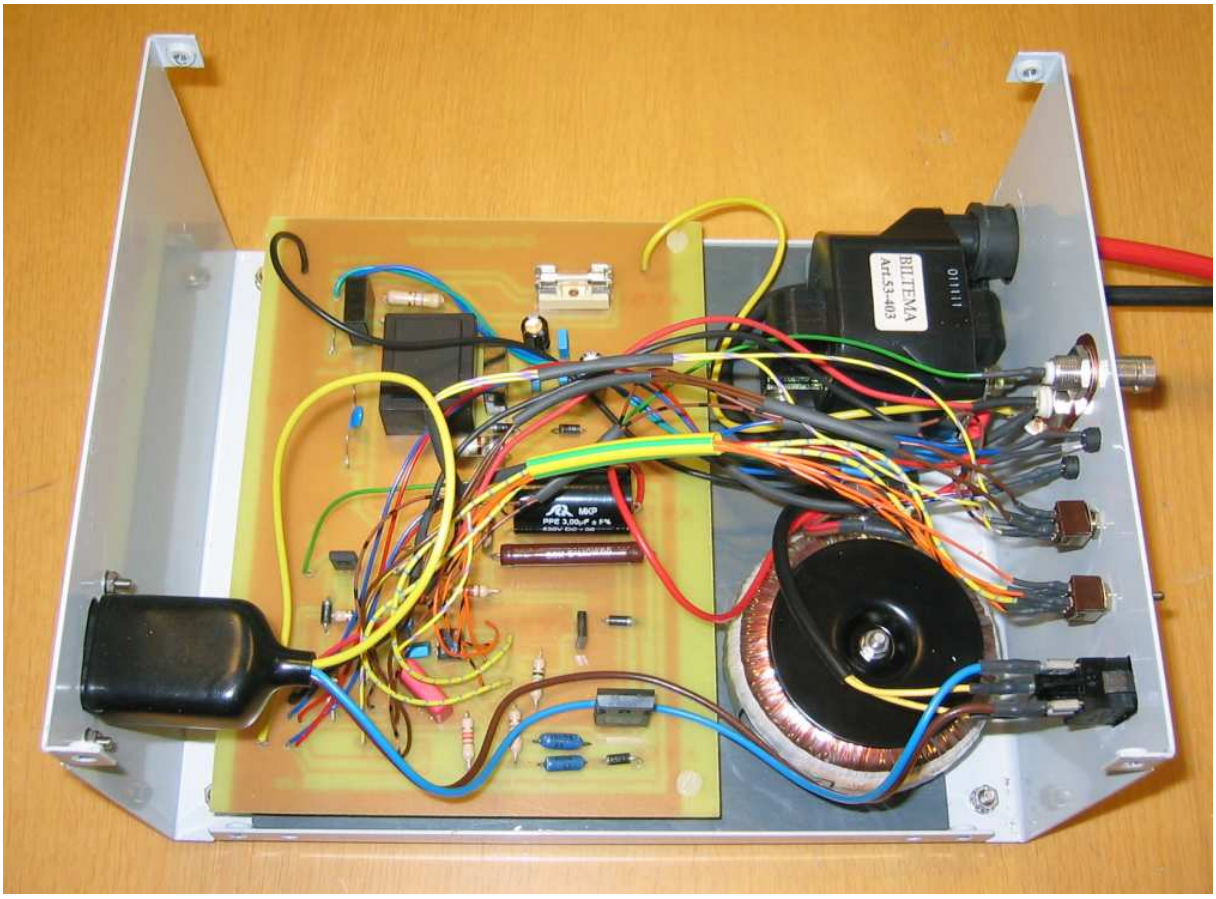

Figure A-2 Inner parts of the electric spark generator

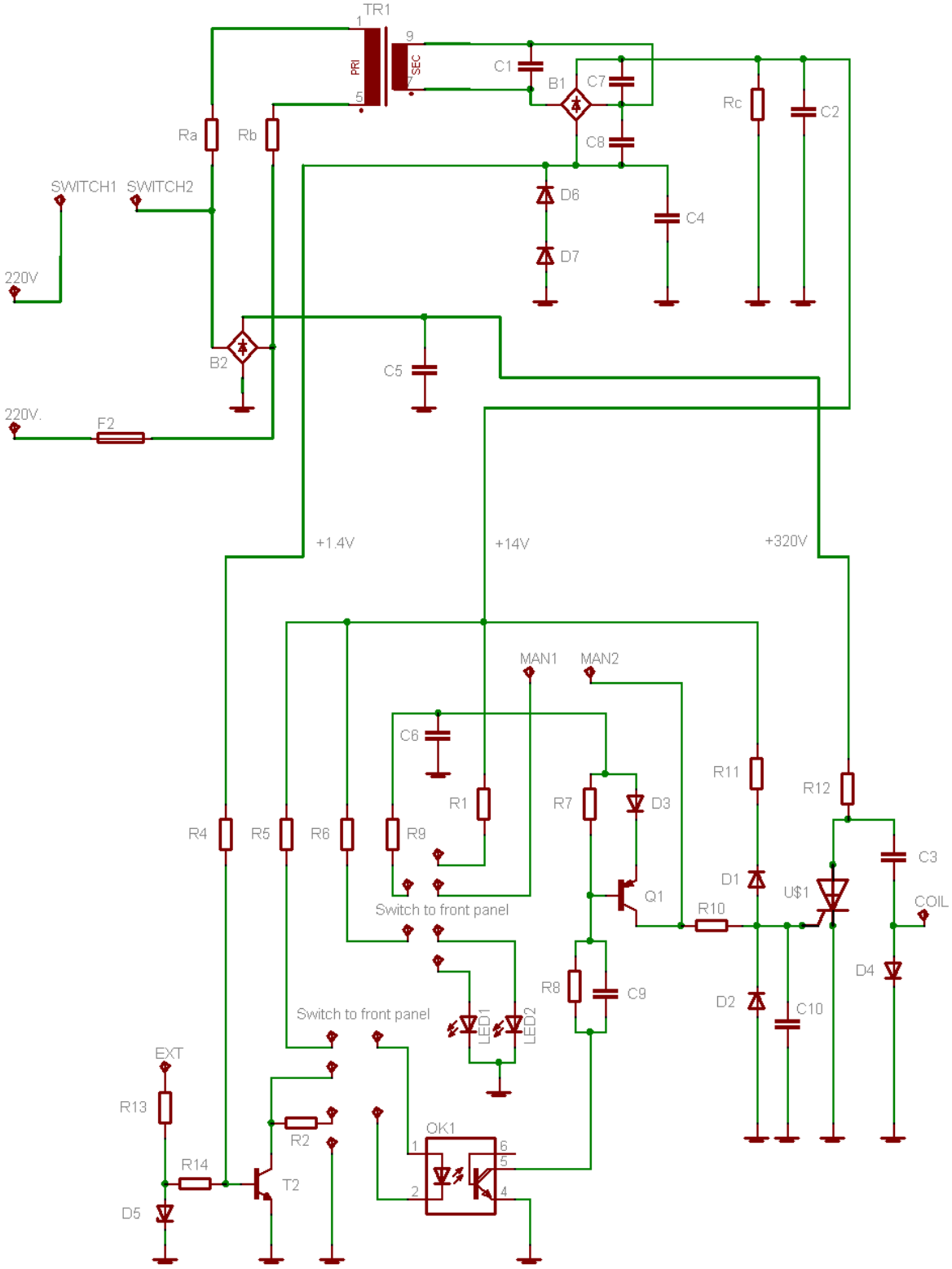

Figure A-3 Electrical circuit for spark generator

Table A-1 Part list for spark generator

Part	Value	Device	
C3	1u/500V	C-EU275-113X316	capacitor
C6	2.2u	C-EU050-025X075	capacitor
C9	0.1u	C-EU025-024X044	capacitor
C10	0.1u	C-EU050-025X075	capacitor
D1	1N4004	1N4004	diode
D2	1N4004	1N4004	diode
D3	1N4004	1N4004	diode
D4	1N4004	1N4004	diode
D5	1N821	1N821	diode
LED1		LED5MM	led
LED2		LED5MM	led
OK1	4N33	4N33	optocoupler
Q1	BD140	BD140	transistor-pnp
R1	100	R-EU_0207/10	resistor
R2	15	R-EU_0207/10	resistor
R4	10k	R-EU_0207/10	resistor
R5	680	R-EU_0207/15	resistor
R6	1.2k	R-EU_0207/10	resistor
R7	1.2k	R-EU_0207/10	resistor
R8	1.2k	R-EU_0207/10	resistor
R9	220	R-EU_0207/10	resistor
R10	15	R-EU_0207/10	resistor
R11	100	R-EU_0207/10	resistor
R12	58K/2W	R-EU_0617/22	resistor
R13	470	R-EU_0207/10	resistor
R14	120	R-EU_0207/10	resistor
T2	BD139	BD139	transistor
U$1	30TPS08	30TPS08	triac
B1		SKB	rectifier
B2		SKB	rectifier
C1	0.1u	C-EU050-025X075	capacitor
C2	100u	C-EU050-025X075	capacitor
C4	100u	C-EU050-025X075	capacitor
C5	0.01u/400V	C-EU275-093X316	capacitor
C7	0.1u	C-EU050-025X075	capacitor
C8	0.1u	C-EU050-025X075	capacitor
D6	1N4004	1N4004	diode
D7	1N4004	1N4004	diode
F2		SH22,5A	fuse
Ra	470/1W	R-EU_0411/15	resistor
Rb	470/1W	R-EU_0411/15	resistor
Rc	680/1W	R-EU_0411/15	resistor
TR1		EI30-1	trafo
coil		Art.53-403	Biltema

A.3 Thermocouples

A thermocouple basically consists of a junction of two different metals. The junction creates a small voltage which increases with temperature. There is a variety of different thermocouples and they are classified by which materials the junction is made of. The most common type of thermocouples is type k, which is used in this project, where the two materials in use are Nickel-Chromium and Nickel-Aluminium. Its temperature range is from -200°C to 1100°C, its sensitivity is approximately 41µV/°C and they got an accuracy of about ±2.5°C (The temp. handbook). The thermocouples are bought from Elfa and the thickness of the metal wires is 0.3 mm. As shown in Figure A-4 below the use of thermocouples can be very easy using only a voltmeter.

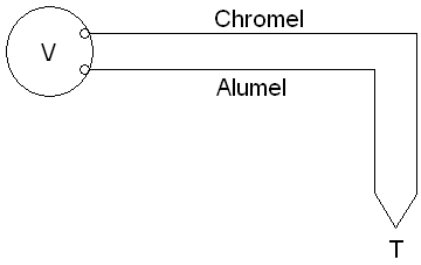

Figure A-4 Schematic of temperature measurements using a thermocouple and voltmeter

However, when sampling during continuous measurements, one has to amplify the signal from the thermocouple in order to get a strong signal and clear signal. Figure A-5 shows the thermocouple circuit used in this thesis, including an operational amplifier (AD597). With this circuit an output voltage of 0V corresponds to a temperature of 0°C, 0.1V corresponds to 10°C, 1V corresponds to 100°C and so on.

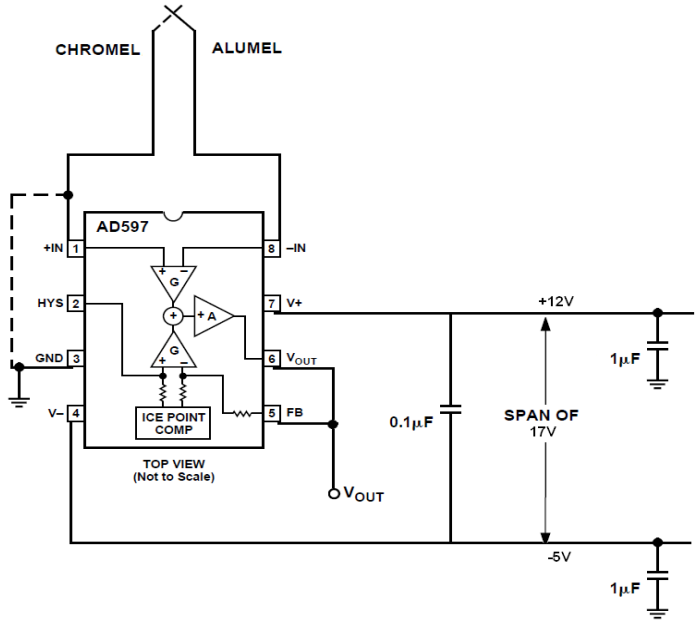

Figure A-5 A thermocouple circuit including an operational amplifier

The thermocouple probes are designed to fit both the 20-litre vessel at UiB and the FAT at Gexcon. Figure A-6 shows a picture of one of the thermocouple probes. The probe holders have been made by the mechanics at the Mechanical workshop at UiB, the welding of the thermocouples is done by the use of a self-made welding apparatus.

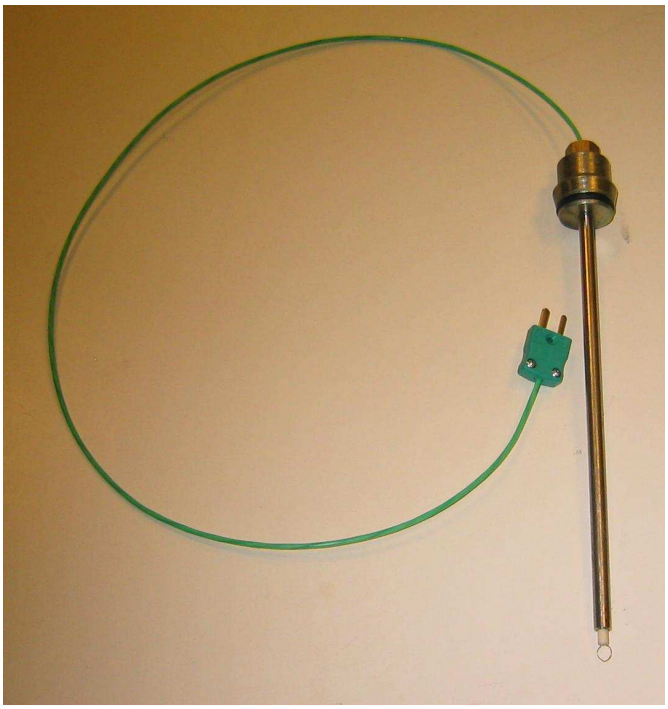

Figure A-6 Thermocouple probe

A.4 Welding Apparatus for Thermocouples

Figure A-7 shows the apparatus that has been made for welding together the two metal wires that the thermoelement consists of. The basic principle behind the apparatus is to first charge a condensator with power from the regular power net via a rectifier, and then to discharge it across the two wires (Figure A-7). This is done by, at one end of the cable, connecting one wire to the positive part of the condensator and the other to the negative part. At the other end of the cable the two wires are gently pushed against eachother until contact is made, and the condensator then discharges through the wires. The wires are then welded together.

To further improve the result, argon is added to the welding point during the process in an attempt to exel oxygen from the welding zone. This will, to some extent, prevent combustion to take place, and the melting/welding of the two materials will be the more dominant process.

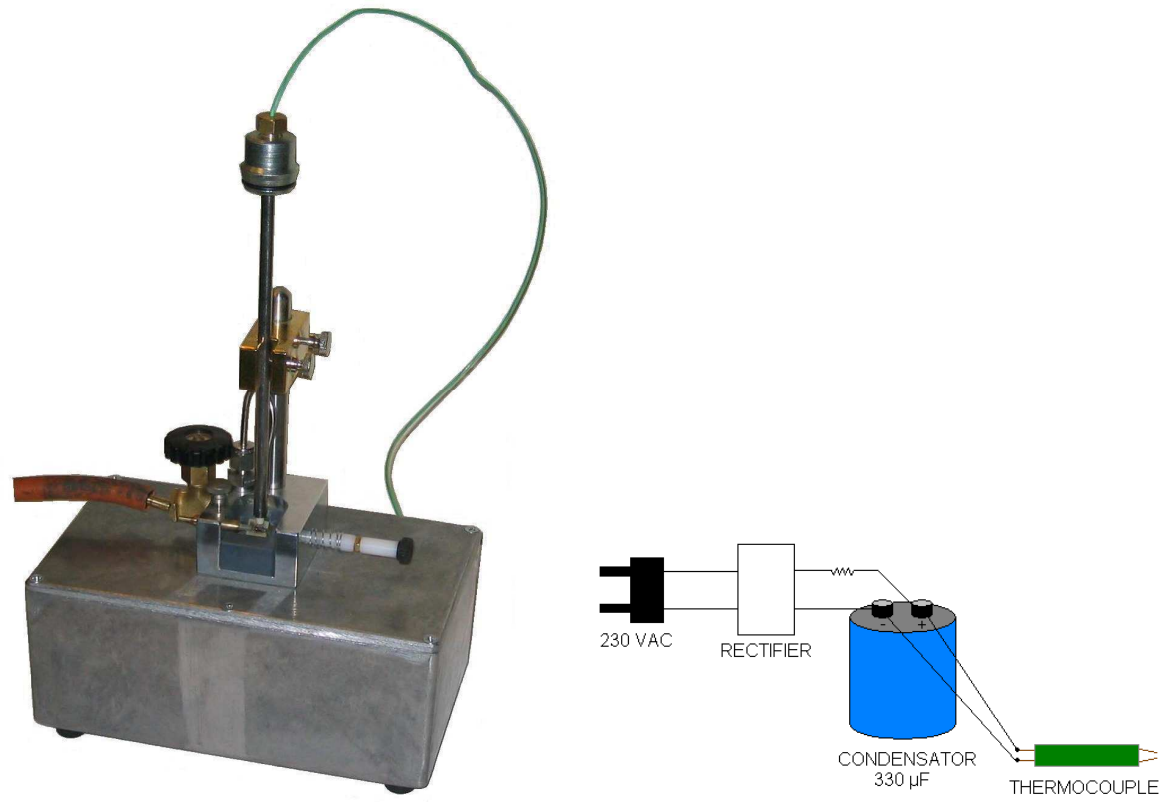

Figure A-7 Left: welding apparatus for thermocouples. Right: simple schematic for welding apparatus.

A.5 Power Supply

A.5.1 V Power-supply circuit

Within the self-made power-supply, there is a circuit which gives an output voltage of 5V and also consists of a trigger function. The 5 V power supply is mainly used for various measurement instruments. Figure A-8 and A-9 below shows the schematic and print board for this circuit.

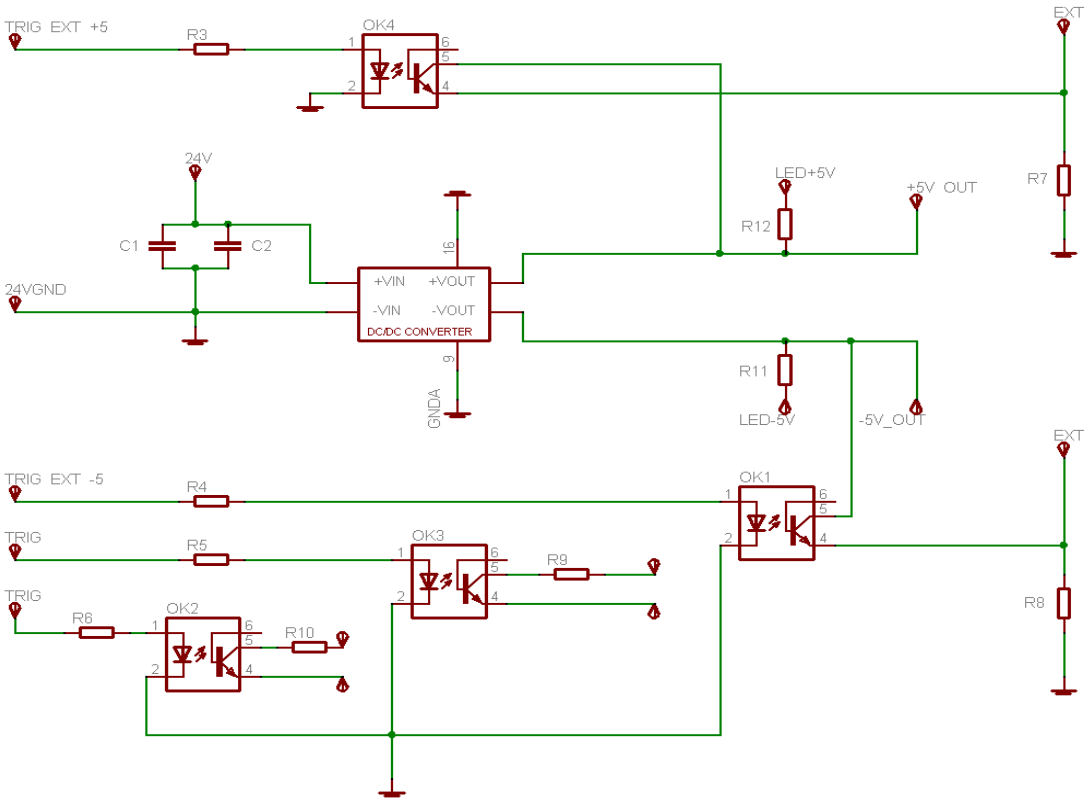

Part	Value	Device	
C1	10u	C2.5/4	capacitor-wima
C2	0.1u	C2.5/4	capacitor-wima
OK1	SFH601G	SFH601G	optocoupler
OK2	SFH601G	SFH601G	optocoupler
OK3	SFH601G	SFH601G	optocoupler
OK4	SFH601G	SFH601G	optocoupler
R3	1k	R-EU_0207/12	resistor
R4	1k	R-EU_0207/12	resistor
R5	1k	R-EU_0207/12	resistor
R6	1k	R-EU_0207/12	resistor
R7	100k	R-EU_0207/12	resistor
R8	100k	R-EU_0207/12	resistor
R9	0	R-EU_0207/12	resistor
R10	0	R-EU_0207/12	resistor
R11	470	R-EU_0207/12	resistor
R12	470	R-EU_0207/12	resistor
U$1	TEN5-2421	TEN5-2421	dc-dc-converter

Figure A-8 Schematic of 5V circuit with belonging partlist.

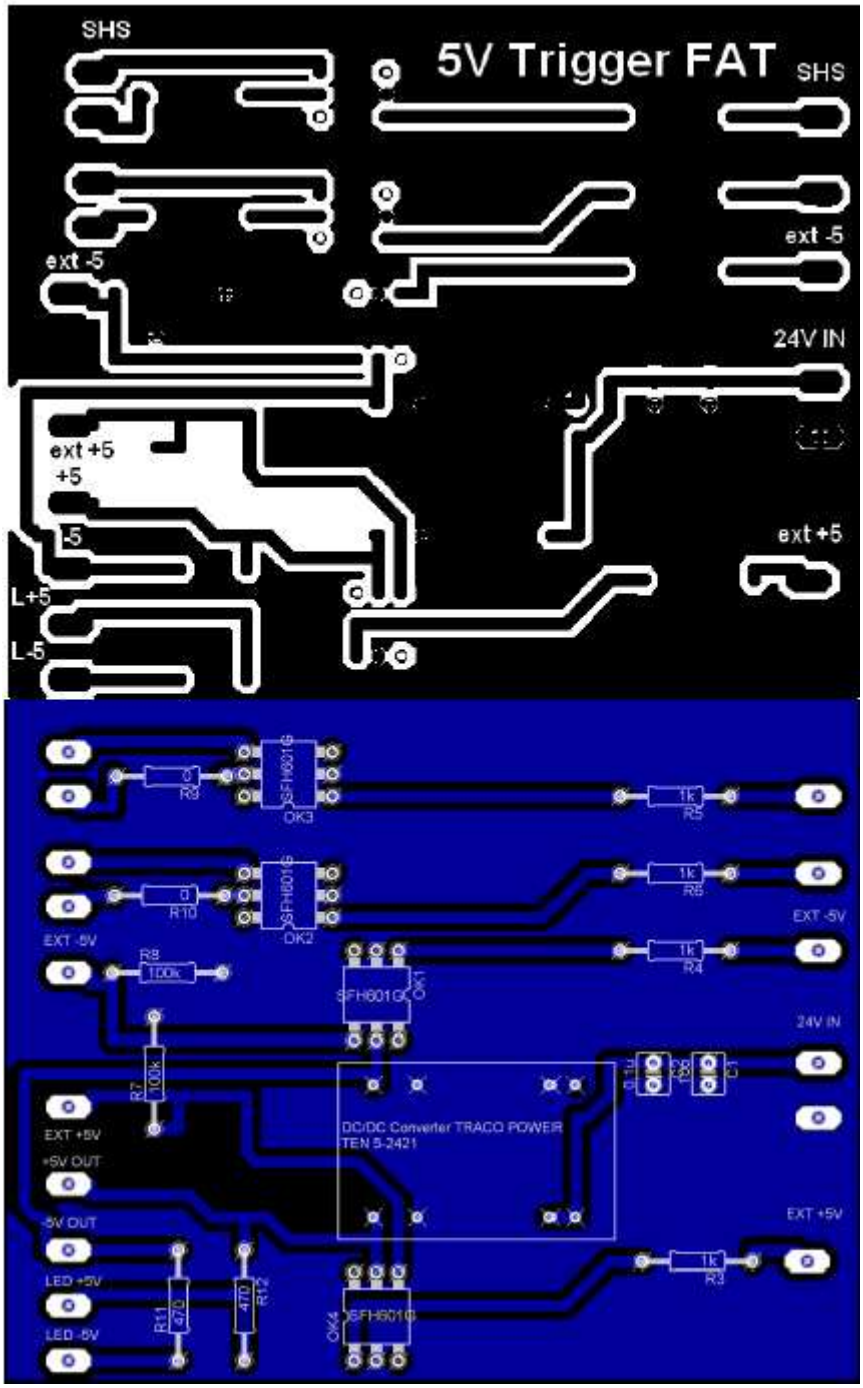

Figure A-9 Circuit board print of 5 V trigger circuit in scale 1:1, with components added on the bottom picture.

A.5.2 12V Power-supply circuit

Within the self-made power-supply, there is a circuit which gives an output voltage of 12V and also consists of a trigger function. The 12V power supply is used for the thermocouples. In Figure A-10 and A-11 below, the schematic and print board is given for this circuit.

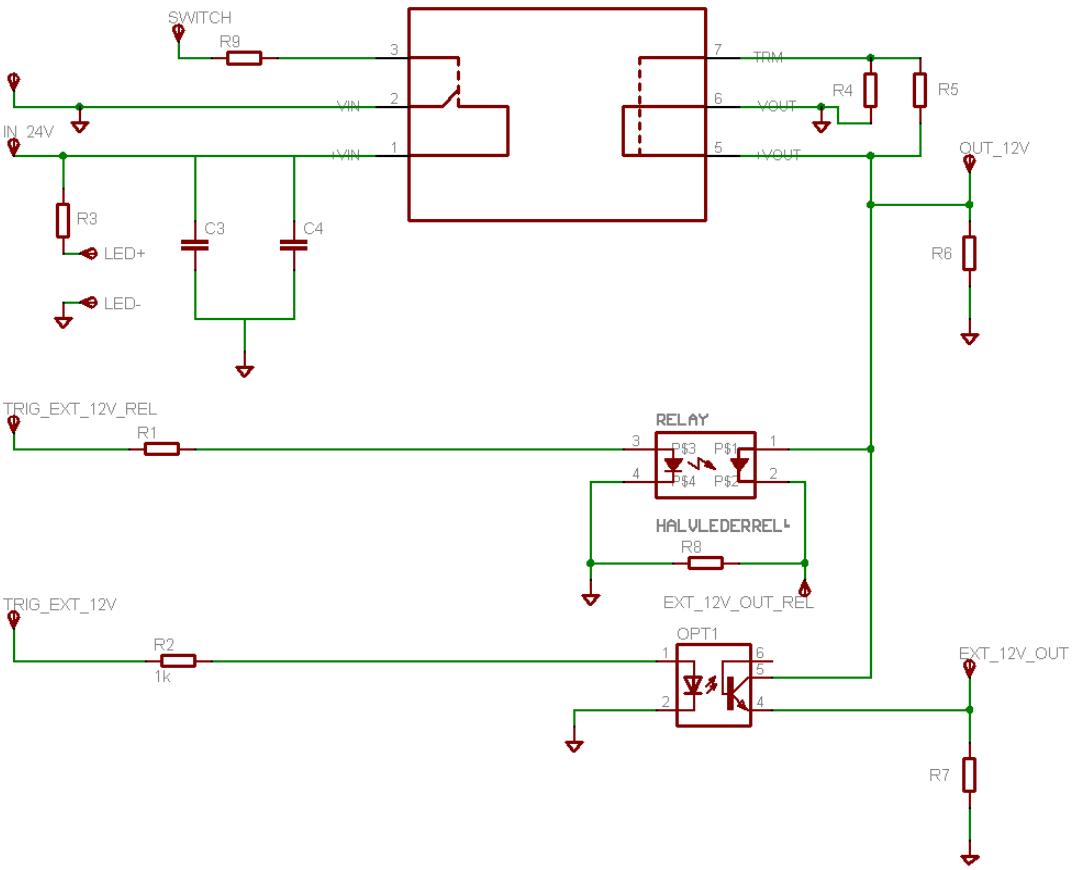

Part	Value	Device	
C3	10u	C2.5/6	capacitor
C4	0.1u	C2.5/6	capacitor
OPT1	SFH601G	SFH601G	optocoupler
R1	0	R-EU_0207/10	resistor
R2	1k	R-EU_0207/12	resistor
R3	1.8k	R-EU_0207/12	resistor
R4	?	R-EU_0309/12	resistor
R5	?	R-EU_0309/12	resistor
R6	100k	R-EU_0309/12	resistor
R7	100k	R-EU_0309/12	resistor
R8	100k	R-EU_0309/12	resistor
R9	0	R-EU_0207/10	resistor
RELAY	HALVLEDERRELÈ	HALVLEDERRELÈ	relay
U$1	TEN25-2412	TEN25-2412	dc-dc-converter

Figure A-10 Schematic of 12V circuit with belonging part list

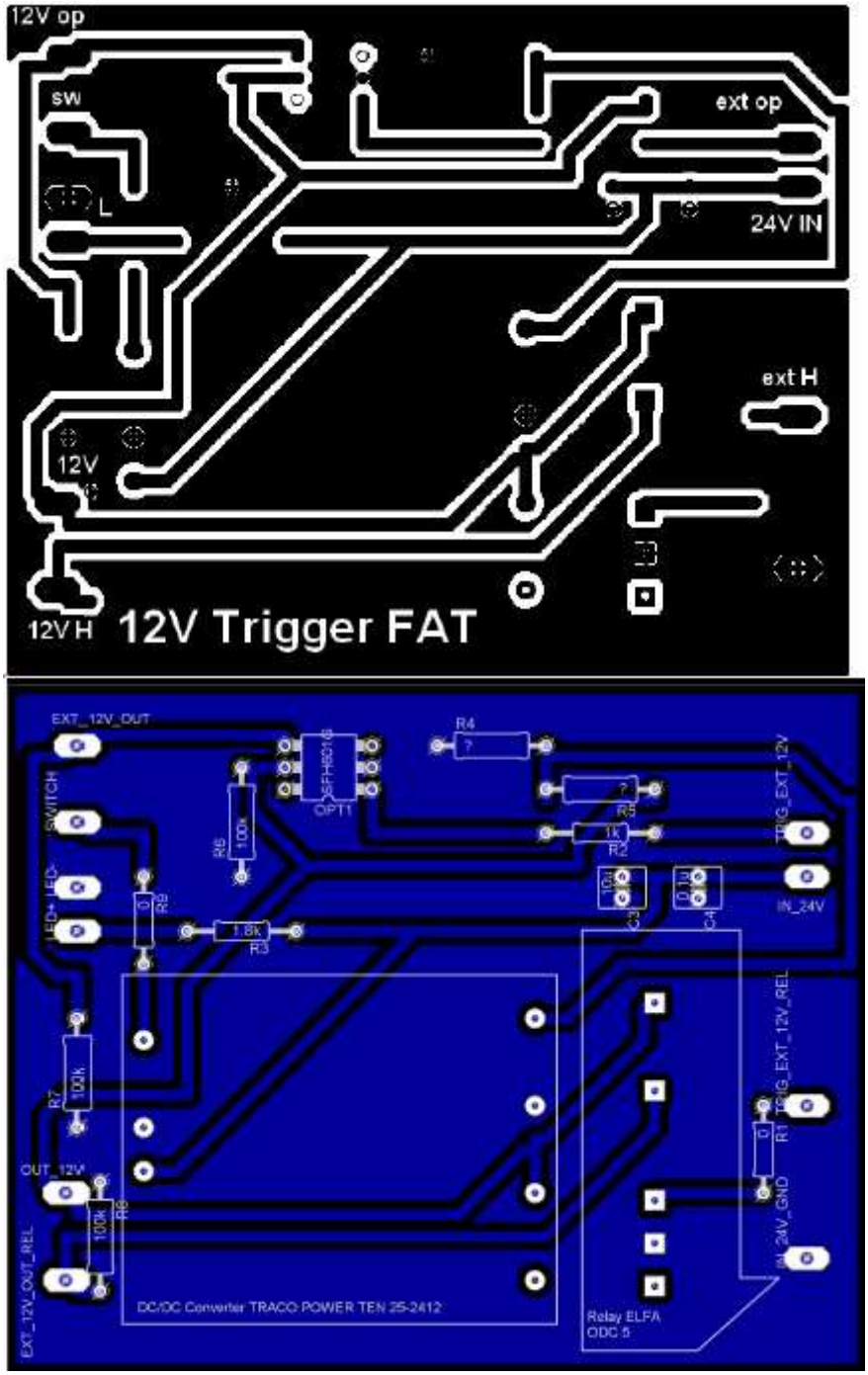

Figure A-11 Circuit board print for 12 V trigger circuit in scale 1:1, with components added on the bottom picture.

A.5.3 24V Power-supply circuit

Within the self-made power-supply, there is a circuit which gives an output voltage of 24V and consists of a trigger function, which is used for the dispersion valves. In Figures A-12, A-13 and A-14 below, the schematic and the print board is given for this circuit.

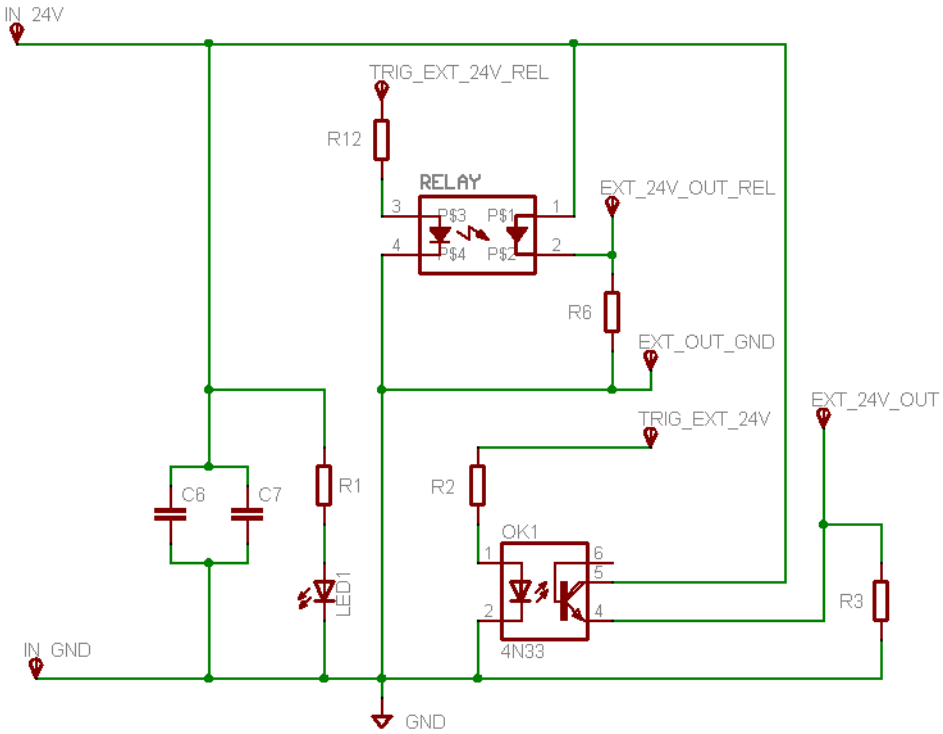

Part	Value	Device	
C6	10u	C-EU050-030X075	capacitor
C7	0.1u	C-EU050-030X075	capacitor
LED1		LED3MM	led
OK1	4N33	4N33	optocoupler
R1	1.8k	R-EU_0411/12	resistor
R2	1.5k	R-EU_0309/12	resistor
R3	100k	R-EU_0204/5	resistor
R6	100k	R-EU_0204/5	resistor
R12	0	R-EU_0411/12	resistor
RELAY	HALVLEDERRELÈ	HALVLEDERRELÈ	relay

Figure A-12 Schematic of 24V circuit with belonging part list

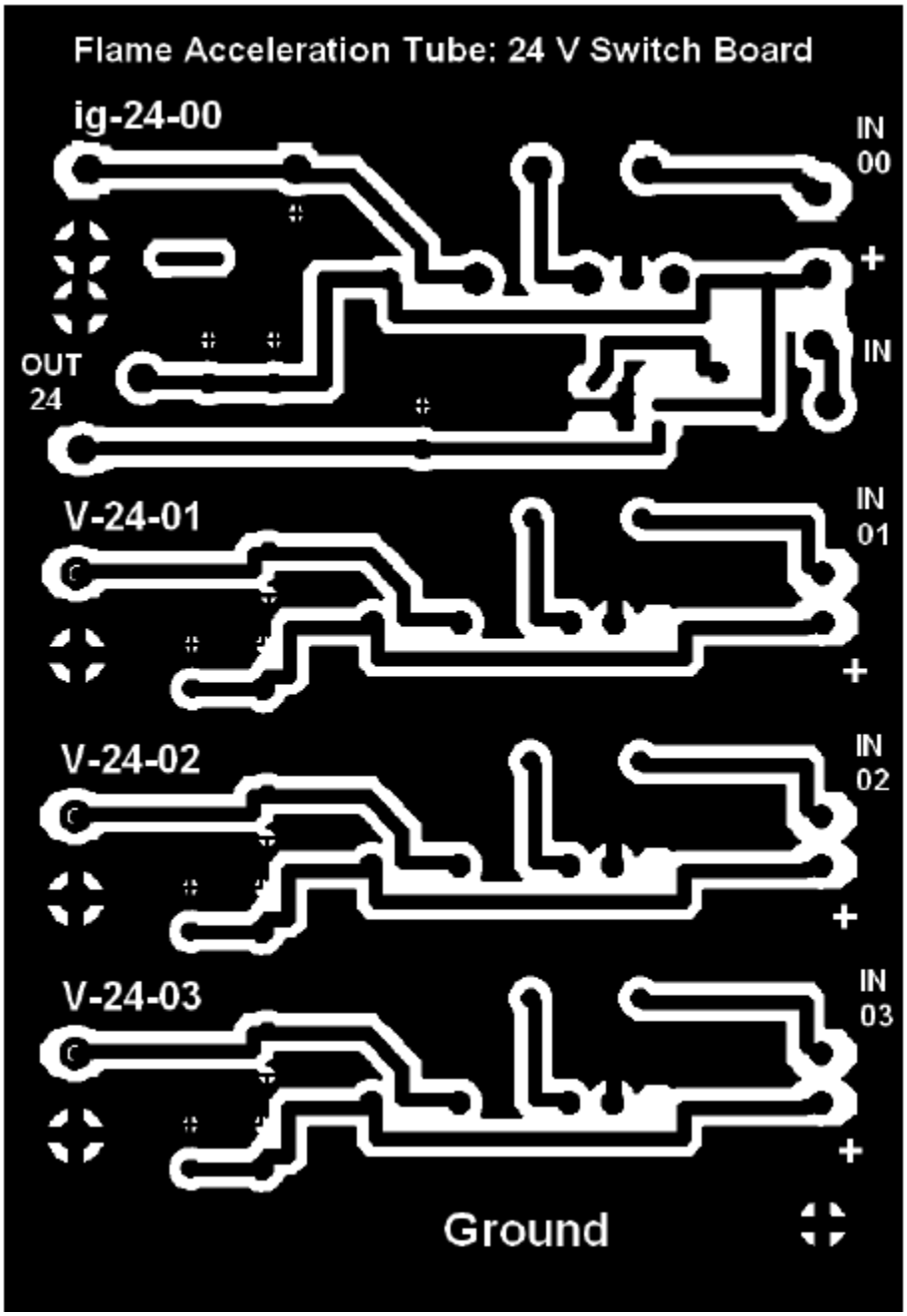

Figure A-13 Circuit board print of 24 V circuit in scale 1:1

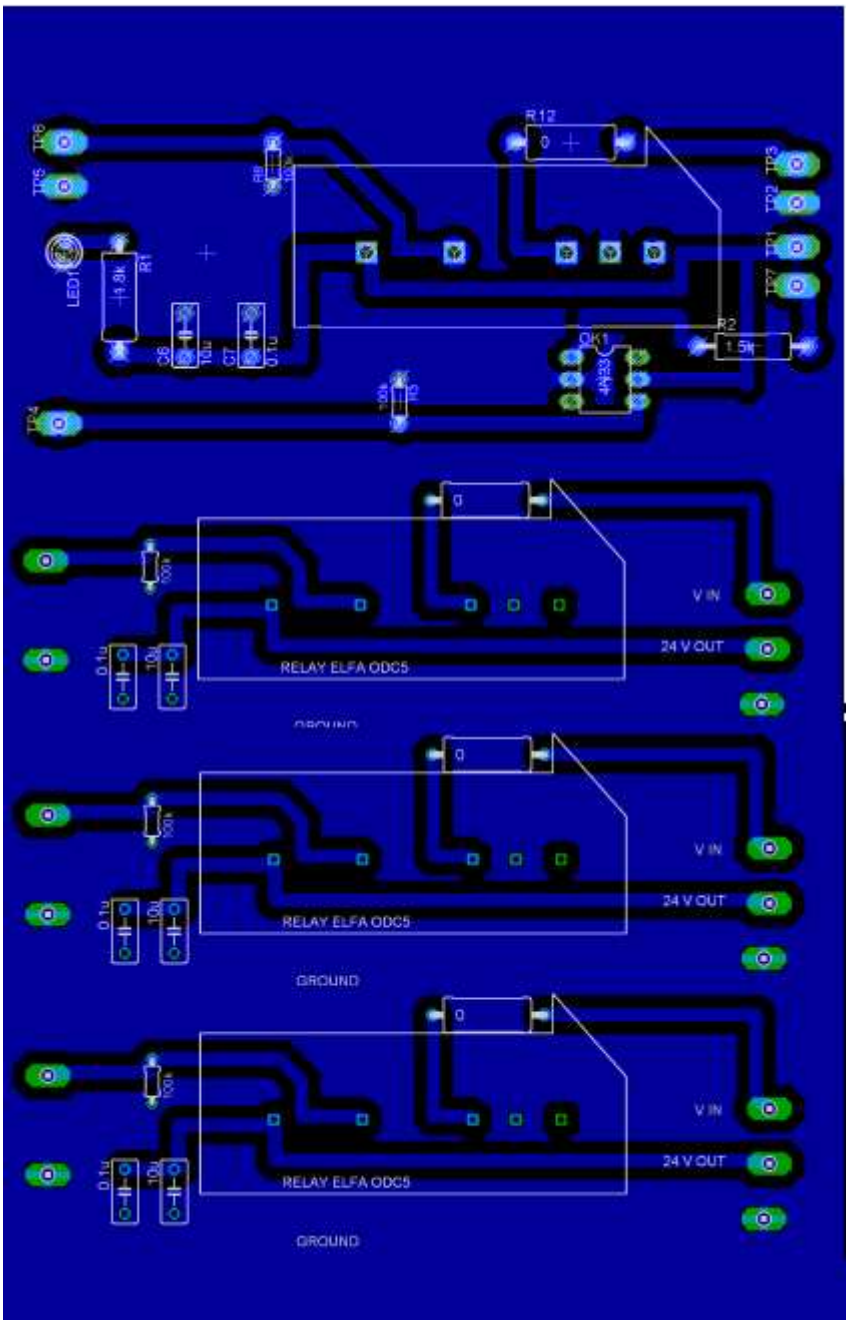

Figure A-14 Circuit board print with components for 24 V circuit in scale 1:1

A.6 Measurement Probe

A.6.1 Mechanical drawing of the measurement probe

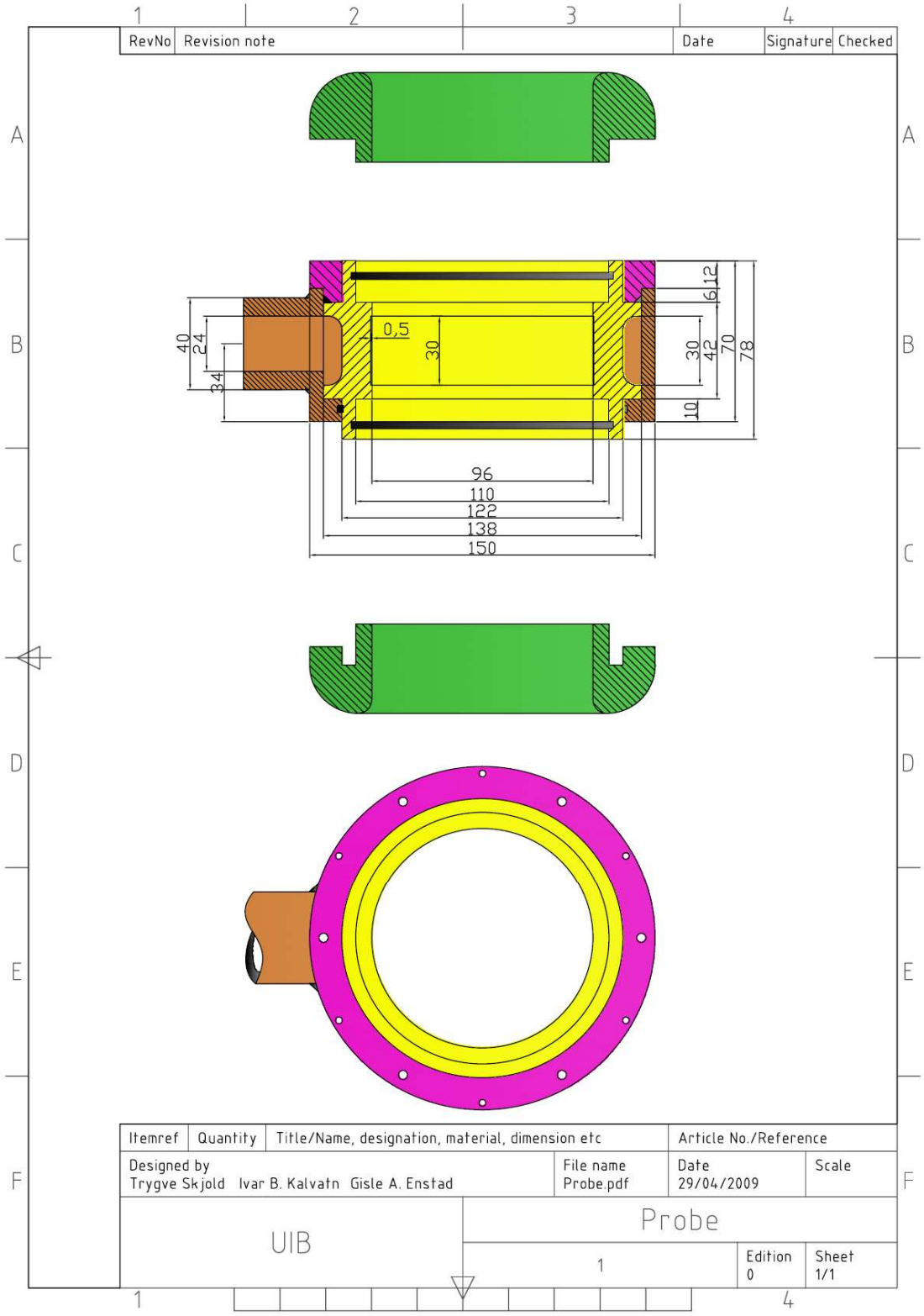

Figure A-15 Mechanical drawing of the optical/capacative probe

A.6.2 The LED power supply

An astable multivibrator powers the LED within the optical dust probe. The design of the astable multivibrator is shown in Figure A-16 below.

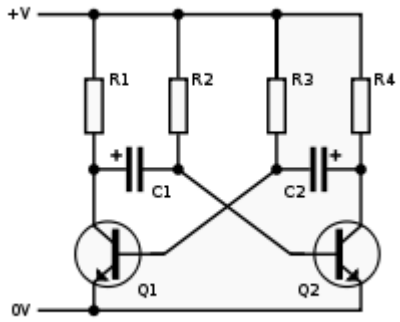

R1, R4 = 18 Ω

R2, R3 = 680 Ω

C1, C2 = 10 µF

Q1,Q2 = NPN transistor BC547

Q1, Q2 = transistor BC 547

Figure A-16 Schematic of an astable multivibrator

This design produces a near to square wave signal. This circuit with the values of resistors and capacitors as indicated above, yields a frequency of about 150 Hz. Each astable multivibrator powers two LEDs. The circuit board has been printed at the electro lab at the UiB and the circuit board print is shown in Figure A-17 in scale 2:1.

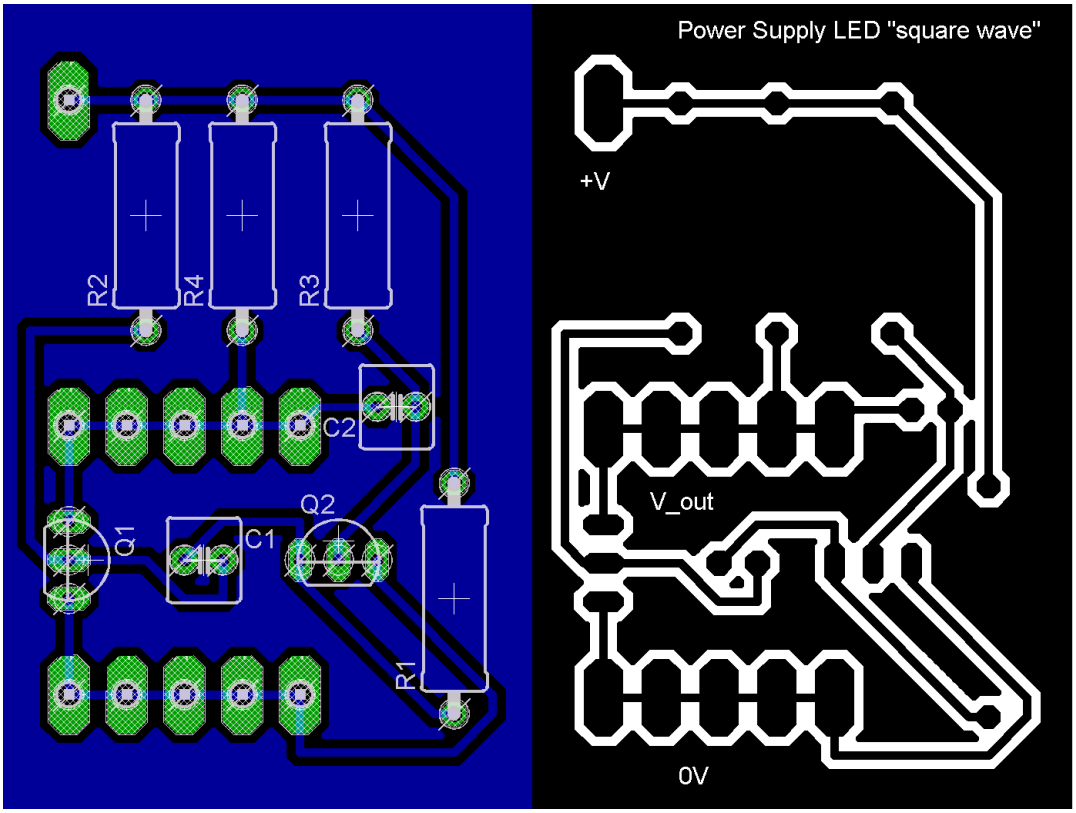

Figure A-17 Circuit board print for the astable multivibrator in scale 2:1 with the components added on the picture to the left

A.6.3 Signal amplifier for photodiode

In order to get an adequate signal for measurements with the NI logging card, signal amplifiers has been made for each photodiode. Figure A-18 shows the design for these amplifiers. The design is mainly based upon Rako (2004). As pointed out by Rako (2004) it is tricky to find an optimal design for photodiode amplifiers for different cases, and indeed it has required a lot of trial and error to find a design that works. The amplifiers are powered by the power supply by -5V to +12V. The circuit boards are printed at the UiB. Please note that Q1 and R3 was added to the design after the circuit boards were made, and were mounted directly on the board and existing components.

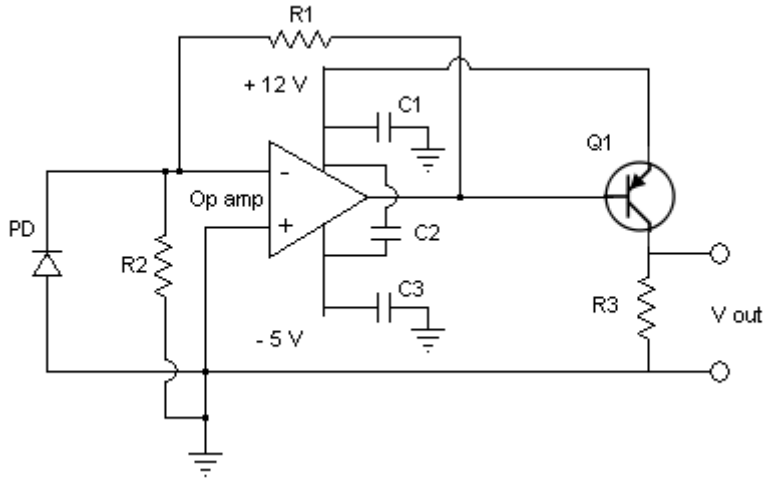

C1 = 1 µF
C2 = 1 µF
C3 = 1 µF
R1 = 1,0 MΩ
R2 = 39Ω
R3 = 200 Ω
Q1 = BC 547
PD = photodiode OP 905
Op amp = OP 64G

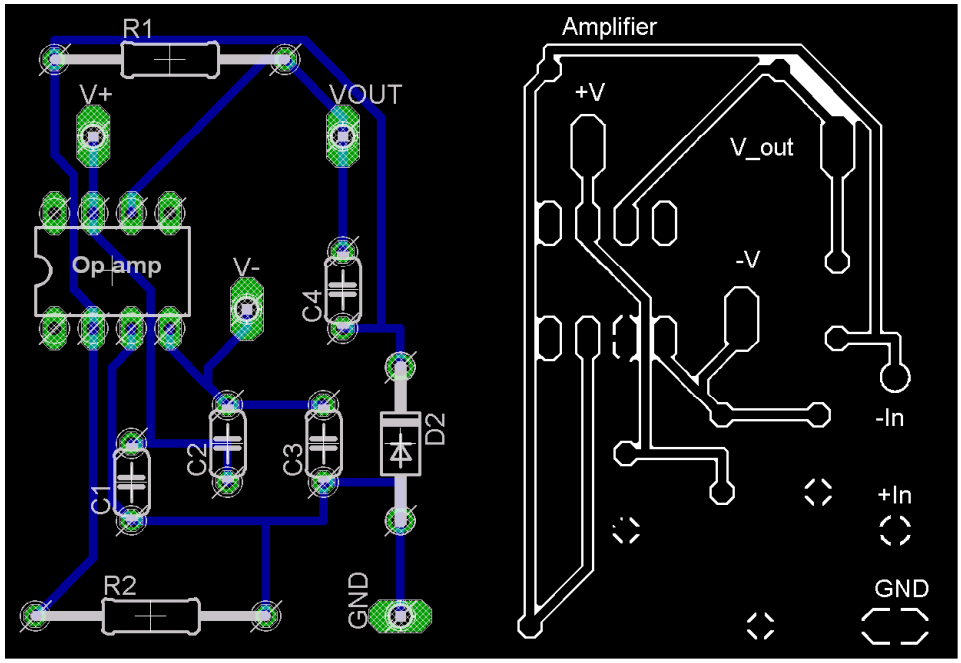

Figure A-18 Upper: schematic for signal amplifiers for photodiodes. Lower: circuit board print for signal amplifier in scale 2:1 with components added on the picture to the left.

A.6.4 Flushing system for the optical probe

It was attempted to use a flushing system to clean the windows in front of the diodes. However, the air tubes connected to the measure-heads (Figure A-19) could not withstand the pressure and temperature from a propane/air-explosion, and jumped out of their positions during the explosion. Due to the restricted time available for doing the experiments, it was decided to plug the system for the tests presented in this thesis. A way to fix the flushing system would be to replace the plastic air tube with brass pipes for a few centimetres out of the measure-head. This way the cooling effect from the brass will prevent the plastic air tube from jumping out of position. However, it will require rebuilding of the measure-head in order for the plug-in system of the measure-heads to work. The brass pipes must be connected to the measure-heads in such a way that they can be mounted while the measure-heads are situated within the probe.

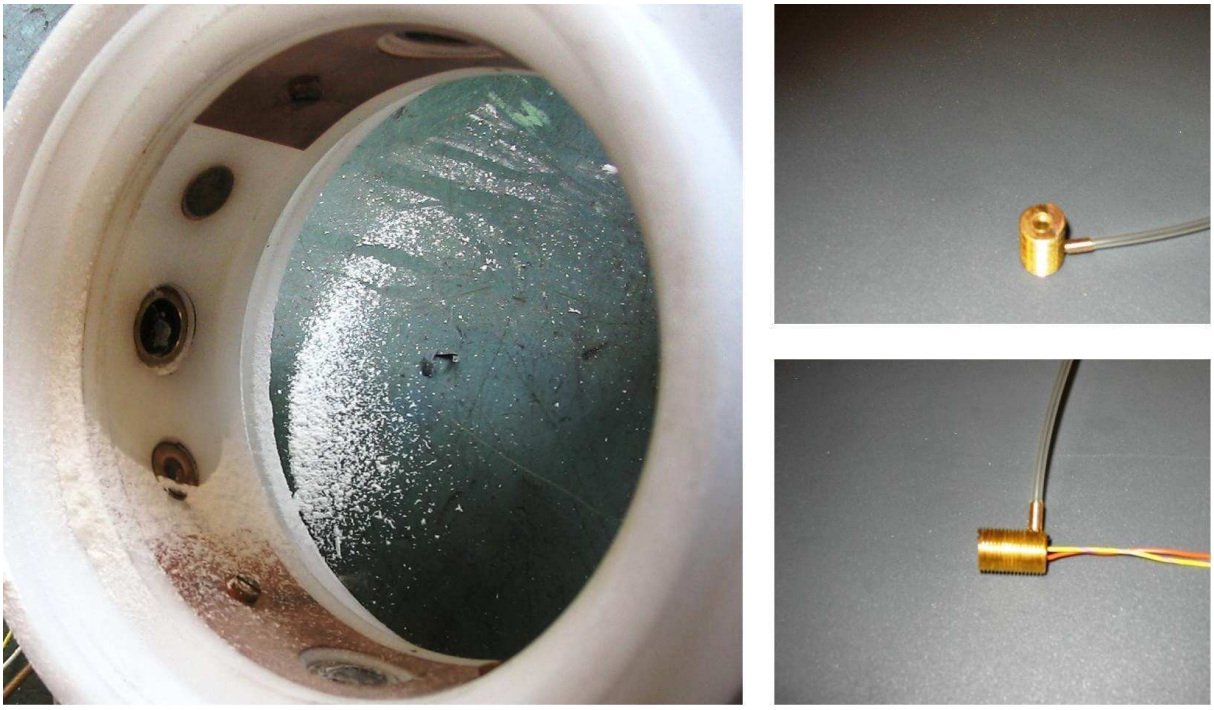

Figure A-19 Left: result from flushing of a window while sifted maize starch fell down on the window. Right: measure-heads with air tubes connected to them.

A.7 User Documents for the FAT

A.7.1 Checklist – FAT

In Table A-2, a checklist for experiments in the FAT is viewed. This checklist is a tool for remembering the most important things in terms of safety and measurements when performing experiments.

Table A- 2 Checklist for the experimental procedure for experiments in the FAT

What to check	
Vacuum	_____ barg
Reservoir pressure	_____ barg
Security valve closed	
Specify filename in labview	
Reset signal amplifier for reservoir pressures	
Close reservoir valves	
Check test number	
Secure area	
Spark generator on	

A.7.2 User guide for the Labview program for running the experiment

A program was made, based on Labview, in order to run the experiment. In the front panel of the program, shown in Figure A-20, timing of dispersion and ignition can be set. In the block diagram, shown in the same figure, input/output-channel settings can be chosen by the use of the data acquisition (DAQ) assistants. To activate the program, press the arrow button in the upper left corner of the front panel. This button does not start the experiment. To make the program ready to start press the OK button. The experiment can now be activated by the externally trigger switch, which is connected to the NI-logging card. Before every experiment it is important that the file name for the logging file is defined. This can be done via the file path dialog box.

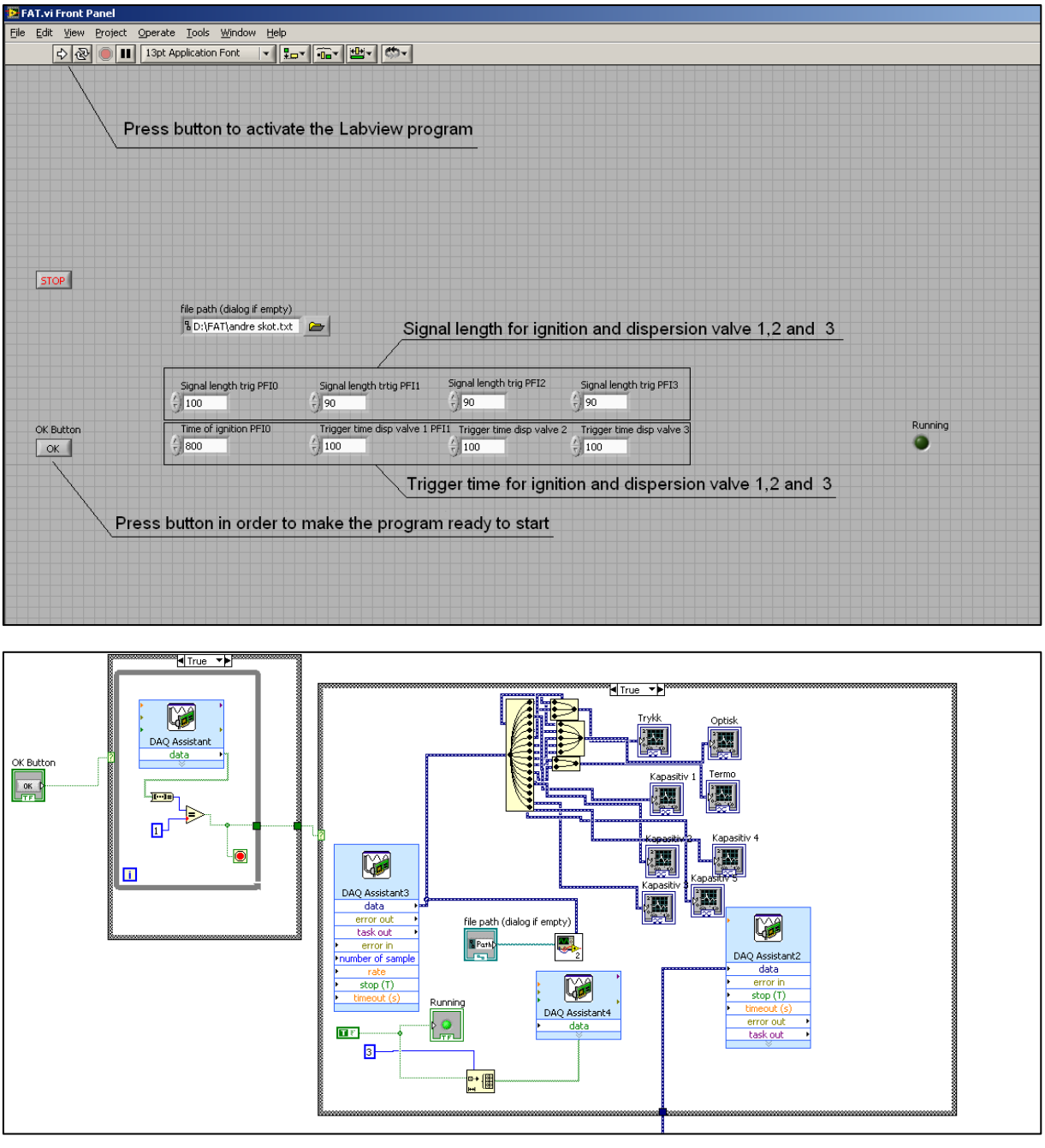

Figure A-20 Upper: front panel for the program. Lower: part of the block diagram with the DAQ assistants.

Appendix B – Measurement Data and Analysis

B.1 Videos and Flame Arrival/Speed and Pressure Measurements in the FAT

Table B-1 views the log for the experiments while pressure measurements are presented in Table B-2. Table B-3 shows data from video observations as well as results from the measurements done with the optical/capacitive probes and the thermoelement in the FAT. Figure B-1 and B-2 shows pictures from the videos recorded of test 7 and 16.

Table B-1 Log for the experiments in the FAT

Log						
Propane/air-mixtures						
Test number	consentration	dispersion 1	dispersion 2	dispersion 3	ignition	comment
5	4,5	100	100	100	800	
6	4,5	100	100	100	800	No video
7	4,5	100	100	100	800	
8	2,4	100	100	100	800	No ignition
9	2,8	100	100	100	800	No initial turbulence, 0,4% filled in ignition end
10	3	100	100	100	800	
11	3	100	100	100	800	
12	6	100	100	100	800	
13	6	100	100	100	800	chemical igniter
14	3	100	100	100	800	no ignition
15	3	100	100	100	800	no initial turbulence
Maize starch						
Test number	consentration	dispersion 1	dispersion 2	dispersion 3	ignition	comment
16	500	100	100	100	800	
17	500	100	100	100	800	no ignition
18	500	100	100	100	800	
19	500	100	100	100	800	
20	250	100	100	100	800	
21	250	100	100	100	800	

Table B-2 Pressure development for tests in the FAT

Pressure development for tests in the Flame Acceleration Tube						
Test number	**Probe station**					**Maximum pressure**
	1	2	3	4	5	
	Pressure bar(a)					
6	1,241	1,699	2,715	3,482	5,517	8,58
7	1,168	1,421	1,896	2,208	5,34	8,18
10	1,107	1,2	1,563	2,454	4,198	6,16
11	1,126	1,248	1,835	2,564	3,561	5,78
12	1,189	1,485	2,078	3,261	5,403	7,38
13	1,167	1,4114	1,9861	3,1704	5,316	6,88
16	1,168	1,488	1,983	3,028	4,432	7,28
18	1,166	1,438	1,939	2,9	4,753	7,18
19	1,189	1,461	1,903	2,842	5,181	6,78

Table B-3 Results from measurements after experiments in the FAT

Flame arrival/speed measurements												
		Location										
Test number	Principle	0 (Ignition)	Speed 01	1	Speed 12	2	Speed 23	3	Speed 34	4	Speed 45	5
5	optical probe											
	capacativ probe											
	video	0,000	24	0,025	90	0,032	120	0,037	180	0,040	45	0,053
	thermocouples											
6	optical probe	0,744	20	0,774	75	0,782	150	0,786	200	0,789	100	0,795
	capacativ probe	0,744	17	0,780	120	0,785	120	0,790	300	0,792	75	0,800
	video											
	thermocouples	0,744						0,790				
7	optical probe	0,791	19	0,823	75	0,831	200	0,834	200	0,837	75	0,845
	capacativ probe	0,791	17	0,826	86	0,833	200	0,836	120	0,841	46	0,854
	video	0,000	24	0,025	90	0,032	180	0,035	120	0,040	51	0,052
	thermocouples	0,791						0,842				
8	optical probe											
	capacativ probe											
	video	----------										
	thermocouples											
9	optical probe	0,786	6	0,888	30	0,908	30	0,928	33	0,946	10	1,009
	capacativ probe	0,785	5	0,895	32	0,914	27	0,936	20	0,966	3	1,142
	video	0,000	13	0,047	28	0,068	30	0,088	20	0,118	7	0,203
	thermocouples											
10	optical probe	0,792	4	0,926	26	0,949	32	0,968	33	0,986	8	1,060
	capacativ probe	0,792	4	0,927	22	0,954	38	0,970	12	1,020	16	1,058
	video	0,000	12	0,052	26	0,075	30	0,095	18	0,128	10	0,188
	thermocouples	0,792						0,973				
11	optical probe	0,754	10	0,814	60	0,824	60	0,834	67	0,843	25	0,867
	capacativ probe	0,752	10	0,814	43	0,828	35	0,845	46	0,858		
	video	0,000	21	0,028	51	0,040	51	0,052	36	0,068	17	0,103
	thermocouples	0,754						0,840				
12	optical probe	0,792	18	0,825	50	0,837	100	0,843	100	0,849	50	0,861
	capacativ probe	0,789	15	0,829	75	0,837	75	0,845	60	0,855	30	0,875
	video	0,000	19	0,032	72	0,040	90	0,047	60	0,057	30	0,077
	thermocouples	0,792						0,845				
13	optical probe	0,788	15	0,828	60	0,838	75	0,846	75	0,854	32	0,873
	capacativ probe	0,788	13	0,833	67	0,842	75	0,850	40	0,865	9	0,930
	video	0,000	18	0,033	60	0,043	90	0,050	60	0,060	20	0,090
	thermocouples	0,788						0,849				
14	optical probe											
	capacativ probe											
	video	----------										
	thermocouples											
15	optical probe	0,788	7	0,880	13	0,925	14	0,968	10	1,030	4	1,168
	capacativ probe	0,786	5	0,899	17	0,934				1,100	6	1,200
	video	0,000	6	0,103	13	0,148	16	0,185	7	0,273	3	0,452
	thermocouples											
16	optical probe	0,788	15	0,828	20	0,858	46	0,871	43	0,885	27	0,907
	capacativ probe	0,788	10	0,847	30	0,867	43	0,881	35	0,898	29	0,919
	video	0,000	11	0,053	33	0,072	40	0,087	51	0,098	24	0,123
	thermocouples											
17	optical probe											
	capacativ probe											
	video	----------										
	thermocouples											
18	optical probe	0,788	12	0,838	21	0,867	30	0,887	43	0,901	30	0,921
	capacativ probe	0,788	8	0,865	35	0,882	33	0,900	40	0,915	17	0,951
	video	0,000	9	0,067	30	0,087	40	0,102	51	0,113	24	0,138
	thermocouples											
19	optical probe	0,787		14		0,874	29	0,895	33	0,913	20	0,943
	capacativ probe	0,787		12		0,891	29	0,912	35	0,929	7	1,018
	video	0,000	9	0,070	26	0,093	30	0,113	36	0,130	18	0,163
	thermocouples											
20	optical probe	0,788		9		0,927	4	1,083	3	1,270	----------	
	capacativ probe	0,788		6		0,997						
	video	0,000	5	0,110	8	0,190	3	0,373	2	0,615	----------	
	thermocouples											
21	optical probe	0,787	7	0,875	2	1,269	----------					
	capacativ probe	0,787	4	0,949	1	1,373						
	video	0,000	4	0,150	1	0,570	----------					
	thermocouples											

Figure B-1 Pictures of video from test 7

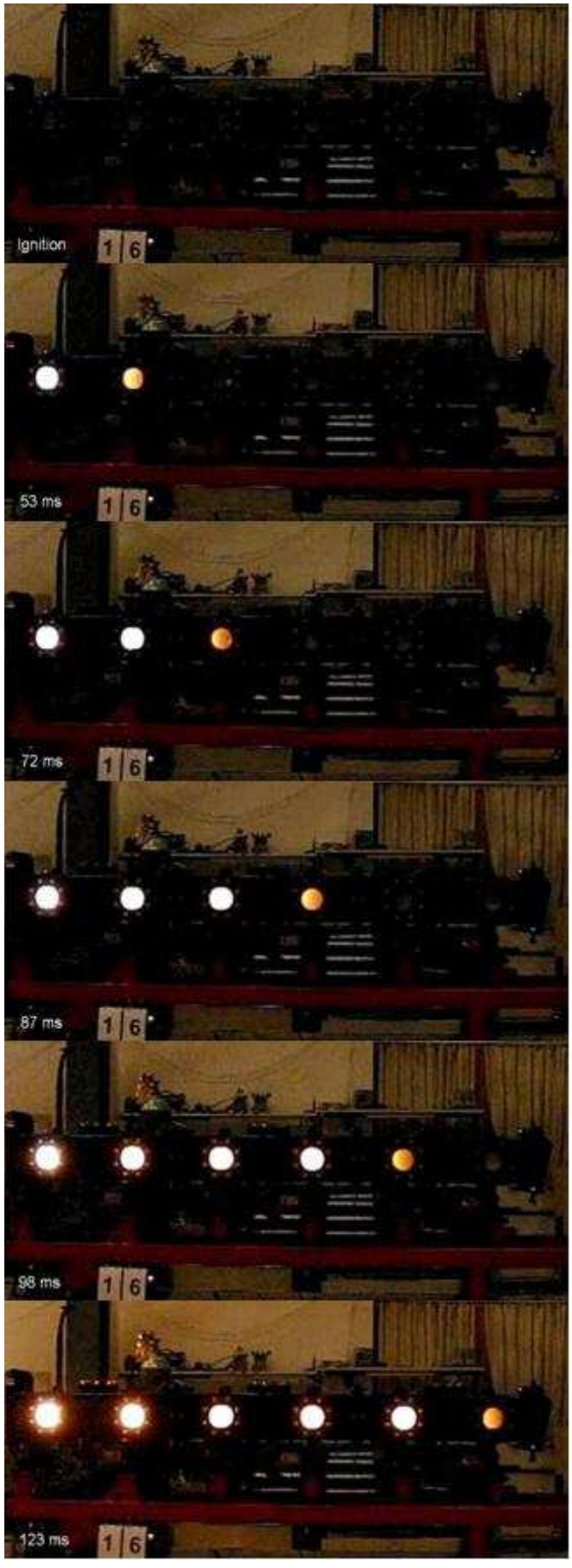

Figure B-2 Pictures of video from test 16

B.2 Results from Preliminary Experiments in the 20-litre Vessel

Thermocouples and piezoelectric pressure sensors

Figure B-3 shows a typical result from a thermocouple test in the 20-litre vessel as well as the pressure development with a concentration of 500 g maize starch /m^3. The ignition delay i.e. the time between dispersion and ignition is 60 ms. The dispersion and ignition signal is so strong that it is registered by the thermocouple measurement system, as can be seen by the two peaks in Figure B-3, and it is very useful as references in the measurement data. As can be seen from Figure B-3 the time between ignition and the flame detection done by the thermocouple is approximately 30 ms. As the thermocouple is placed 7,5 cm from the centre of the vessel, where ignition takes place, one can do an estimate of the flame propagation speed:

$$S = \frac{0{,}075}{0{,}030} = 2{,}5\frac{m}{s}$$

The order of magnitude of the flame speed is sensible however; it is not a good measurement of the flame speed when using only one thermocouple. Since the thermocouple got an unknown response time it is more appropriate to use several thermocouples with a known distance between them, and register the different times at which they measures a temperature rise. The thermocouples will then measure relative to each other and the response time is then not that interesting. Due to the small volume and lack of space, the implementation of more than one thermocouple has not been possible in the 20-litre vessel with our probes. The peak temperature registered by the thermocouple is approximately 900°C. However, the maximum temperature might be higher but due to the response time of the thermocouple, it might not be registered.

The pressure development, viewed in Figure B-3, shows that the pressure reaches a maximum value of 8.4 bar(g). This is in accordance with values presented by Siwek (1996) and Skjold (2003). Based upon the maximum dp/dt value obtained from the pressure-time measurement the K_{st} value can be estimated:

$$K_{st} = \left(\frac{dp}{dt}\right)_{\max} \cdot V^{1/3} = 616 \cdot 0{,}02^{1/3} = 167 bar \cdot m/s$$

The order of magnitude of the K_{st} is in accordance with previous work.

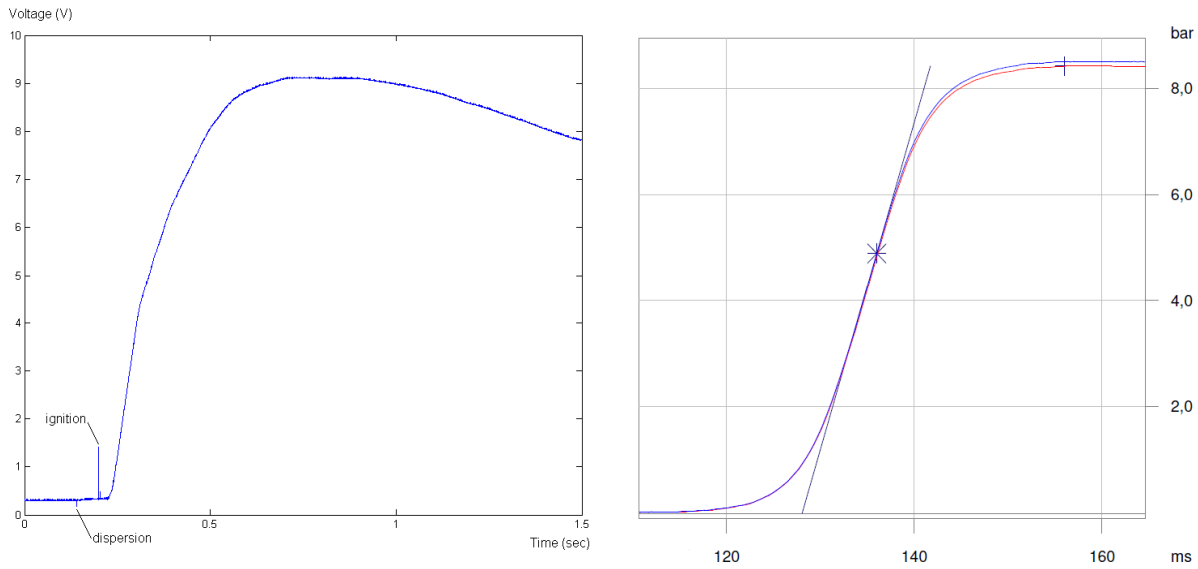

Figure B-3 Left: typical result from a thermocouple test in the 20-litre vessel. Right: typical pressure development in the 20-litre vessel.

B.3 The Matlab Program FileReader.m

```
% This program reads measurement data from the logging files and exports
% the measurement data in a file, with a binary format, for each measurement
% channel

clear all
for test = 22:22;
fid  = fopen(['test' num2str(test) '.txt'],'r');

A = zeros(200000,16);
for i = 1:200000
Line = fgetl(fid);
Line = strrep(Line,',','.');
line = str2num(Line);
A(i,1:16)=line;
i
end
fclose(fid)
capch = [13,14,15,3,16]
optproch = [1,2,7,8]
thermoch = [10]
prch = [4,5,6]

PrRes = A(:,1:3);
Time = 0:1/50000:4;
PrTub = [Time(1:end-1)', A(:,prch)];
CapPro = [Time(1:end-1)', A(:,capch)];
TempPro = [Time(1:end-1)', A(:,thermoch)];
OptPro = [Time(1:end-1)', A(:,optproch)];

fid = fopen(['cap' num2str(test) '.bin'], 'w+');
count = fwrite(fid, CapPro, 'double');
fclose 'all'

fid = fopen(['opt' num2str(test) '.bin'], 'w+');
count = fwrite(fid, OptPro, 'double');
fclose 'all'

fid = fopen(['Temp' num2str(test) '.bin'], 'w+');
count = fwrite(fid, TempPro, 'double');
fclose 'all'

fid = fopen(['PrTub' num2str(test) '.bin'], 'w+');
count = fwrite(fid, PrTub, 'double');
fclose 'all'
end
```

B.4 The Matlab Program analysis.m

```
% This program plots the results from measurements done by the optical
% probes, and calculates the transmission of light during the explosion
% based upon the measurements. Before this program can be used,
% one must run FileReader.m
% ------------------------------------------------------------------------ %

clear all
test=13;                            % enter test number
str1=num2str(test);
file=['opt' str1 '.bin'];           % opens a file defined by Filereader.m
fid = fopen(file, 'r');
A = fread(fid,'float64');
measurements=200000;                % number of measurements
f=50000;                            % frequenzy in Hz
t=A(1:measurements);                % time vector
B=A(200001:400000);                 % probe 1
C=A(400001:600000);                 % probe 2
D=A(600001:800000);                 % probe 3
E=A(800001:1000000);                % probe 4
F=A(1000001:1200000);               % probe 5

% chose step in order to define the size of the intervals where the program
% shall calculate the transmission

step=1600;                          % covers approximately five square waves
n=measurements-step;
o=1:(n/step);
t2=o./(f/step);                     % time vector for transmission plot
c=0;
s=0.6;                              % distanse between probes [m]

% adjusting for noise for each probe

bcut=min(B(1:(measurements/100)));    % cut values for noise
ccut=min(C(1:(measurements/100)));
dcut=min(D(1:(measurements/100)));
ecut=min(E(1:(measurements/100)));
fcut=min(F(1:(measurements/100)));

for i=1:measurements;
    if B(i)==0;
        B(i)=0;
    elseif B(i)<bcut;
        B(i)=B(i-1);
    else B(i)=B(i);
    end
```

```
    if C(i)<ccut;
        C(i)=C(i-1);
    else C(i)=C(i);
    end

    if E(i)<ecut;
        E(i)=E(i-1);
    else E(i)=E(i);
    end

    if F(i)<fcut;
        F(i)=F(i-1);
    else F(i)=F(i);
    end
end

for i=1:30000;
    if D(i)<dcut;
        D(i)=D(i-1);
    else D(i)=D(i);
    end
end

% transmission of light

Bn=B-min(B);
Cn=C-min(C);
Ds=-D;
Dn=Ds-min(Ds(1:5000));
En=E-min(E);
Fn=F-min(F);
u1=10000;
u2=150000;
tt=t(u1:u2);

for i=1:step:n;
    c=c+1;
    bmean(c)=mean(Bn((i:(i+step))));
    cmean(c)=mean(Cn((i:(i+step))));
    dmean(c)=mean(Dn((i:(i+step))));
    emean(c)=mean(En((i:(i+step))));
    fmean(c)=mean(Fn((i:(i+step))));
end

Transmissionb=bmean./bmean(1);
Transmissionc=cmean./cmean(1);
Transmissiond=dmean./dmean(1);
Transmissione=emean./emean(1);
Transmissionf=fmean./fmean(1);
```

```
for i=1:numel(Transmissionb);
    if Transmissionb(i)>1;
        Transmissionb(i)=1;
    else Transmissionb(i)=Transmissionb(i);
    end

    if Transmissionc(i)>1;
        Transmissionc(i)=1;
    else Transmissionc(i)=Transmissionc(i);
    end

    if Transmissiond(i)>1;
        Transmissiond(i)=1;
    else Transmissiond(i)=Transmissiond(i);
    end

    if Transmissione(i)>1;
        Transmissione(i)=1;
    else Transmissione(i)=Transmissione(i);
    end

    if Transmissionf(i)>1;
        Transmissionf(i)=1;
    else Transmissionf(i)=Transmissionf(i);
    end
end

% plotting

scrsz = get(0,'ScreenSize');
figure('Position',[1 scrsz(4)/2 scrsz(3)/2 scrsz(4)/2],'Name','measurements')

subplot(2,1,1),plot(t,B,t,C,t,D,t,E,t,F)
title(['Signal from the optical probes: test ',num2str(test)])
legend('probe 1','probe 2','probe 3','probe 4','probe 5',-1);

subplot(2,1,2),plot(t2,Transmissionb,t2,Transmissionc,t2,Transmissiond,t2,Transmissione
,t2,Transmissionf)
title('transmission')
xlabel('time [s]')
legend('probe 1','probe 2','probe 3','probe 4','probe 5',-1);

scrsz = get(0,'ScreenSize');
figure('Position',[1 scrsz(4)/2 scrsz(3)/2 scrsz(4)/2],'Name','measurements')
plot(tt,Bn(u1:u2),tt,Cn(u1:u2),tt,Dn(u1:u2),tt,En(u1:u2),tt,Fn(u1:u2))
title(['Signal from the optical probes: test ',num2str(test)])
xlabel('time [s]')
ylabel('voltage [V]')
legend('probe 1','probe 2','probe 3','probe 4','probe 5',2)
```

Appendix C - Abstracts for Work in Progress Posters

Abstracts for work in progress posters are presented in the following pages. The first is a poster that is to be presented at the 22nd International Colloquium on the Dynamics of Explosions and Reactive Systems (ICDERS) in Minsk, Belarus. This poster describes the ongoing work with the FAT. The second poster was presented last year in Montreal, Canada at the 32nd International Symposium on Combustion, and it is about the modified balloon experiment for dust explosions. This experiment were performed at the workshop at the UiB, and also worked as a preliminary experiment to the FAT-project.

Experimental investigation of the influence of obstacles on flame propagation in propane-air mixtures and dust-air suspensions in a 3.6 m flame acceleration tube

Trygve Skjold [1,2], Ivar B. Kalvatn [1], Gisle A. Enstad [1] & Rolf K. Eckhoff [1]

[1] University of Bergen, Dept. Physics & Technology, Allégaten 55, Bergen, Norway
[2] GexCon AS, Fantoftvegen 38, Bergen, Norway

1 Introduction

Dust explosions pose a hazard whenever a sufficient amount of combustible material is present as fine powder, there is a possibility of dispersing the material forming an explosive dust cloud within a relatively confined volume of air, and there is an ignition source present. Detailed modelling of industrial dust explosions from first principles is a formidable task, and current methods for mitigating the effects of industrial dust explosions therefore rely on empirical correlations obtained from a limited number of experiments. Recent efforts at simulating the course of dust explosions by combining computational fluid dynamics (CFD) and correlations for turbulent flame propagation with combustion parameters derived from standardized experimental tests have produced promising results [1]. However, the results indicate that the correlations for turbulent burning velocity used in various CFD codes for gaseous fuel-air mixtures are less successful in reproducing the experimental trends observed for dust explosions [1, 2]. The aim of the present work is to investigate these discrepancies further, and to develop improved models that can benefit future use of CFD-codes in consequence assessments for industrial plants. This paper describes an experimental study performed in a 3.6 metres flame acceleration tube on the influence of obstacles on flame propagation in two types of combustible mixtures: propane-air mixtures, and mechanical suspensions of maize starch in air.

2 Experiments

The experimental approach is similar to that of Pu *et al.* [3], but with a somewhat larger apparatus, and with an up-to-date data acquisition system. The flame acceleration tube consists of three equal sections of length 1.2 metres, and internal cross-section 0.27 m × 0.27 m (Figure1). The tests described here are limited to constant volume explosions, but the tube also allows for vented explosions. For gaseous fuels, the explosive mixture is prepared by evacuating the tube and controlling the addition of gas by monitoring the pressure. Tests are typically performed with initial turbulence generated by injecting air from a high pressure reservoir, and this secures thorough mixing prior to ignition. For solid fuels, air from the high pressure reservoir disperses the dust in a pre-dispersion chamber, before the dust is injected into the vessel through nozzles (Figure 2). An ignition source, either a spark or a chemical igniter, initiates the combustion process in one end of the tube. Different types of sensors (thermocouples, capacitive sensors, optical sensors, and high-speed video) measure flame arrival along the length of the tube, and piezoelectric pressure transducers measure pressure development inside the tube.

Correspondence to: trygve@gexcon.com

Figure 1 The 3.6 meter flame acceleration tube.

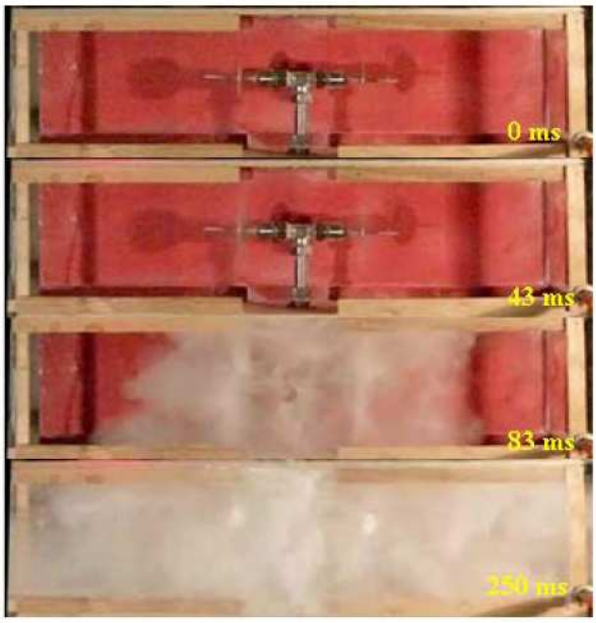

Figure 1 Sequence of pictures from initial testing of the dispersion system in a replica of a 1 metre section with the same cross section area as the flame acceleration tube.

References

[1] Skjold, T., Pu, Y.K., Arntzen, B.J., Hansen, O.J., Storvik, I.E., Taraldset, O.J. & Eckhoff, R.K. (2005). Simulating the influence of obstacles on accelerating dust and gas flames. Poster, *Twentieth International Colloquium on Dynamics of Explosive and Reactive Systems* (ICDERS), July 31 - August 5, Montreal, Canada.

[2] Skjold, T. (2007). Review of the DESC project. *Journal of Loss Prevention in the Process Industries*, **20**: 291-302.

[3] Pu, Y.K., Mazurkiewicz, J., Jarosinski, J. & Kauffman, C.W. (1988). Comparative study of the influence of obstacles on the propagation of dust and gas flames. Twenty-second *Symposium (Int.) on Combustion*: 1789-1797.

A MODIFIED BALLOON EXPERIMENT FOR DUST EXPLOSIONS

T. Skjold [1, 2 *], R.K. Eckhoff [1], G.A. Enstad [1], I.B. Kalvatn [1], M. van Wingerden [2], K. van Wingerden [2]

[1] *Department of Physics and Technology, University of Bergen, Norway;* [2] *GexCon AS, Norway*

trygve.skjold@ift.uib.no

Dust explosions continue to cause serious accidents in the powder handling industries, and the available methods for predicting the course of dust explosions in complex geometries are still of limited use in many practical situations [1]. Dust explosions are inherently complex phenomena, involving transient turbulent particle-laden flow with chemical reactions, often in complex geometries. Nevertheless, recent modelling efforts involving computational fluid dynamics (CFD) have produced promising results [2]. A conventional way of characterizing the reactivity of combustible powders is the maximum rate of pressure rise in constant volume explosion vessels. Although such parameters are convenient to measure, and often provide a useful way of classifying dust samples, they reveal limited information on the actual burning velocity and the structure of the flame. Moreover, the effect of pressure on the rate of combustion complicates the interpretation of the experimental results.

The purpose of the present study is to investigate dust explosions by an alternative experimental method, namely the traditional balloon experiment. A previous study resulted in an experimental apparatus that produced promising results [3]. Rotational flow from a high-pressure reservoir fluidizes the dust in a pre-dispersion chamber, before the suspension flows into the balloon through a pipe and a specially designed nozzle. In the first version, a small blasting cap ignited the dust cloud inside the balloon after a preset ignition delay time. A high-speed video camera captures the dispersion process and the subsequent explosion. The figure below shows some selected frames from one of these experiments. However, the blasting cap produced sparks that could ignite the flammable mixture some distance away from the original point of ignition, and even punctuate the balloon on some occasions. Furthermore, it was not always straightforward to support the balloon in an upright position. Hence, in the present contribution, the flow from the pre-dispersion chamber will enter the balloon from above (hanging balloon), and an electric discharge will ignite the flammable mixture at a specified ignition delay time. The experimental program includes tests with both maize starch and flammable gas (propane).

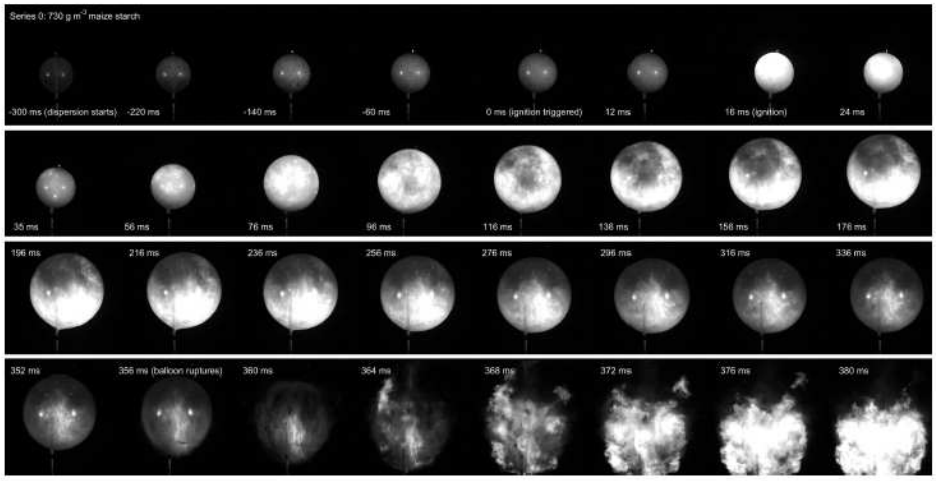

Although the experimental setup is relatively simple, the results may reveal fundamental differences in the structure of turbulent flames involving combustible dusts and flammable gases. The results are also valuable for validating sub-grid models describing the initial phase of flame propagation in CFD codes.

[1] Eckhoff, R.K. (2003). *Dust explosions in the process industries.* Third edition, Gulf Professional Publishing, Amsterdam.

[2] Skjold, T. (2007). Review of the DESC project. *Journal of Loss Prevention in the Process Industries*, 20, 291-302.

[3] Skjold, T. & Eckhoff, R.K. (2006). A balloon experiment for dust explosions. *Thirty-first Symposium (Int.) on Combustion*, Work-in-Progress Poster Session, August 6-11 2006, Heidelberg, 606.